AD_____

GRANT NUMBER: DAMD17-95-1-5027

TITLE: Cholinesterase Structure: Identification of Residues and Domains Affecting Organophosphate Inhibition and Catalysis

PRINCIPAL INVESTIGATOR: Palmer W. Taylor, Ph.D.

CONTRACTING ORGANIZATION: University of California, San Diego
La Jolla, California 92093-0934

REPORT DATE: April, 1997

TYPE OF REPORT: Annual

PREPARED FOR: U.S. Army Medical Research and Materiel Command
Fort Detrick, Frederick, Maryland 21702-5012

REPORT DOCUMENTATION PAGE

Form Approved
OMB No. 0704-0188

1. AGENCY USE ONLY (Leave blank)	2. REPORT DATE	3. REPORT TYPE AND DATES COVERED
	April 1997	Annual (6 Mar 96 - 5 Mar 97)

4. TITLE AND SUBTITLE
Cholinesterase Structure-Identification of Residues and Domains Affecting Organophosphate Inhibition and Catalysis

5. FUNDING NUMBERS
DAMD17-95-1-5027

6. AUTHOR(S)
Palmer W. Taylor, Ph.D.

7. PERFORMING ORGANIZATION NAME(S) AND ADDRESS(ES)
The University of California, San Diego
La Jolla, California 92093-0934

8. PERFORMING ORGANIZATION REPORT NUMBER

9. SPONSORING/MONITORING AGENCY NAME(S) AND ADDRESS(ES)
U.S. Army Medical Research and Materiel Command
Fort Detrick, Frederick, MD 21702-5012

10. SPONSORING/MONITORING AGENCY REPORT NUMBER

11. SUPPLEMENTARY NOTES

12a. DISTRIBUTION/AVAILABILITY STATEMENT
Approved for public release; distribution unlimited

12b. DISTRIBUTION CODE

13. ABSTRACT *(Maximum 200 words)*

In the second year of the grant, we have made excellent progress in several arenas:

1) The crystal structure of a mouse acetylcholinesterase-fasciculin 2 complex has provided an essential template for structure-function studies.
2) Studies with a series of enantiomeric organophosphates have been completed; they have yielded vital information on their binding orientation in the ground and transition states. Residues governing enantiomer specificity and leaving group orientation have been defined.
3) Studies in oxime reactivation of cholinesterase inhibited by the enantiomeric phosphates show two faces of attack between the oxime and the conjugated phosphonate.
4) The interactions of fasciculin 2 with acetylcholinesterase have been studied by kinetic and site-specific mutagenesis methods. The fasciculin2-acetylcholinesterase complex has enabled us to study entry of ligands to the active center gorge.

14. SUBJECT TERMS
Cholinesterase Structure, Organophosphate, Inhibition and Catalysis, Acetylcholinesterase, Enantiomers, Oxime Reactivators, Fasciculin, X-ray Crystal Structure, Site-Specific Mutagenesis

15. NUMBER OF PAGES
80

16. PRICE CODE

17. SECURITY CLASSIFICATION OF REPORT	18. SECURITY CLASSIFICATION OF THIS PAGE	19. SECURITY CLASSIFICATION OF ABSTRACT	20. LIMITATION OF ABSTRACT
Unclassified	Unclassified	Unclassified	Unlimited

FOREWORD

Opinions, interpretations, conclusions and recommendations are those of the author and are not necessarily endorsed by the U.S. Army.

____ Where copyrighted material is quoted, permission has been obtained to use such material.

____ Where material from documents designated for limited distribution is quoted, permission has been obtained to use the material.

____ Citations of commercial organizations and trade names in this report do not constitute an official Department of Army endorsement or approval of the products or services of these organizations.

____ In conducting research using animals, the investigator(s) adhered to the "Guide for the Care and Use of Laboratory Animals," prepared by the Committee on Care and use of Laboratory Animals of the Institute of Laboratory Resources, national Research Council (NIH Publication No. 86-23, Revised 1985).

____ For the protection of human subjects, the investigator(s) adhered to policies of applicable Federal Law 45 CFR 46.

X ____ In conducting research utilizing recombinant DNA technology, the investigator(s) adhered to current guidelines promulgated by the National Institutes of Health.

X ____ In the conduct of research utilizing recombinant DNA, the investigator(s) adhered to the NIH Guidelines for Research Involving Recombinant DNA Molecules.

X ____ In the conduct of research involving hazardous organisms, the investigator(s) adhered to the CDC-NIH Guide for Biosafety in Microbiological and Biomedical Laboratories.

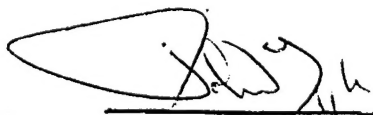

3/31/97

PI - Signature Date

TABLE OF CONTENTS:

Page #'s

(5) INTRODUCTION:

This project is directed towards examining ligand interactions, particularly organophosphates and oximes, with acetylcholinesterase, by kinetic, physicochemical, computational and recombinant DNA methods. The studies are directed to analyzing mechanisms of inhibition by organophosphates, their spontaneous hydrolysis, reactivation by oximes and the sites of interaction of reversible inhibitors. Through these studies we not only hope to understand mechanisms of acetylcholinesterase catalysis, inhibition and reactivation, but also develop means for making recombinant DNA derived cholinesterases as useful antidotes for organophosphate poisoning.

(6) BODY:

A. Recombinant DNA-derived Acetylcholinesterase (AChE) and the Crystal Structure Template

Our studies, to date, have employed site-specific mutagenesis, kinetic analysis, X-ray crystallography, fluorescence spectroscopy and ligand design. Below are described the projects in which we have made substantive inroads. In the last progress report, we described procedures of production of large quantities of AChE by expression from cDNAs and its crystallization (cf: Marchot et al., 1996, Appendix) and the crystal structure of the fasciculin-AChE complex (Bourne et al., 1995, Appendix). Since this is the first mammalian AChE structure to be reported, it now serves as our template for the analysis of structure. To date, we have prepared by recombinant DNA means over a gram of enzyme and supplied several laboratories for their studies. Our success in obtaining a homogeneity sufficient for crystallization stems from rapid production over short time intervals and immediate purification. Earlier modeling only used the *Torpedo* enzyme.

In collaboration with Drs. Yves Bourne and Pascale Marchot, we have now succeeded in obtaining crystals of the mouse enzyme in the absence of fasciculin at about 3Å resolution. New data are now being collected on the synchrotron in Grenoble which should yield a high resolution structure. The initial diffraction patterns show that the back side of each cholinesterase molecule (Cys265-Cys272 loop) adopts the position of fasciculin in the structure. However, the gorge remains in its narrow or closed state.

B. Studies of Enantiomeric Specificity of the Organophosphates

These studies using a series of R- and S-alkyl methylphosphonylcholines and neutral alkyl methylphosphonylthioates are now complete. Data for several charged residue and acyl pocket mutations have been analyzed by a thermodynamic mutant cycle analysis in three dimensions (X = R and S chirality; Y = charge on the leaving group thioate; Z = acyl pocket substitutions (Hosea et al., 1995 & 1996, Appendix). Analysis of the second order rate constants for organophosphate inhibition of AChE reveal that: (a) chiral selectivity is dictated primarily by acyl pocket dimensions, particularly the 297 residue. By mutation from Phe to Ile, the S to R preference inverts going from 230 to 0.3. (b) Asp74, but not Glu202 or Glu450, governs the enhanced reactivity of the cationic organophosphates, (c) ligand orientation in the transition state requires that: (1) the phosphonyl oxygen fit in the oxyanion hole, (2) the phosphorus be positioned for nucleophilic attack by the serine, and (3) the leaving group be positioned to exit from the gorge. Three dimensional plots of the free energy diagrams clearly reveal these requirements for enantiomeric selectivity.

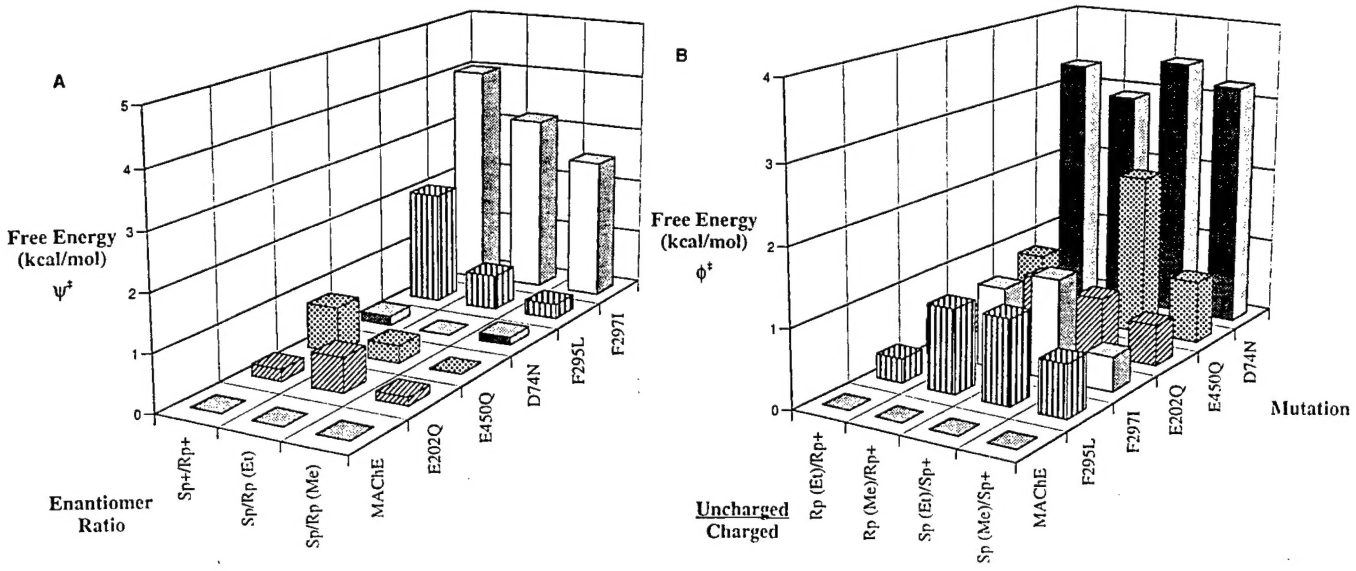

Fig. 1: Relationship between the change in free energy of activation, selected mutations in acetylcholinesterase, and structures of cycloheptyl methylphosphonyl thioates. (A) Selectivity for the S_p and R_p enantiomers. (B) Selectivity for charged and uncharged phosphonates: +, cationic cyclopheptyl methylphosphonyl thiocholine; Me, uncharged cycloheptyl methylphosphonyl thiomethane; and Et, uncharged cycloheptyl methylphosphonyl thioethane. The scheme for the thermodynamic mutant cycle analysis is shown in Hosea et al., 1996, appendix.

Future studies will be directed to ligands with small leaving groups (i.e., the fluoridates). The R and S enantiomers should correspond to P(+) and P(-) isomers of soman and sarin.

C. Studies on Modes of Ligand Entry to the Active Center of Acetylcholinesterase

We had shown previously that specificity of fasciculin for AChE over butyrylcholinesterase arises from three aromatic residues found only in AChE (Trp 284, Tyr 72 and Tyr 124) [Radic et al., 1995]. Subsequent studies also show a role for Asp 74 and His 285 in the energetics of fasciculin binding, but these residues are of lesser consequence than the three above residues. The crystal structure of the complex substantiates these findings since residues 284, 72 and 124 play a dominant role in the interfacial contact between fasciculin (loop 2) and AChE. Loop 1 forms contact with a furrow near the top of the enzyme and a protrusion involving Pro 76 contacts a crotch region between loops 2 and 3 on the toxin. Loop 3 forms little contact in the complex. See Bourne et al., 1995.

The crystal structure of mouse AChE with fasciculin shows that the peptide plugs the gorge entry raising the question of why there remains residual activity (0.1% for acetylthiocholine but higher for *p*-nitrophenylacetate). Moreover, inhibitors like trifluoroketones and organophosphates, can still access the active center, albeit more slowly.

To examine the mode of ligand entry, we conducted an extensive study of the ionic strength dependence of ligand inhibition wherein surface residues on the enzyme are modified. Association rates of cationic ligands (*m*-trimethylammoniotrifluoro acetophenone (TFK^+), a trifluoroketone and fasciculin, a peptide) decrease with an increase in ionic strength showing the masking effect on the electrostatic attraction between the cationic ligand and the anionic enzyme. The influence is roughly proportional to the charge on the respective ligands...fasciculin (+4) and TFK^+ (+1). Neutralization

of anionic residues on the enzyme, by site-specific mutagenesis to the corresponding carboxamides, also results in a predictable diminution in the electrostatic enhancement of rate. No effect of ionic strength is seen for the dissociation rates.

Of paramount interest is the influence of bound fasciculin on the ionic strength dependence of small ligand entry to the complex for bound fasciculin actually inverts the dependence of TFK^+ where the masking effect of increased ionic strength accelerates the reaction. This inverted influence is not seen when charge on the enzyme is reduced equivalently by +4 through mutation of four Glu and Asp to Gln and Asn. Hence, the entering TFK^+ projectile must traverse closely to the bound fasciculin, and the transition state for diffusion into the gorge of restricted dimensions is reflected in the proximity to fasciculin in the transition state. Representative data for TFK^+ and fasciculin are shown in fig. 2. The inverted ionic strength dependence for TFK^+ association with the fasciculin-AChE complex when compared with mutant AChE containing equivalent charge neutralization as the complex is shown in fig. 3b.

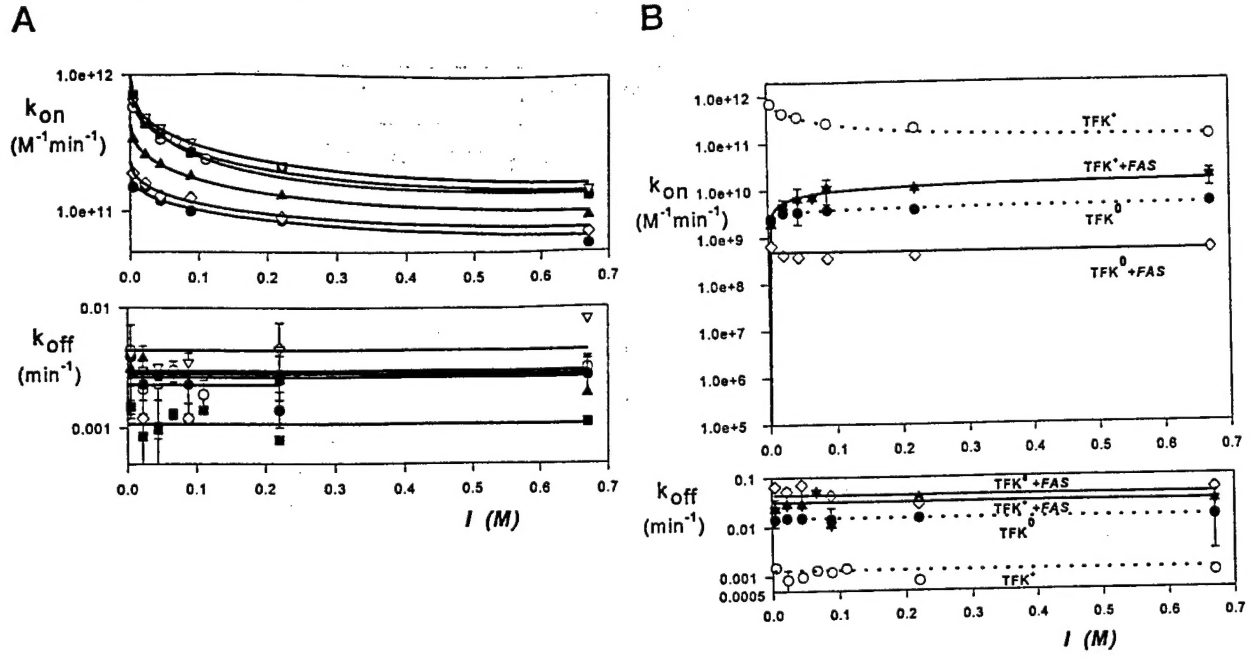

FIG. 2A. **Ionic strength dependence of TFK^+; second-order rate constant (k_{on}) and first-order dissociation constant (k_{off}) with wild-type (■) and mutant mouse AChEs.** All *curves* were calculated as a best fit of data to the Debye Hukel limiting law. A, surface mutants: D280V (▽), D280V/D283N (○), E84Q/E91Q/D280V/D283N (▲), E84Q/E91Q/D280V/D283N/D372N (◊), and E84Q/E91Q/D280V/D283N/E292Q/D372N (●)

Fig. 2B. **Ionic strength dependences of rate constants for ligands and AChE-FAS2 complex (*solid lines* and AChE alone (*dashed lines*).** *Curves* were calculated as best fits of the data to the Debye Hukel limiting law, association (k_{on}) and dissociation (k_{off}) rate constants of inhibitors. TFK° is uncharged isostere [*m*-(*t*-butyl)trifluoroacetophenone].

D. Studies on Oxime Reactivation of Phosphoryl and Phosphonyl-Conjugated Cholinesterases

Having accumulated substantial data on enantiomeric selectivity for the phosphorylation reaction with wild-type and mutant enzymes, we have begun to study oxime reactivation of the enantiomeric conjugates (actually diasteriomers). The data base for this is our previous work on

oxime reactivation of the ethoxymethylphosponyl conjugate (Ashani et al., 1995) where the enantiomeric pair was used. New data that we have generated using the conjugated R and S enantiomers and reactivation with 2-PAM and HI-6 are shown in Tables 1, 2 and 3. An example of the kinetic profiles for reactivation are shown in fig. 3. Data are calculated according to Scheme I.

Scheme 1:

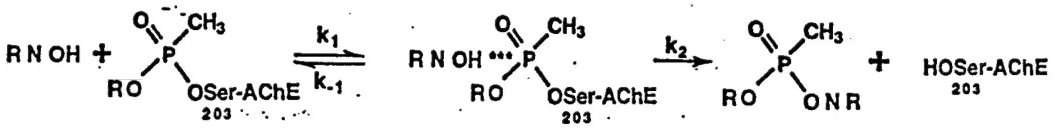

where $k_{obs}=\frac{k_2}{(1+K'_{ox}/RNOH)}$ and $K'_{ox}=\frac{k_1+k_2}{k_1}$

While these studies are still in progress, several trends are evident. (1) Large enantiomeric preferences are seen with the S enantiomers being more susceptible to reactivation, (2) opening of the acyl pocket can enhance reactivation provided geometric access is correct, (3) the oxyanion hole stabilizes the transition state in the reactivation reaction, (4) attack by the oximes can occur from two directions (ie: two faces of the conjugated phosphonate), and (5) the efficiency of reactivation by different oximes depends on the structure of the conjugated phosphonate.

Table I
Bimolecular Rate Constants ($min^{-1}M^{-1}$) for Reactivation of Mouse AChE by HI6.

Enzyme	(Sp) CHMP	(Sp) IPMP	(Sp)DBMP
AChE	$0.19x10^3$	$1.5x10^3$	$0.18x10^3$
F295L	$2.4x10^3$	$3.8x10^3$	$1.2x10^3$
F297I	$0.41x10^3$	$2.4x10^3$	$0.25x10^3$

*Rp compounds have yet to be analyzed since reactivation is less than 50%.

Table II
Bimolecular Rate Constants ($min^{-1}M^{-1}$) for Reactivation of Mouse AChE by 2-PAM.

Enzyme	(Sp)CHMP	(Rp)CHMP	(Sp)IPMP	(Rp)IPMP	(Sp)DBMP	(Rp)DBMP
AChE	0.45	UD	160	36	0.23	0.47
F295L	1.4	UD	ND	ND	ND	ND
F297I	ND	ND	ND	ND	ND	ND

UD= undetermined, less than 20% reactivation; ND= not determined
CHMP, cycloheptylmethylphosphono-AChE; DBMP, 3,3 dimethylbutylmethylphosphono-AChE; IPMP, isopropylmethylphosphono-AChE

Table III: Aging of Phosphonylated-AChE Conjugates as Determined by 2mM HI6 Reactivation Half Lives of the Conjugated Enzymes (in hours).

Enzyme	Sp-cycloheptylmethyl phosphono-AChE	Sp-isoproylmethyl phosphono-AChE	Sp-3,3dimethylbutylmethyl phosphono-AChE
AChE	24.1	49.0	NO
F295L	14.4	ND	NO
F297I	30.8	ND	NO

ND= not determined; NO= no aging observed

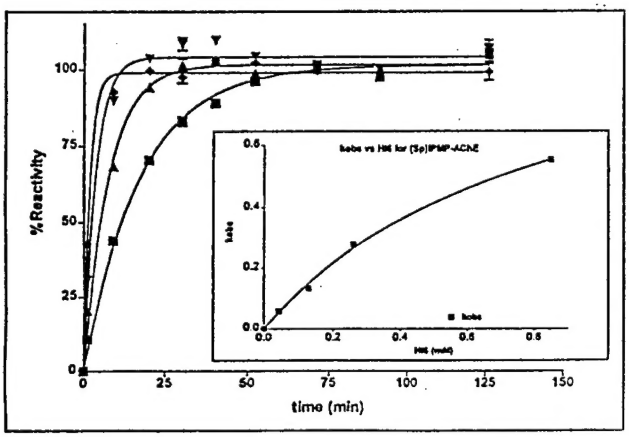

Fig. 3: Reactivation of S_p-IPMP-AChE by varying concentrations of HI-6, 0.0425mM, ▲, 0.128mM; ▼, 0.25mM; ◆, 0.85mM. Inset shows the concentration dependence for the rate constant of reactivation.

(7) CONCLUSIONS:

The studies of the structure of AChE coupled with the detailed analysis of enantiomeric phosphonates and other specific inhibitors have yielded important information on enzyme structure in relation to function. We will continue this line of study, but also will extend the work to conformation in solution since we feel that the crystal structure does not reflect the catalytically active conformational states of acetylcholinesterase. Particular emphasis will be placed on oxime reactivation studies in the next year since the efficacy of particular oximes will depend on the structure of the conjugated phosphonate or phosphorate.

(8) REFERENCES:

Radic', Z., Duran, R., Vellom, D.C., Li, Y., Cervenansky, C. and Taylor, P. Site of Fasciculin Interaction with Acetylcholinesterase. *J. Biol. Chem.* 269: 11233-11239 (1994).

Ashani, Y., Radić, Z., Tsigelny, I., Vellom, D.C., Pickering, N.A., Quinn, D.M., Doctor, B.P. and Taylor, P. Amino Acid Controlling Reactivation of a Chiral Organophosphonyl Conjugate of Acetylcholinesterase by Mono- and Bisquaternary Oximes. *J. Biol. Chem.* 270:6370-6380 (1995).

Hosea, N.A., Berman, H.A. and Taylor, P. Specificity and Orientation of Trigonal Carboxyl Esters and Tetrahedral Alkylphosphonyl Esters in Cholinesterases, *Biochemistry* 34:11528-11536 (1995).

Bourne, Y., Taylor, P. and Marchot, P. Acetylcholinesterase Inhibition by Fasciculin: Crystal Structure of the Complex. *Cell* 83:502-512 (1995).

Publications in 1996 & 1997 arising from these studies:

1. Marchot, P., Ravelli, R.B.G., Raves, M.L., Bourne, Y., Vellom, D.C., Kanter, J., Camp, S., Sussman, J.L. and Taylor, P. Soluble Monomeric Acetylcholinesterase from Mouse: Expression, Purification, and Crystallization in Complex with Fasciculin. *Protein Science* 5: 672-679 (1996).

2. Hosea, N.A., Radic, Z., Tsigelny, I., Berman, H.A., Quinn, D.M. and Taylor, P. Aspartate 74 as a Primary Determinant in Cholinesterase Governing Specificity to Cationic Organophosphates. *Biochemistry* 35:10995-11004 (1996).

3.. Taylor, P., Hosea, N.A., Tsigelny, I., Radić, Z. and Berman, H.A. Determining Ligand Orientation and Transphosphonylation Mechanisms on Acetylcholinesterase by Rp, Sp Enantiomer Selectivity and Site-Specific Mutagenesis. *Enantiomer*, In Press.

4. Taylor, P., Hosea, N., Marchot, P., Radić, Z., and Berman, H.A. The Cholinesterases at Atomic Resolution: Application of Structural Studies to Mechanisms of Inhibition. Medical Defense Bioscience Review Proceedings Vol. 1, pp. 1-12 (1996)

5. Marchot, P, Prowse, C.N., Kantor, J., Camp, S., Ackermann, E.J., Radic, Z., Bougis, P.E. and Taylor, P. Expression and Activity of Mutants of Fasciculin, a Peptidic Acetylcholi-nesterase Inhibitor from Mamba Venom. *J. Biol. Chem.* 272, 3502-3510, (1997)

(9) APPENDIX:

Copies of the above five articles are enclosed.

Protein Science (1996), *5*:672–679. Cambridge University Press. Printed in the USA.

Soluble monomeric acetylcholinesterase from mouse: Expression, purification, and crystallization in complex with fasciculin

PASCALE MARCHOT,[1,6] RAIMOND B.G. RAVELLI,[2] MIA L. RAVES,[3,5] YVES BOURNE,[1,4,7] DANIEL C. VELLOM,[1,8] JOAN KANTER,[1] SHELLEY CAMP,[1] JOEL L. SUSSMAN,[3,5] AND PALMER TAYLOR[1]

[1] Department of Pharmacology, University of California at San Diego, La Jolla, California 92093-0636
[2] Department of Crystal and Structural Chemistry, Bijvoet Center for Biomolecular Research, Padualaan 8, 3584 CH Utrecht, The Netherlands
[3] Biology Department, Brookhaven National Laboratory, Upton, New York 11973
[4] Department of Molecular Biology, The Scripps Research Institute, La Jolla, California 92037
[5] Department of Structural Biology, Weizmann Institute of Science, Rehovot 76100, Israel

(RECEIVED October 25, 1995; ACCEPTED January 12, 1996)

Abstract

A soluble, monomeric form of acetylcholinesterase from mouse (mAChE), truncated at its carboxyl-terminal end, was generated from a cDNA encoding the glycophospholipid-linked form of the mouse enzyme by insertion of an early stop codon at position 549. Insertion of the cDNA behind a cytomegalovirus promoter and selection by aminoglycoside resistance in transfected HEK cells yielded clones secreting large quantities of mAChE into the medium. The enzyme sediments as a soluble monomer at 4.8 S. High levels of expression coupled with a one-step purification by affinity chromatography have allowed us to undertake a crystallographic study of the fasciculin–mAChE complex. Complexes of two distinct fasciculins, Fas1-mAChE and Fas2-mAChE, were formed prior to the crystallization and were characterized thoroughly. Single hexagonal crystals, up to 0.6 mm × 0.5 mm × 0.5 mm, grew spontaneously from ammonium sulfate solutions buffered in the pH 7.0 range. They were found by electrophoretic migration to consist entirely of the complex and diffracted to 2.8 Å resolution. Analysis of initial X-ray data collected on Fas2-mAChE crystals identified the space group as $P6_122$ or $P6_522$ with unit cell dimensions $a = b = 75.5$ Å, $c = 556$ Å, giving a V_m value of 3.1 Å^3/Da (or 60% of solvent), consistent with a single molecule of Fas2-AChE complex (72 kDa) per asymmetric unit. The complex Fas1-mAChE crystallizes in the same space group with identical cell dimensions.

Keywords: acetylcholinesterase; crystallization; fasciculin; peptide–macromolecule complex; snake toxin

Reprint requests to: Palmer Taylor, Department of Pharmacology, University of California at San Diego, La Jolla, California 92093-0636.

[6] Permanent address: Laboratoire de Biochimie, CNRS, Unité de Recherche Associée 1455, Institut Fédératif de Recherche Jean Roche, Université d'Aix-Marseille II, Faculté de Médecine Secteur Nord, 13916 Marseille cedex 20, France.

[7] Permanent address: Laboratoire de Cristallisation et Cristallographie des Macromolécules Biologiques, CNRS, Institut Fédératif de Recherche Concertée-1, 31 Ch. Joseph Aiguier, 13402 Marseille cedex 20, France.

[8] Present address: Department of Biochemistry, Brooklyn College of the City University of New York, Brooklyn, New York 11210-2889.

Abbreviations: mAChE, mouse acetylcholinesterase; $(NH_4)_2SO_4$, ammonium sulfate; BSA, bovine serum albumin; CMV, cytomegalovirus; DTNB, dithiobis-2-nitrobenzoic acid; FPLC, fast performance liquid chromatography; HEK, human embryonic kidney; ImMal, imidazole malate; PEG, polyethyleneglycol; PNGaseF, peptide:*N*-glycanase F; Mes, 2-(*N*-morpholino)ethane sulfonic acid; NaAc, sodium acetate.

Acetylcholinesterase's only well-documented action is the termination of receptor activation by the neurotransmitter, acetylcholine, at synaptic junctions through ester hydrolysis (cf. Massoulié et al., 1993; Taylor & Radić, 1994). Inhibition of acetylcholinesterase gives rise to a panoply of symptoms. In skeletal muscle, fasciculations are observed initially, followed by flaccid paralysis.

Fasciculins are the only known peptide inhibitors of AChE, with dissociation constants as low as 1–10 pM. These 7-kDa peptides, which are found in mamba snake venoms (cf. Cerveñansky et al., 1991), form three loops emerging from a dense core containing the disulfide bridges. They belong to the structural family of three-fingered peptidic toxins from Elapidae venoms, which include the nicotinic receptor-blocking α-neurotoxins (Changeux et al., 1970; Endo & Tamiya, 1991), the muscarinic receptor peptide agonists (Adem et al., 1988; Segalas et al., 1995), and the

cardiotoxins that interact with cell membranes (Bougis et al., 1981; Dufton & Hider, 1991). Despite a common structural motif, the toxins in this family are directed to diverse targets, yet their modes of action are highly selective. Several lines of evidence show that the fasciculins bind to a peripheral site of AChE, a region distinct from the catalytic center and located at the rim of the active site gorge. This site shares a common region with the binding site, of peripheral-site cationic inhibitors and with the site at which the substrate, when present in large excess, binds. In addition, fasciculins appear not to totally occlude access of small molecules to the catalytic site (Marchot et al., 1993; Radić et al., 1995). Rather, they influence AChE catalysis in an allosteric fashion, although a partial gating influence may also restrict the rate of entry into the gorge for substrates whose catalysis is rate-limited or near-limited by diffusion (Eastman et al., 1995; Radić et al., 1995; van den Born et al., 1995).

The X-ray structure of a dimeric AChE from *Torpedo californica* has been solved at 2.8 Å resolution (Sussman et al., 1991). Since then, substantial information regarding the fasciculin binding site on mouse AChE has been obtained by site-directed mutagenesis (Radić et al., 1994, 1995). The X-ray structures of fasciculins, Fas1 and Fas2, have been solved at 1.9 Å and 2.0 Å resolution, respectively (Le Du et al., 1992, 1995). Analysis of the structures, however, allowed one only to hypothesize on the nature of the fasciculin determinants responsible for binding to AChE.

The predominant monomeric and dimeric forms of native AChE contain a hydrophobic domain at their carboxyl-terminus, either as an attached glycophospholipid or an amphipathic sequence (Massoulié et al., 1993), both being likely to limit the propensity for crystallization. In the dimeric *Torpedo* AChE, the diglyceride on the glycophospholipid, which serves as the hydrophobic anchor in the membrane, was enzymatically cleaved prior to crystallization (Sussman et al., 1988).

We have generated a soluble, monomeric AChE from mouse (mAChE), a catalytic subunit (~65 kDa), from a cDNA lacking the coding sequence for the extreme carboxyl terminus. High levels of expression in HEK cells, coupled with a one-step purification by affinity chromatography on an inhibitor-conjugated resin, have allowed us to undertake an X-ray crystallographic study of the fasciculin–AChE complex.

Results and discussion

Insertion of a stop codon in place of the Cys 549 codon of mouse AChE (Rachinsky et al., 1990; Li et al., 1991, 1993) maintains the catalytic core of the molecule, but truncates 37 amino acids from the nascent peptide. This eliminates the signal for attachment of the hydrophobic glycophospholipid to the carboxy-terminal residue (Gly 557) of the processed native enzyme (Fig. 1). Thus, the recombinant DNA-derived enzyme is nine residues shorter than the processed amphiphilic enzyme and, importantly, lacks a hydrophobic glycophospholipid or amphipathic helix at its carboxyl-terminus found on other forms of AChE. HEK cells in which the mutated cDNA was stably integrated were grown in the presence of serum, then allowed to express mAChE in a serum-free medium. Typically, 0.2–0.5 mg of mAChE was secreted over a 3-day period in a 10-cm dish covered with 10 mL of medium, and secretion at a high level could

```
                 5         5
                 4         5
                 9         7
-SATATEAPCTCPSPAHGEAAPRPGPDLALSLLFFLFLLHSGLPWL
<--||-->
exon 4  exon 5          cleaved glycophospholipid anchor signal peptide


-SATATEAP
<--||-->
exon 4  exon 5
```

Fig. 1. Carboxyl-terminal sequences of native and truncated mouse AChE. The signal for attachment of the hydrophobic glycophospholipid to Gly 557 in the processed native enzyme (top sequence) has been eliminated by insertion of a stop codon in place of the Cys 549 codon. The resulting enzyme, mAChE, is monomeric and devoid of a carboxyl-terminal hydrophobic segment (bottom sequence). Sequence Ser-Ala-Thr is encoded by the end of exon 4; sequence Ala-Thr-Glu is encoded by the beginning of exon 5 (Li et al., 1993). Mouse AChE residue numbering is used.

be maintained for up to one month. Sedimentation of mAChE from the collected medium on sucrose gradients in the presence of 1% Triton X-100 yielded a single, symmetric peak sedimenting at 4.8 S (Fig. 2), consistent with the recombinant enzyme sedimenting as a monomer. Indeed, dimers of the catalytic subunit containing the glycophospholipid sediment at 6.0 S, whereas cleavage of the phospholipid yields a sedimentation constant of 6.5 S (D.C. Vellom, unpubl. data). Similar behavior has been reported for corresponding forms of *Torpedo* AChE (Duval et al., 1992).

Purification and characterization of mAChE

Similar to the procedure adopted for purification of the 11S form of *T. californica* AChE (Taylor & Jacobs, 1974), affinity chromatography was used to purify milligram quantities of mAChE from the tissue culture medium. Typically, 30–50 mg of enzyme in 2–4 L of medium were subjected to purification by selective retention on an *m*-aminophenyltrimethyl-ammonium-

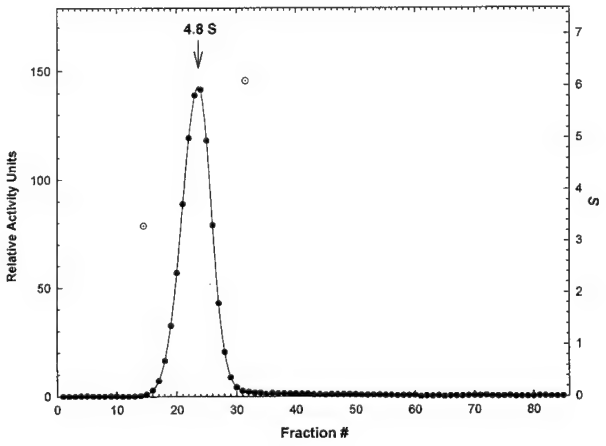

Fig. 2. Hydrodynamic analysis of mAChE-containing harvested culture media. The sample (100 μL), supplemented with sedimentation standards, was centrifuged in a 3–20% sucrose gradient in the presence of Triton X-100, then fractionated as described in the text. Sedimentation positions of two standards, carbonic anhydrase (3.3 S) and alkaline phosphatase (6.1 S), are shown as dotted open circles.

conjugated column and subsequent elution by decamethonium. Owing to the high concentration of decamethonium used, mAChE eluted as a single, sharp peak with only minor tailing representing a few percent of the initial activity loaded on the column. Purification yields ranged from 60% to 95% of the activity initially detected in the medium. The specific activity of purified mAChE, 2,206 units mg^{-1}, corresponds to a k_{cat} of 16.2×10^4 min^{-1}, in good agreement with the value reported previously (Vellom et al., 1993). Routine storage at −20 °C of purified mAChE mixed with glycerol 1:1 (v/v) was not consistent with reliable crystallization. An immediate and dramatic loss of activity was observed upon flash-freezing of the purified enzyme in liquid nitrogen. mAChE, however, could be stored for weeks on ice without loss of activity or alteration of the gel-filtration or SDS-PAGE patterns.

Electrophoretic analysis of the purified mAChE suggests that the enzyme displays slight heterogeneity. Indeed, SDS-PAGE resulted in two diffuse and partially overlapping bands with a ratio of about 1:1 and an average apparent mass of ca. 65 kDa (Figs. 3, 4A), whereas native gel electrophoresis resulted in a diffuse and particularly broad band, larger than expected from a protein with three *N*-glycosylation sites (Fig. 4B). Reducing the volume of the loaded sample and/or increasing the crosslinking of the stacking gel did not change these patterns significantly. Removal of the N-linked carbohydrate side chains from mAChE by digestion with PNGaseF, then subsequent analysis by SDS-PAGE, resulted in sharpening of the two bands, causing them to migrate closer to each other, and lowering their apparent mass to ca. 55 kDa (Fig. 3). The purified mAChE could therefore be composed of two roughly equal populations of monomeric enzyme differing slightly in their carbohydrate composition or some other post-translational modification. Similar observations have been reported for purified recombinant human AChE (Velan et al., 1992). Independent analysis of the chromatographic fractions from the affinity column showed that the two bands co-elute throughout the elution peak, suggesting identical binding properties for the two forms. The two forms were still observed upon SDS-PAGE analysis of the fasciculin–mAChE complexes and of the dissolved crystals (Fig. 4; see below), and therefore are not distinguished by complexation with fasciculin and subsequent crystallization.

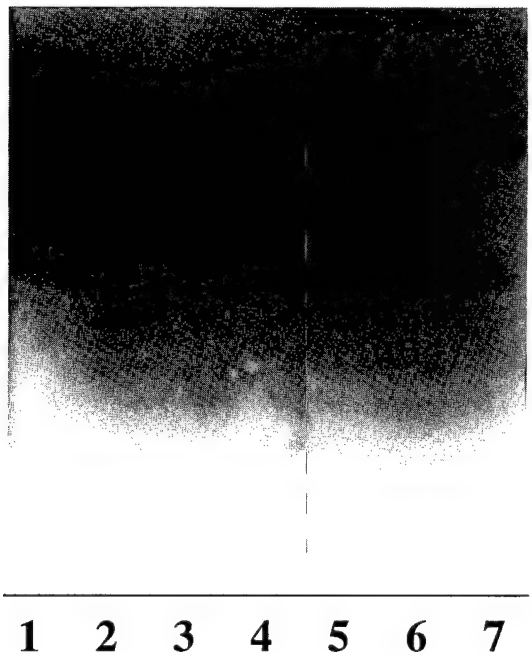

Fig. 3. Electrophoretic analysis of native and deglycosylated mAChE. SDS-PAGE (15% resolving/5% stacking gel, 20 cm × 20 cm) under reducing conditions: lanes 1 and 6, purified mAChE; lanes 2 and 7, BSA (66 kDa); lanes 3 and 4, mAChE deglycosylated with PNGaseF; lane 5, BSA treated with PNGaseF. The thin band at the bottom of the gel corresponds to PNGaseF (36 kDa, lanes 3, 4, and 5).

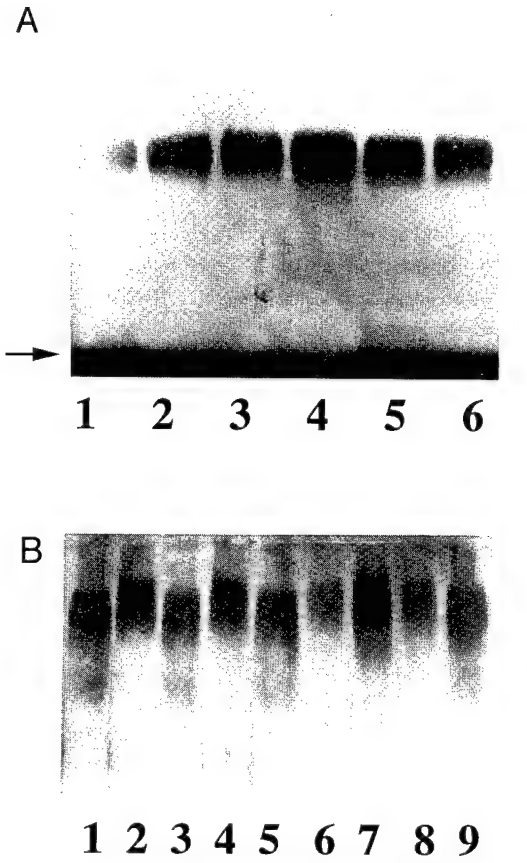

Fig. 4. Electrophoretic analysis of mAChE and fasciculin–mAChE complexes. **A:** SDS-PAGE (4–20% gradient gel, 8 cm × 8 cm) under reducing conditions: lanes 2, 3, and 4, purified mAChE; lane 1, mAChE complexed to Fas1; lane 5, mAChE complexed to Fas2; lane 6, washed and dissolved Fas2-mAChE hexagonal crystal; mAChE migrates as two diffuse and overlapping bands; arrow at the bottom of the gel indicates the fasciculin band (lanes 1, 5, and 6). **B:** Native gel electrophoresis (7.5% resolving/5% stacking gel, 8 cm × 8 cm) with migration toward the anode: lanes 1, 3, 5, and 9, purified mAChE; lane 2, mAChE complexed to Fas1; lane 4, mAChE complexed to Fas2; lanes 6, 7, and 8, washed and dissolved triangular, needle-shaped, and hexagonal Fas2-mAChE crystals, grown in $(NH_4)_2SO_4$; the shift toward the cathode in the position of the complexes (lanes 2, 4, 6, 7, and 8) relative to the free mAChE is evident.

Complexation of mAChE with fasciculins and characterization of the complexes

Special care has been taken for complexation of Fas1 and Fas2, respectively, to mAChE and characterization of the complexes

prior to crystallization. The fasciculin–mAChE complexes were preformed at, or close to, the high protein concentrations required for crystallization, i.e., a concentration $\sim 10^8$-fold greater than the K_i of Fas2 for mouse AChE (Radić et al., 1994), together with an 1.2 molar excess of fasciculin. Slightly higher residual activity was observed repeatedly for the Fas2-mAChE complex compared to the Fas1-mAChE complex. Both complexes were analyzed by gel electrophoresis (after removal of the unbound excess fasciculin) and gel filtration chromatography (before and after removal). SDS-PAGE of the complexes was performed with a gradient gel appropriate for the large difference in size of the fasciculin and the mAChE molecules (Fig. 4A). Although fasciculin migrated together with the free dodecylsulfate, it ran as a thin, intense band at the bottom of the gel. The migration pattern of initially complexed mAChE was found to be identical to free mAChE. In order to establish actual complexation of Fas1 or Fas2 to mAChE and not only their simultaneous presence, native gel electrophoresis was performed both on the free and complexed mAChE (Fig. 4B). The bound fasciculin was found to diminish the mobility of mAChE, as expected from the increased Mw or/and basicity of the complex compared to the free enzyme. Identical electrophoretic patterns were observed for the Fas1- and Fas2-mAChE complexes.

Gel filtration chromatography of the free mAChE and the fasciculin–mAChE complexes led to single, symmetric absorbance peaks (data not shown). No difference in the chromatographic mobility of the fasciculin–mAChE complexes with regard to mAChE could be detected, most probably because of the limited resolution for a mass change from ~65 kDa to ~72 kDa. Screening the chromatographic fractions for their AChE activity, however, required 10^3-fold less dilution of the fasciculin–mAChE fractions than the mAChE fractions, consistent with the level of residual activity (in the 0.1% range) recorded upon complexation of mAChE. Screening for fasciculin activity of the fractions eluting from chromatography of the fasciculin–mAChE complexes performed *before* removal of the unbound fasciculin revealed an included free fasciculin peak eluting at a position consistent with its mass. No such fasciculin peak was detected upon equivalent screening of the fractions eluting from chromatography of the fasciculin–mAChE complexes performed *after* removal of the unbound fasciculin, thereby affirming the total removal of the excess fasciculin.

Crystallization of the fasciculin–mAChE complexes

Crystals spontaneously grew within 2–5 days in hanging drops and within a week in sitting drops. Various crystal morphologies were obtained in two major conditions based on the use of PEG or $(NH_4)_2SO_4$ as precipitating agents. Thick needles with hexagonal sections, extending across the droplet and sometimes hollowed at one end, grew similarly from PEG 600, 2000, 4000, or 10000 solutions buffered with 0.1 M NaAc or ImMal at pHs between 6.5 and 7.5. In contrast, three different crystal forms were obtained from 1.25 M to 1.45 M $(NH_4)_2SO_4$, buffered to pH 6.5 to 7.5 with ammonia. Short and large needles with hexagonal sections, thick triangles, stars, and crowns, all made of stacked thin triangular platelets, as well as symmetric hexagons with slightly variable geometry, were generally found in the same drop, although with varying distribution depending on the precise $(NH_4)_2SO_4$ concentration or pH (Fig. 5A,B). Growth of hexagonal needles as perpendicular axes from the triangles or

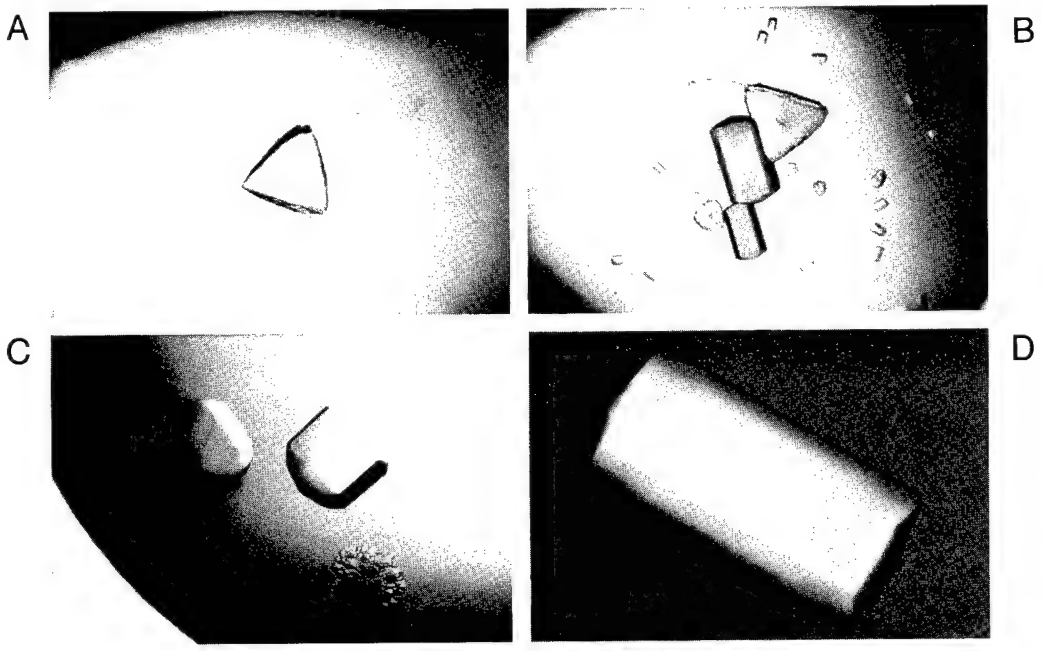

Fig. 5. Photographs of fasciculin-mAChE crystals. **A,B:** Fas1-mAChE and Fas2-mAChE crystals spontaneously grown in a 4-μL hanging drop from 1.35 M $(NH_4)_2SO_4$, pH 6.75. **C:** Half Fas2-mAChE crystals (0.6 mm × 0.5 mm × 0.25 mm) spontaneously grown in a 10-μL sitting drop from 1.35 M $(NH_4)_2SO_4$, pH 7.25. **D:** Fas2-mAChE crystal (1 mm × 0.5 mm × 0.5 mm) grown from 1.35 M $(NH_4)_2SO_4$, pH 7.0, by macroseeding of a 10-μL drop.

as parallel axes from the hexagons was sometimes observed, suggesting that the three forms crystallize in related, if not identical, space groups. Buffering the $(NH_4)_2SO_4$ solutions with 0.1 M NaAc, ImMal, or $NaKPO_4$, as well as adding 0.25% (w/v) β-octylglucoside, did not change the crystallization behavior significantly. Triangular crystals could not be dissociated to monocrystals, even when grown in the presence of 0.25% or 0.5% (w/v) β-octylglucoside or 0.1% (w/v) heptanediol or the detergent screening kit solutions. Growing the hexagonal Fas2-AChE crystals in sitting drops occasionally led to half-crystals adhering tightly to the siliconized cover-slip, presumably arising from epitaxial nucleation (Fig. 5C).

Except for the hexagonal form, which grew almost specifically from the Fas2-mAChE complex (only three hexagonal Fas1-mAChE crystals were obtained in a unique drop after ~10 weeks of equilibration), the same crystal forms were obtained for the two complexes. They all could be enlarged by macroseeding. Larger hexagonal Fas2-mAChE crystals were so obtained (Fig. 5D). Cross-seeding of the Fas1-mAChE complex with seeds from a hexagonal Fas2-mAChE crystal led to both triangular and hexagonal Fas1-mAChE crystals, although the latter grew more slowly than their Fas2 counterparts and displayed a slightly different geometry (not shown). The two fasciculins differ by a single substitution Fas1-Tyr to Fas2-Asn at position 47. No difference, however, could be found in their affinity for mAChE (P. Marchot, unpubl. data). Differences in solubility of the two complexes should therefore account for their different crystallization behavior. The protein content of all crystal forms was checked by SDS-PAGE and native-gel electrophoresis after several successive rinses of the crystals in decreasing concentrations of the precipitating agent, then dissolution in distilled water (Fig. 4A,B). In all cases, the patterns were the same as observed initially upon analysis of the complexes in solution, indicating actual crystallization of the fasciculin–mAChE complexes rather than mAChE alone. Free mAChE, even when concentrated to 18–20 mg mL^{-1}, remained totally soluble in all conditions that yielded fasciculin–mAChE crystals.

Data collection

Preliminary X-ray studies were performed at beam line X12B of the National Synchrotron Light Source (NSLS) equipped with a standard MarResearch imaging plate detector. The highest diffracting patterns (2.8 Å) were obtained for the hexagonal Fas2-mAChE crystals as compared to triangles (3.5 Å) and PEG- or $(NH_4)_2SO_4$-grown needles (5 Å) from both complexes, but the diffraction limit dropped to about 4 Å after the first 15° rotation of data collection. With the aim of protecting the crystals from radiation damage, numerous cryoprotection and flash-cooling assays were performed, but all failed because of immediate cracking of the crystal or/and dramatic loss of resolution. Preliminary data were therefore collected at 4 °C. The crystals belong to space group $P6_122$ or $P6_522$ with cell dimensions $a = b = 75.5$ Å, $c = 556$ Å, giving a V_m value of 3.1 $Å^3$/Da or 60% of solvent, consistent with the presence of a single molecule of complex (72 kDa) in the asymmetric unit (Matthews, 1968). Efforts to collect data at beam line X12B, however, were hampered by the large dimension of the c axis and the resulting overlap of the diffraction spots. Diffraction data were therefore collected at beam line X12C of the NSLS, equipped with a MarResearch imaging plate detector mounted on an Enraf Nonius 4-circle goniometer. A distance of 540 mm (λ = 1.5 Å) and 860 mm (λ = 1.0 Å) with a tilt of 11° and 12°, respectively, was used with 2° oscillation steps. A total of ca. 62,200 observations was obtained at 3.2 Å from four Fas2-mAChE crystals, giving ca. 14,500 unique reflections (85% complete, R_{sym} = 8.9%). Further details on the crystallographic parameters of the Fas2-mAChE complex have been presented elsewhere (Bourne et al., 1995).

The same resolution limit was observed for the spontaneously grown hexagonal Fas1-mAChE crystals, which belong to the same space group with similar cell dimensions $a = b = 75.4$ Å, $c = 550$ Å. In spite of the apparently different conformations of their first disulfide loop, loop I (Le Du et al., 1992, 1995), Fas1 and Fas2 would be expected to adopt the same conformation upon binding to mAChE. The crystals, however, were most probably heterogeneous because double diffraction patterns were obtained. Diffraction patterns from triangles and needles were also consistent with a particularly long c axis.

In summary, the expression of a recombinant cDNA-derived form of AChE, truncated by nine amino acids from native mouse AChE, has yielded a monomeric enzyme appropriate for structural studies. The solubility of mAChE decreased in the presence of fasciculin, and crystals of fasciculin–mAChE complexes suitable for X-ray analysis have been obtained (Bourne et al., 1995). This structure offers a new template for further structure–function studies of mammalian cholinesterases. The structures of the fasciculin–AChE complexes (Bourne et al., 1995; Harel et al., 1995) contribute to at least three lines of investigation. First, they help reveal how fasciculin inhibits AChE. Second, they represent the first structures of three-fingered snake toxins bound to their macromolecular receptors. Third, establishing the contact points between fasciculin and AChE provides a framework for understanding the bases of the high affinities and unusual specificities of the family of three-fingered peptidic toxins.

Materials and methods

Materials

HEK-293 cells were obtained from American Type Culture Collection. Ultraculture cell culture medium was purchased from Biowhittaker. Dialysis tubing (Spectra/Por6) was from Spectrum Medical Industries. Centriprep, Centricon, and Microcon concentration units were from Amicon. Sterile 0.22-μm SpinX units were from Costar. The BCA kit for protein assays was from Pierce. The prepacked Superose-12 HR 10/30 column was from Pharmacia. Gel-filtration molecular weight markers (Mw-GF-70 Kit) were from Sigma. Precast Tris-glycine 4–20% gradient gels were from Novex. Prestained protein Mw standards for SDS-PAGE (14,300–200,000 Mw range) were from Gibco BRL. PNGaseF (S.A., 12,500,000 U mg^{-1}) was from BioLabs. DTNB, ATCh, decamethonium bromide, and PEG 200 were from Sigma. All other PEG (600, 2000, 4000, and 10000), as well as ammonium sulfate of biochemical grade, were from Fluka. The Detergent Screening Kit was from Hampton Research. All buffers used for crystallization were made with deionized water from a Millipore MilliRO/MilliQ system and filtered through 0.22-μm cellulose acetate membrane filtration units (Corning).

Proteins

Fas1 and Fas2 were from the same purification batches as those used previously for crystallization and structure determination (Le Du et al., 1989, 1992, 1995). The concentrations of stock solutions were determined from their UV spectra (ϵ_{276nm} = 6,300 M^{-1} cm^{-1} for Fas1 and 4,900 M^{-1} cm^{-1} for Fas2). mAChE was a soluble molecular form derived from the cDNA encoding the glycophospholipid-linked form of mouse AChE (Li et al., 1993). The cDNA was truncated after Pro 548 by insertion of a stop codon (TGA) in place of the Cys 549 codon (Fig. 1). Sequence of the mutant cDNA was confirmed by direct sequencing of the insert. The cDNA was inserted behind a CMV promoter. Transfection into HEK cells was with $Ca_3(PO_4)_2$ co-precipitation (Vellom et al., 1993). Selection of clones depended on incorporation of the neomycin-resistance gene and selection of cells with G418 sulfate (800 μg mL^{-1}) (Radić et al., 1993; Vellom et al., 1993). HEK-293 cells in which the mutated mAChE cDNA was stably integrated were grown to confluency in Dulbecco's modified Eagle's medium supplemented with 10% fetal bovine serum, then switched into serum-free media (Ultraculture) for collection of secreted mAChE.

Assay of AChE activity

AChE activity measurements were conducted spectrophotometrically (Ellman et al., 1961) with 0.5 mM acetylthiocholine iodide and 0.33 mM DTNB in 100 mM NaH_2PO_4/Na_2HPO_4, pH 7.0, BSA 0.1 mg mL^{-1}, to a final volume of 1.5 mL (room temperature). Initial kinetics of duplicate samples were recorded at $\lambda = 412$ nm during 5 min with a Response™ spectrophotometer (Gilford). A specific activity of 30,000 ΔA min^{-1} mg^{-1} was used. Relative AChE activities were screened at room temperature by microtitration on a Vmax kinetic microplate reader (Molecular Devices Corp.) with $\lambda = 405$ nm. Gel-filtration fractions were diluted 20–50,000-fold for screening of free mAChE and 30-fold for screening of the residual activity of the fasciculin–AChE complexes. Free fasciculin in the chromatographic fractions was screened by recording the residual activity of an extra AChE sample (~8 pM) after incubation for 1 h at 37 °C with a 30–100-fold dilution of the fractions (Marchot et al., 1993).

Sedimentation velocity analysis

mAChE-containing culture medium was sedimented into linear 3–20% sucrose gradients containing 0.1 M NaCl, 0.04 M $MgCl_2$, 0.01 M Tris-HCl, pH 8.0, and 0.1% (v/v) Triton X-100, for 20 h at 200,000 × *g* (4 °C). The layered sample (100 μL) was supplemented with carbonic anhydrase (20 μg, 3.3 S), alkaline phosphatase (0.2 μg, 6.1 S), catalase (2 μg, 11.4 S), and β-galactosidase (0.4 μg, 16 S) as sedimentation standards (Camp et al., 1995). The sedimented 12-mL tubes were fractionated in 96-tube racks with the microtitration plate format allowing further screening of the respective enzyme activities.

Purification and characterization of mAChE

Soluble mAChE was purified by affinity chromatography using *m*-trimethylaminophenyl amine coupled to Sepharose through a successively coupled succinic acid and diaminodipropylamine arm (Taylor & Jacobs, 1974). The conjugated resin was stored as a 50% suspension in 100 mM NaCl, 40 mM $MgCl_2$, 10 mM $NaHCO_3$, pH 8.0, containing NaN_3 0.02% (w/v). Harvested Ultraculture medium containing the expressed mAChE was centrifuged (2,000 g, 15 min, 4 °C) to remove cell debris, and assayed for AChE activity. $MgCl_2$ (1 M) was added to a final concentration of 40 mM, then the resin suspension (1 mL for each 2 mg AChE), and the mixture was allowed to stir in a spinner flask overnight at 4 °C in the presence of NaN_3 0.02% (w/v). The mixture was assayed for residual AChE activity and, if required, supplemented with the exact amount of resin necessary to achieve total inhibition of the enzyme. It was poured into a Bio-Rad econo column, allowed to pack by sedimentation, then washed with the equilibrating buffer (50–100-fold the bed volume). The bound AChE was eluted with 100 mM decamethonium bromide (30 × K_i, Radić et al. 1993) in the same buffer, at a low flow rate (1–1.5 mL h^{-1}). Elution fractions were assayed for AChE activity with a 10^6-fold final dilution, which reduced the final decamethonium concentration to well below its K_i for the mouse enzyme. The purified enzyme was dialyzed *extensively* against the crystallization buffer with SpectraPor6 dialysis tubing, then rinsed again and concentrated to 10–20 mg mL^{-1} in a Centriprep3 or Centricon3 unit. Purified mAChE was quantified independently from catalytic activity, BCA protein assay, absorbance at $\lambda = 280$ nm, and titration by Fas2 (Marchot et al., 1993), all of which yielded a close correlation. It was stored on ice.

N-linked carbohydrate removal

Purified mAChE (20 μg in 100 μL) was boiled for 10 min in denaturing buffer: 20 mM Tris-HCl, pH 8.0, 5 mM EDTA, 5 mM β-mercaptoethanol, 0.5% (w/v) SDS, cooled, added with 1% (v/v) Nonidet P-40, then incubated in the presence of PNGaseF (2,000 U) for 5 h at 37 °C. A further aliquot of 2,000 U was added after 2 h of incubation.

Complexation of mAChE with fasciculins and crystallization of the complexes

The respective complexes were formed in 50 mM NaCl, 1 mM Mes, pH 6.5, NaN_3 0.01% (w/v) (crystallization buffer) with a fasciculin-to-AChE molar ratio of 1.2:1 to preclude stoichiometric deficiency assuming a maximal 10% error in the quantification of protein and peptide. After equilibration overnight on ice, the complexes were assayed for residual AChE activity and free fasciculin, respectively. The enzyme was considered to be totally complexed to fasciculin when no decrease in its residual activity (usually 0.1–0.5% of the initial activity of the sample) was observed upon further addition of fasciculin and extended incubation, and when free fasciculin could be detected in the mixture through inhibition of a second AChE sample. Excess fasciculin was then dialyzed from the complexes with the crystallization buffer in a Centricon10 or Microcon10 concentrator, until no free fasciculin could be detected in both the filtrate and the sample. Total removal was confirmed by gel-filtration chromatography. The complexes were concentrated to 12–15 mg mL^{-1}, then filtered through a SpinX unit. They were stored on ice and were used within a week with no change in their crystallization behavior. Both Fas1- and Fas2-AChE complexes were crystal-

lized at 20 °C by the vapor diffusion method using hanging drops (4 μL) or sitting drops (10 μL) with a protein-to-well solution ratio of 1:1. Macroseeding of 10 μL sitting drops previously equilibrated overnight was performed according to Stura and Wilson (1992).

Electrophoresis

SDS-PAGE under reducing conditions and native gel electrophoreses of mAChE and Fas-AChE complexes were performed according to the discontinuous system of Laemmli (1970) with a vertical gel electrophoresis apparatus (JM Specialty Parts) or a Mighty Small Slab gel electrophoresis unit (Hoefer Scientific Instruments). Precast Tris-glycine 4–20% gradient gels, or 15% or 10% resolving/5% stacking gels, were used for SDS-PAGE. A 7.5% resolving/5% stacking gel made with no SDS was used for native gel electrophoresis. Samples loaded were typically 5 μL and contained 10% (v/v) glycerol. Silver nitrate staining was performed according to Morrisey (1981).

Gel-filtration chromatography

Analytical gel-filtration chromatography of mAChE and fasciculin–AChE complexes was conducted at 4 °C on a Superose-12 column using the FPLC system from Pharmacia. The column was equilibrated in, then eluted with, the crystallization buffer (flow rate, 0.5 mL min^{-1}). The loaded samples were 5 μL of the concentrated protein solutions used for complexation (mAChE) or crystallization (complexes), sandwiched into 25 μL of the crystallization buffer. Absorbance of column effluents was monitored at $\lambda = 280$ nm. Fractions (0.5 mL) were collected and assayed for AChE activity. The column was calibrated with a molecular weight standard kit.

Acknowledgments

We thank Dr. P.E. Bougis, in whose group at the Centre National de la Recherche Scientifique the fasciculins have been purified; Dr. John A. Tainer at The Scripps Research Institute and Dr. K.I. Varughese at UCSD, for the use of their crystallization facilities; and Dr. Robert M. Sweet, for access to the National Synchrotron Light Source beam line X12C. Expert assistance from Malcom Capel at the NSLS beam line X12B is much appreciated. This work was supported by USPHS GM18360 and DAMD 17C grants to P.T. and the Biology Department at the Brookhaven National Laboratory to J.L.S.

References

Adem A, Asblom A, Johansson G, Mbugua PM, Karlsson E. 1988. Toxins from the venom of the green mamba *Dendroaspis angusticeps* that inhibit the binding of quinuclidinylbenzylate to muscarinic acetylcholine receptors. *Biochim Biophys Acta 968*:340–345.

Bougis P, Rochat H, Piéroni G, Verger R. 1981. Penetration of phospholipid monolayers by cardiotoxins. *Biochemistry 20*:4915–4920.

Bourne Y, Taylor P, Marchot P. 1995. Acetylcholinesterase inhibition by fasciculin: Crystal structure of the complex. *Cell 83*:503–512.

Camp S, Bon S, Li Y, Getman DK, Engel AG, Massoulié J, Taylor P. 1995. Patients with congenital myasthenia associated with end-plate acetylcholinesterase deficiency show normal sequence, mRNA splicing, and assembly of catalytic subunits. *J Clin Invest 95*:333–340.

Cerveñansky C, Dajas F, Harvey AL, Karlsson E. 1991. Fasciculins, anticholinesterase toxins from mamba venoms: Biochemistry and pharmacology. In: Harvey AL, ed. *Snake toxins*. New York: Pergamon Press Inc. pp 303–321.

Changeux JP, Kasai M, Lee CY. 1970. The use of a snake venom toxin to characterize the cholinergic receptor protein. *Proc Natl Acad Sci USA 67*:1241–1247.

Dufton MJ, Hider RC. 1991. The structure and pharmacology of elapid cytotoxins. In: Harvey AL, ed. *Snake toxins*. New York: Pergamon Press Inc. pp 259–302.

Duval NE, Krejci E, Grassi J, Coussen F, Massoulié J, Bon S. 1992. Molecular architecture of acetylcholinesterase collagen-tailed forms; construction of a glycolipid-tailed tetramer. *EMBO J 11*:3255–3261.

Eastman J, Wilson EJ, Cerveñansky C, Rosenberry TL. 1995. Fasciculin 2 binds to the peripheral site on acetylcholinesterase and inhibits substrate hydrolysis by slowing a step involving proton transfer during enzyme acylation. *J Biol Chem 270*:19694–19701.

Ellman GL, Courtney KD, Andres V Jr, Featherstone RM. 1961. A new rapid combination method for acetylcholinesterase activity. *Biochem Pharmacol 7*:88–95.

Endo T, Tamiya N. 1991. Structure–function relationship of postsynaptic neurotoxins from snake venoms. In: Harvey AL, ed. *Snake toxins*. New York: Pergamon Press Inc. pp 165–222.

Harel M, Kleywegt GJ, Ravelli RBG, Silman I, Sussman JL. 1995. Crystal structure of an acetylcholinesterase–fasciculin complex: Interaction of a three-fingered toxin from snake venom with its target. *Structure 3*: 1355–1366.

Laemmli UK. 1970. Cleavage of structural proteins during the assembly of the head of bacteriophage T4. *Nature (Lond) 227*:680–685.

Le Du MH, Housset D, Marchot P, Bougis PE, Navaza J, Fontecilla-Camps JC. 1996. Crystal structure of fasciculin 2 from mamba snake venom: Evidence for unusual loop flexibility. *Acta Crystallogr D52*:8.

Le Du MH, Marchot P, Bougis PE, Fontecilla-Camps JC. 1989. Crystals of fasciculin 2 from green mamba snake venom: Preparation and preliminary X-ray analysis. *J Biol Chem 264*:21401–21402.

Le Du MH, Marchot P, Bougis PE, Fontecilla-Camps JC. 1992. 1.9 Å resolution structure of fasciculin 1, an anti-cholinesterase toxin from green mamba snake venom. *J Biol Chem 267*:22122–22130.

Li Y, Camp S, Rachinsky TL, Getman D, Taylor P. 1991. Gene structure of mammalian acetylcholinesterase. *J Biol Chem 266*:23083–23090.

Li Y, Camp S, Taylor P. 1993. Tissue-specific expression and alternative mRNA processing of the mammalian acetylcholinesterase gene. *J Biol Chem 268*:5790–5797.

Marchot P, Khélif A, Ji YH, Mansuelle P, Bougis PE. 1993. Binding of ^{125}I-fasciculin to rat brain acetylcholinesterase. The complex still binds diisopropyl fluorophosphate. *J Biol Chem 268*:12458–12467.

Massoulié J, Pezzementi L, Bon S, Krejci E, Vallette FM. 1993. Molecular and cellular biology of the cholinesterases. *Prog Neurobiol 41*:31–91.

Matthews BW. 1968. Solvent content of protein crystals. *J Mol Biol 33*: 491–497.

Morrisey J. 1981. Silver stain for proteins in polyacrylamide gels; a modified procedure with enhanced uniform sensitivity. *Anal Biochem 117*:307–310.

Rachinsky TL, Camp S, Li Y, Ekström J, Newton M, Taylor P. 1990. Molecular cloning of mouse acetylcholinesterase: Tissue distribution of alternatively spliced mRNA species. *Neuron 5*:317–327.

Radić Z, Duran R, Vellom DC, Li Y, Cerveñansky C, Taylor P. 1994. Site of fasciculin interaction with acetylcholinesterase. *J Biol Chem 269*: 11233–11239.

Radić Z, Pickering NA, Vellom DC, Camp S, Taylor P. 1993. Three distinct domains in the cholinesterase molecule confer selectivity for acetyl- and butyrylcholinesterase inhibitors. *Biochemistry 32*:12074–12084.

Radić Z, Quinn DM, Vellom DC, Camp S, Taylor P. 1995. Allosteric control of acetylcholinesterase catalysis by fasciculin. *J Biol Chem 270*:20391–20399.

Segalas I, Roumestand C, Zinn-Justin S, Gilquin B, Ménez R, Ménez A, Toma F. 1995. Solution structure of a green mamba toxin that activates muscarinic acetylcholine receptors, as studied by nuclear magnetic resonance and molecular modeling. *Biochemistry 34*:1248–1260.

Stura E, Wilson IA. 1992. Seeding techniques. In: Ducruix A, Giege R, eds. *Crystallization of nucleic acids and proteins, a practical approach*. Oxford: IRL Press, Oxford University Press. pp 99–126.

Sussman JL, Harel M, Frolow F, Oefner C, Goldman A, Toker L, Silman I. 1991. Atomic structure of acetylcholinesterase from *Torpedo californica*: A prototypic acetylcholine-binding protein. *Science 253*:872–879.

Sussman JL, Harel M, Frolow F, Varon L, Toker L, Futerman AH, Silman I. 1988. Purification and crystallization of a dimeric form of acetylcholinesterase from *Torpedo californica* subsequent to solubilization with phosphatidylinositol-specific phospholipase C. *J Mol Biol 203*:821–823.

Taylor P, Jacobs NM. 1974. Interaction between bisquaternary ammonium ligands and acetylcholinesterase: Complex formation studied by fluorescence quenching. *Mol Pharmacol 10*:93–107.

Taylor P, Radić Z. 1994. The cholinesterases: From genes to proteins. *Annu Rev Pharmacol Toxicol 34*:281–320.

van den Born HKL, Radić Z, Marchot P, Taylor P, Tsigelny I. 1995. Theoretical analysis of the structure of the peptide fasciculin and its docking to acetylcholinesterase. *Protein Sci 4*:703–715.

Velan B, Kronman C, Leitner M, Grosfeld H, Flashner Y, Marcus D, Lazar A, Kerem A, Bar-Nun S, Cohen S, Shafferman A. 1992. Molecular organization of recombinant human acetylcholinesterase. In: Shafferman A, Velan B, eds. *Multidisciplinary approches to cholinesterase functions*. New York: Plenum Press. pp 39–47.

Vellom DC, Radić Z, Li Y, Pickering NA, Camp S, Taylor P. 1993. Amino acid residues controlling acetylcholinesterase and butyrylcholinesterase specificity. *Biochemistry 32*:12–17.

Aspartate 74 as a Primary Determinant in Acetylcholinesterase Governing Specificity to Cationic Organophosphonates

Natilie A. Hosea, Zoran Radić, Igor Tsigelny, Harvey Alan Berman, Daniel M. Quinn, and Palmer Taylor

Department of Pharmacology,
University of California at San Diego, La Jolla, California 92093-0636,
Department of Biochemical Pharmacology,
State University of New York at Buffalo, Buffalo, New York 14260,
and Department of Chemistry, The University of Iowa,
Iowa City, Iowa 52242

Biochemistry®

Reprinted from
Volume 35, Number 33, Pages 10995–11004

Aspartate 74 as a Primary Determinant in Acetylcholinesterase Governing Specificity to Cationic Organophosphonates†

Natilie A. Hosea,‡ Zoran Radić,‡ Igor Tsigelny,‡ Harvey Alan Berman,§ Daniel M. Quinn,|| and Palmer Taylor*,‡

Department of Pharmacology, University of California at San Diego, La Jolla, California 92093-0636, Department of Biochemical Pharmacology, State University of New York at Buffalo, Buffalo, New York 14260, and Department of Chemistry, The University of Iowa, Iowa City, Iowa 52242

Received May 10, 1996; Revised Manuscript Received June 24, 1996⊗

ABSTRACT: Through site-specific mutagenesis, we examined the determinants on acetylcholinesterase which govern the specificity and reactivity of three classes of substrates: enantiomeric alkyl phosphonates, trifluoromethyl acetophenones, and carboxyl esters. By employing cationic and uncharged pairs of enantiomeric alkyl methylphosphonyl thioates of known absolute stereochemistry, we find that an aspartate residue near the gorge entrance (D74) is responsible for the enhanced reactivity of the cationic organophosphonates. Removal of the charge with the mutation D74N causes a near equal reduction in the reaction rate constants for the R_p and S_p enantiomers and exerts a greater influence on the cationic organophosphonates than on the charged trimethylammonio trifluoromethyl acetophenone and acetylthiocholine. This pattern of reactivity suggests that the orientation of the leaving group for both enantiomers is directed toward the gorge exit and in apposition to Asp 74. Replacement of tryptophan 86 with alanine in the choline subsite also diminishes the reaction rates for cationic organophosphonates, although to a lesser extent than with the D74N mutation, while not affecting the reactions with the uncharged compounds. Hence, reaction with cationic OPs depends to a lesser degree on Trp 86 than on Asp 74. Docking of S_p and R_p cycloheptyl methylphosphonyl thiocholines and thioethylates in AChE as models of the reversible complex and transition state using molecular dynamics affords structural insight into the spatial arrangement of the substituents surrounding phosphorus prior to and during reaction. The leaving group of the R_p and S_p enantiomers, regardless of charge, is directed to the gorge exit and toward Asp 74, an orientation unique to tetrahedral ligands.

Acetylcholinesterase (AChE)[1] catalyzes the hydrolysis of the neurotransmitter acetylcholine (ACh) at a rate approaching a diffusion-controlled process (Rosenberry, 1975; Fersht, 1985; Quinn, 1987), thereby terminating neurotransmission. The X-ray crystal structure of AChE from *Torpedo californica* (TAChE; Sussman et al., 1991) and mouse (MAChE; Bourne et al., 1995) reveals that ACh must travel down a gorge of 20 Å in depth to reach the catalytic serine, the proximal nucleophile in the ester hydrolysis mechanism. The great speed at which the enzyme catalyzes the hydrolysis is thought to arise, in part, from a dipole aligned with the gorge and directed to the active site that electrostatically drives the positively charged substrate to the catalytic center (Tan et al., 1993; Ripoll et al., 1993). Trifluoromethyl acetophenone (TFK) transition state analogs of ACh, which conjugate with the active center serine of AChE at diffusion-controlled rates without requiring the departure of a leaving group (Nair et al., 1993, 1994), also demonstrate that the electric field of AChE accelerates quaternary ammonium binding to the active site (Quinn et al., 1995); in fact, the association rate constants for cationic and uncharged substituted TFK compounds differ by 20−70-fold (Nair et al., 1994). This electrostatic enhancement of catalysis agrees with kinetics of aromatic cation binding (Nolte et al., 1980) and calculations detailing the electrostatic attractions between AChE and the ligands (Tan et al., 1993).

Organophosphonates (OPs) also react rapidly with cholinesterase by phosphonylating the active site serine (Oosterbann & Cohen, 1964; Aldridge & Reiner, 1972). However, the resulting phosphonyl enzymes react slowly with water; thus, these compounds become irreversible inhibitors, rendering AChE inactive upon reaction (Froede & Wilson, 1971). Their reaction rates with AChE depend on the size, nature, and stereochemical arrangement of the substituents about the phosphate where the rates differ between cationic and uncharged alkyl phosphonates by 2−3 orders of magnitude with a preference for the charged OP. Moreover, an enantiomeric preference of greater than 200-fold has been found (Berman & Leonard, 1989). The acyl pocket region, comprised of two phenylalanines at 295 and 297, dictates the preference for the S_p isomer by sterically hindering the approach of the R_p isomer and its positioning for optimal phosphonyl transfer. However, the acyl pocket region has essentially no role in dictating AChE's selectivity for the cationic OPs (Hosea et al., 1995).

The tetrahedral geometry of OPs adds an additional dimension to analysis of specificity compared to the trigonal, planar carboxyl ester substrates and the TFK transition state analogs. Thus, the tetrahedral phosphonates possess a

† Supported by USPHS Grant GM 18360 and DAMD Grant 17-95I 5027 to P.T. and by the U.S. Army Research Office (Research Triangle Park, NC) and NIH ES-03085 to H.A.B.

‡ University of California at San Diego.

§ State University of New York at Buffalo.

|| The University of Iowa.

⊗ Abstract published in *Advance ACS Abstracts,* August 1, 1996.

[1] Abbreviations: AChE, acetylcholinesterase; TAChE, *Torpedo californica* AChE; MAChE, mouse AChE; TFK, trifluoromethyl acetophenone; TFK$^+$, *m*-(*N,N,N*-trimethylammonio) TFK; TFK^o, *m*-(*tert*-butyl) TFK; OP, organophosphonate; ACh, acetylcholine; ATC, acetylthiocholine; CHMP, cycloheptyl methylphosphonyl; iPrMP, isopropyl methylphosphonyl; DMBMP, 3,3-dimethylbutyl methylphosphonyl; k_{on}, bimolecular rate constant of association for TFK; k_i, bimolecular rate constant for OP acylation of AChE.

S0006-2960(96)01122-1 CCC: $12.00

different spatial arrangement for acylation, and the contribution of residues to their stabilization will differ from those stabilizing ACh and TFKs. Nevertheless, parallels between the three classes of ligands should exist since they all react with a common serine in an equivalent, asymmetric environment (Sussman et al., 1991, 1995).

Three regions of AChE—the acyl pocket, the choline subsite, and the peripheral site—are highly aromatic in amino acid content. Whereas aromatic side chains in the acyl pocket sterically exclude ligands with a particular size and dimension, the choline subsite contributes to stabilization of a positively charged quaternary ammonium moiety as found in ACh, TFK, and edrophonium conferring selectivity to cationic ligands (Sussman et al., 1991, 1995; Harel et al., 1996). Additionally, interaction of an aromatic residue with a cationic substituent, coined a "cation−π" interaction, is suggested to arise through the quadrupole moment of the aromatic ring and to be electrostatic in nature (Dougherty & Stauffer, 1990; Mecozzi et al., 1996). This structural model has been supported kinetically by analysis of AChE mutations of Trp 86, where replacement by an Ala significantly diminishes catalytic efficiency with cationic ligands but only moderately alters reaction rates with uncharged ligands (Ordentlich et al., 1993a, 1995; Radić et al., 1995).

AChE also contains three nonvariant anionic residues (Cygler et al., 1993; Gentry & Doctor, 1995) in and near the active center: Asp 74 at the rim of the gorge and Glu 202 and 450 at the base of the gorge. The X-ray crystal structure of TAChE in complexes with edrophonium and tacrine reveals that Glu 202 and 450 hydrogen bond with water molecules in the active site (Harel et al., 1993). This network of hydrogen bonding is thought to contribute to efficient acylation of AChE (Radić et al., 1992) and dealkylation during "aging" of OP−AChE conjugates (Michel et al., 1967; Saxena et al., 1993; Ordentlich et al., 1993b; Qian & Kovach, 1993).

Herein, we report on a mutational analysis of AChE to elucidate the determinants responsible for its large selectivity for cationic ligands and assess the contribution by aromatic residues of the choline subsite and peripheral site regions. Information gained from the mutational analysis of the acyl pocket (Hosea et al., 1995) provided evidence for steric determinants dictating phosphonate reactivity and suggested an orientation of the leaving group of the isomers directed out of the gorge. Our findings reported here substantiate that orientation for both the R_p and S_p enantiomers and reveal Asp 74 as a primary determinant in dictating specificity to cationic OPs. In conjunction with kinetic data, computational docking of charged and uncharged enantiomeric alkyl methylphosphonates in a reversible complex and in a trigonal bipyramidal model of the transition state enables one to refine the spatial arrangements of the substituents about the phosphonate prior to and during the phosphonylation reaction.

MATERIALS AND METHODS

Materials. Acetylthiocholine (ATC) iodide and 5,5′-dithiobis(2-nitrobenzoic acid) (DTNB) were products of Sigma Chemical Co. (St. Louis, MO). (S_p)- and (R_p)-alkyl methylphosphonyl thioates were synthesized and isolated as resolved S_p and R_p enantiomers as described previously (Berman & Leonard, 1989). 7-[[(Methylethoxy)phosphinyl]-oxyl]-1-methylquinolinium iodide (MEPQ) was a gift of Drs. Y. Ashani and B. P. Doctor (Walter Reed Army Research Center, Washington, DC; Levy & Ashani, 1986). *m*-(*N*,*N*,*N*-Trimethylammonio) trifluoromethyl acetophenone and *m*-*tert*-butyl trifluoromethyl acetophenone (TFK^+ and TFK^o, respectively) were synthesized as described (Nair et al., 1993,1994).

Production of Enzymes. Wild-type and mutant mouse AChE cDNA constructs were generated as described in Radić et al. (1993). The pRCCMV (Invitrogen) expression plasmids were purified by standard procedures involving polyethylene glycol precipitation and centrifugation in CsCl gradients.

Human embryonic kidney (HEK-293) cells obtained from American Type Culture Collection (Atlanta, GA) were plated at 2×10^6 cells per 10 cm plate in 10% fetal bovine serum-supplemented Dulbecco's modified Eagle's (DME) medium 24 h prior to transfection. Cells were transfected with 15 μg of plasmid/plate of mutant or wild-type cholinesterase-pRCCMV using a standard HEPES-based calcium phosphate precipitation protocol (Ausubel et al., 1994). After 16−24 h, the transfected plates were washed with phosphate-buffered saline and maintained in serum free DME medium for 48−72 h. The medium, containing the expressed cholinesterase, was collected, and the transfected cells were replenished with serum free DME medium. This process was continued for three or four harvests of enzyme. Batches of media were then concentrated to approximately 1−2% of original volume and stored at 4 °C using Centriprep 30 Centricons (Amicon, Beverly, MA).

To produce larger quantities of enzyme for detailed kinetic studies, stable transfectants were generated by selecting transfected HEK cells with G418 for 2−3 weeks or until cell death subsided. Pools of selected cells were frozen in 10% serum and 5% DMSO-containing DME medium for future use.

Enzyme Activity Measurements and Active Site Quantitation. Wild-type and mutant AChE activities were measured in 0.1 M sodium phosphate buffer (pH 7.0) and 0.3 mM DTNB at 22 °C according to Ellman et al. (1961) using ATC as the substrate. Maximum concentrations of ATC did not exceed 100 mM due to appreciable spontaneous substrate hydrolysis. Active sites were quantitated according to Levy and Ashani (1986) and Radić et al. (1992) by titrating the enzyme samples with known concentrations of MEPQ.

Inhibition. Enzyme samples (tens of picomoles) were incubated for designated times with the (S_p)- and (R_p)-alkyl phosphonylthioates in the above assay mixture in the absence of substrate; typically, four inhibitor concentrations were used. The inhibition reaction was stopped by addition of 5−10 mM ATC (a concentration 30−50-fold above the K_m), and residual activity was measured. From the slopes of semilogarithmic plots of activity versus time, pseudo-first-order rate constants (k_{obs}) were plotted against inhibitor concentration to obtain the bimolecular rate constants (k_i) (Aldridge & Reiner, 1972; Radić et al., 1992). When semilogarithmic plots of inhibition versus time were nonlinear, the initial rates were taken as the k_{obs}.

Inhibition by TFK^+ and TFK^o was measured as above which parallels the stopped-time assay reported in Nair et al. (1994). The resulting activities analyzed as a function of time were then fit using nonlinear regression according to the following equation:

$$\%V = (\%V_0 - \%V_{ss})e^{-k_{obs}(t)} + \%V_{ss}$$

where $\%V$, $\%V_0$, and $\%V_{ss}$ are the AChE activities expressed as a percentage of control activity at times t, 0, and infinity, respectively, and k_{obs} is the observed first-order rate constant. The association rate constant, k_{on}, was determined by the following equation:

$$k_{obs} = k_{on}[\text{inhibitor}] + k_{off}$$

The dissociation rate constant, k_{off}, under the experimental conditions was negligible except for the E202Q mutation.

Computer Modeling. Two sequential stages in reaction of (S_p)- and (R_p)-cycloheptyl methylphosphonyl thiocholines and (S_p)- and (R_p)-cycloheptyl methylphosphonyl thioethylates with the enzyme were analyzed: the tetrahedral noncovalent reversible complex preceding phosphonylation and the pentavalent transition state during phosphonylation. Models of the inhibitor structures were built and energy minimized using the Insight II package (Biosym, San Diego, CA) with their partial charges calculated using the MOPAC module of Insight II. The best conformation for each inhibitor in the model of the reversible complex with *T. californica* AChE was obtained after simulated annealing calculations starting from a series of inhibitor orientations in the AChE active center. A mild distance restraint resulted in a harmonic force with a maximum of about 40 kcal/Å applied between the γ-oxygen of Ser 203 of AChE (200 of TAChE)[2] and the phosphorus atom of the inhibitors in order to reduce the number of resulting conformations to the productive ones that lead to phosphonylation. Transition state models were then built by covalent bonding of the inhibitor phosphorus atom to γ-oxygen of Ser 203. The geometry of the substituents attached to the phosphorus atom was adjusted to an ideal trigonal bipyramidal structure (Westheimer, 1968): 180° from apical to apical, 120° from equatorial to equatorial, and 90° from apical to equatorial positions. Simulated annealing calculations were then started (Ashani et al., 1995) to obtain a family of energetically favorable conformations reflecting the pentavalent transition state. In all calculations, residues of the *T. californica* AChE crystal structure were kept fixed except for Ser 203; only this side chain and the conjugated inhibitor were allowed free rotation.

RESULTS

Electrostatic Influences on Reaction Rates with Cationic and Uncharged Organophosphonates. The acyl pocket region of the active site of cholinesterases is the primary determinant in the enantiomeric specificity of chiral phosphonates; however, this region is not involved in distinguishing between the cationic and uncharged thioate leaving groups (Hosea et al., 1995). To explore the electrostatic influences of AChE on reaction rates with charged and uncharged phosphonates, rates of inhibition by enantiomeric alkyl methylphosphonates containing either a thiocholine or thioalkyl leaving group (Figure 1) were examined with MAChE which was mutated at three anionic residues near or within the active center gorge—Asp 74, Glu 202, and Glu

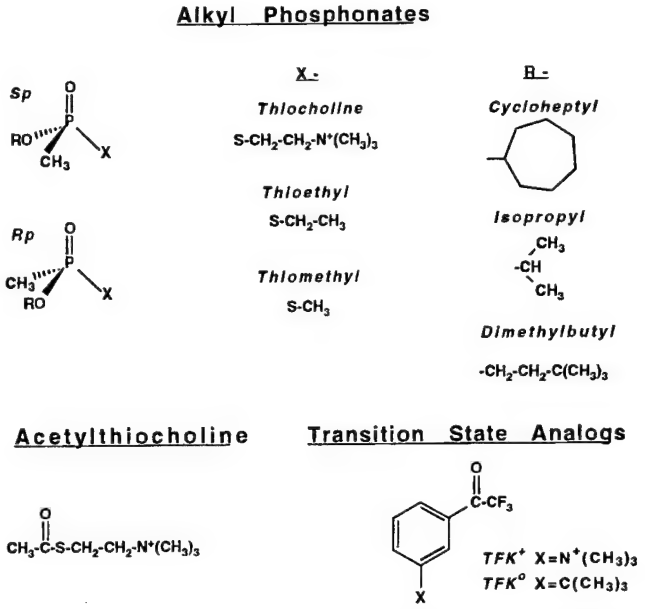

FIGURE 1: Structures of ligands used in the analysis. The leaving group is denoted by X, and the alkyl substituent is denoted by R for the alkyl phosphonates.

450—to the corresponding neutral isosteric residues, Asn and Gln, respectively. The resulting bimolecular rate constants (k_i values) for the inhibition by enantiomers of cycloheptyl methylphosphonyl, isopropyl methylphosphonyl, and 3,3-dimethylbutyl methylphosphonyl (CHMP, iPrMP, and DMBMP, respectively) thiocholines and of CHMP *S*-methyl- or *S*-ethylthioates (thiomethylate and thioethylate, respectively) are shown in Table 1a,b.

The differences in reaction rate constants between the cationic and uncharged CHMP compounds span nearly 3 orders of magnitude for AChE. These congeners differ only in the leaving group substituent which imparts the difference in charge (Figure 1). Mutations in which the anionic residues at the base of the gorge are replaced by isosteric neutral residues, E202Q and E450Q, reduce the reaction rate constants for the charged and uncharged CHMP congeners to approximately the same degree. Thus, Glu 202 and Glu 450 do not account for the large preference of AChE wild-type for the thiocholine-substituted phosphonates. On the other hand, the Asp 74 mutation to Asn reduces the rate constants for cationic CHMP-thiocholines at least 100-fold, whereas the mutation appears to slightly increase rate constants for uncharged S_p and R_p CHMP-thioates. The resulting bimolecular rate constants for the charged and uncharged compounds are of similar magnitude in the Asn 74 enzyme. Thus, the presence of Asp 74 at the rim of the gorge solely accounts for the 2−3 orders of magnitude enhancement of reaction with the thiocholine-substituted CHMP isomers. The effect of charge neutralization with the D74N mutation on the rates of reaction with the thiocholine compounds maintains the enantiomeric preference, suggesting that the quaternary ammonium moieties of the S_p and R_p isomers reside at similar distances from D74.

Contribution by Aromatic Residues to Alkyl Phosphonate Specificity. AChE mutants encompassing the choline binding site (Trp 86 mutated to Ala; Tyr 337 mutated to either Ala or Phe) and the peripheral site (Trp 286 mutated to either Ala or Arg) were analyzed with the cationic and uncharged alkyl phosphonates (Figure 1) to determine the contribution of the aromatic residues on the specificity of these com-

[2] The numbers in parentheses denote residue positions in the *T. californica* AChE sequence from which the molecular models were built.

Table 1: Bimolecular Rate Constants (10^3 M^{-1} min^{-1})[a] Determined for the Inhibition of Recombinant DNA-Derived Mouse Cholinesterases with Mutations of Anionic Residues by (a) Alkyl Methylphosphonyl Thiocholine Enantiomers and (b) Cycloheptyl Methylphosphonyl Thioate Enantiomers

(a) alkyl substitution	cycloheptyl			isopropyl			3,3-dimethylbutyl		
enzyme	S_p	R_p	S_p/R_p	S_p	R_p	S_p/R_p	S_p	R_p	S_p/R_p
AChE	190000 ± 20000	820 ± 50	230	16000 ± 1000	150 ± 10	110	400000 ± 40000	11000 ± 1000	36
D74N	1400 ± 200	8.0 ± 0.2	180	110 ± 10	1.7 ± 0.3	65	11000 ± 2000	230 ± 20	48
E202Q	21000 ± 2000	130 ± 10	160	490 ± 20	38 ± 2	13	120000 ± 10000	2700 ± 100	44
E450Q	1400 ± 300	23 ± 3	61	180 ± 20	5.9 ± 0.3	31	12000 ± 3000	490 ± 60	24

(b) thioate substitution	SCH_3			SCH_2CH_3		
enzyme	S_p	R_p	S_p/R_p	S_p	R_p	S_p/R_p
AChE	310 ± 20	1.7 ± 0.3	180	74 ± 5	0.16 ± 0.02	460
D74N	530 ± 50	2.3 ± 0.2	230	190 ± 30	0.41 ± 0.04	460
E202Q	14 ± 1	0.060 ± 0.004	230	2.3 ± 0.3	0.014 ± 0.001	160
E450Q	9.0 ± 0.4	0.050 ± 0.002	180	14 ± 2	0.018 ± 0.004	780

[a] Data shown as means ± standard error of the mean typically from three measurements.

Table 2: Bimolecular Rate Constants (10^3 M^{-1} min^{-1})[a] Determined for the Inhibition of Recombinant DNA-Derived Mouse Cholinesterases with Mutations of Aromatic Residues by (a) Alkyl Methylphosphonyl Thiocholine Enantiomers and (b) Cycloheptyl Methylphosphonyl Thioate Enantiomers

(a) alkyl substitution	cycloheptyl			isopropyl			3,3-dimethylbutyl		
enzyme	S_p	R_p	S_p/R_p	S_p	R_p	S_p/R_p	S_p	R_p	S_p/R_p
AChE	190000 ± 20000	820 ± 50	230	16000 ± 1000	150 ± 10	110	400000 ± 40000	11000 ± 1000	36
W86A	4800 ± 1100	25 ± 5	190	43 ± 6	23 ± 7	1.9	37000 ± 14000	1700 ± 200	22
Y337A	120000 ± 10000	840 ± 40	140	24000 ± 3000	340 ± 40	71	750000 ± 20000	19000 ± 1000	39
Y337F	720000 ± 30000	3700 ± 100	190	140000 ± 10000	1000 ± 100	140	1100000 ± 100000	30000 ± 1000	37
W286A	230000 ± 20000	2000 ± 100	120	20000 ± 1000	230 ± 10	87	470000 ± 30000	13000 ± 1000	36
W286R	45000 ± 2000	350 ± 10	130	8700 ± 600	98 ± 2	89	60000 ± 1000	1800 ± 100	33

(b) thioate substitution	SCH_3			SCH_2CH_3		
enzyme	S_p	R_p	S_p/R_p	S_p	R_p	S_p/R_p
AChE	310 ± 20	1.7 ± 0.3	180	74 ± 5	0.16 ± 0.02	460
W86A	170 ± 20	0.75 ± 0.01	230	63 ± 9	0.27 ± 0.002	230
Y337A	81 ± 4	0.46 ± 0.02	180	27 ± 2	0.047 ± 0.002	570
Y337F	320 ± 10	0.94 ± 0.04	340	92 ± 8	0.13 ± 0.02	710
W286A	530 ± 40	1.6 ± 0.2	330	160 ± 10	0.43 ± 0.09	370
W286R	710 ± 30	2.1 ± 0.2	340	200 ± 30	0.35 ± 0.09	570

[a] Data shown as means ± standard error of the mean typically from three measurements.

pounds; the bimolecular rate constants are summarized in Table 2a,b. Replacement of Trp 86 with Ala gives rise to a large reduction in reaction rate constants for both enantiomers of CHMP-thiocholine and, to a lesser extent, with DMBMP-thiocholines while conserving the enantiomeric preference seen for wild-type AChE. Although the rate constant of inhibition for iPrMP-thiocholine was also decreased, this mutation gave a significant shift in enantiomeric preference. A large decrease in the rate constant of reaction with the S_p isomer relative to the R_p isomer was evident, resulting in a 100-fold loss in selectivity for the S_p enantiomer.

Unlike that seen with the cationic alkyl phosphonates, the W86A mutation had a minimal influence on the reaction rate constant for the uncharged phosphonothioates where the k_i values for the thiomethylate and thioethylate compounds were affected at most 2-fold. This observation is consistent with W86 playing a role in stabilization of cationic ligands such as ATC while having little influence on the catalysis of uncharged ligands (Ordentlich et al., 1993a).

The second residue mutated in the choline subsite, Tyr 337 to either Ala or Phe, had a minimal effect on the rate constant of reaction for the thiocholine- and thioalkyl-substituted OPs as shown in Table 2a. Although small differences exist between rate constants for the wild-type and 337 mutant AChEs, it is noteworthy that the Y337A mutation reduced the reaction rate constants of the uncharged phosphonothioates 3−4-fold, indicating an aromatic residue at 337 slightly enhances the reaction.

The final aromatic residue analyzed, W286, resides in the peripheral site at the lip of the gorge and was mutated to either Ala or Arg. As shown in Table 2a, replacing Trp 286 with Ala at the rim of the gorge had little influence on the rate constants for the cationic OPs, showing at most a 2-fold enhancement for R_p CHMP-thiocholine. Introducing an Arg at the 286 position did, however, decrease the rate of inhibition by the cationic OPs. Most notably, the rate constants for CHMP- and DMBMP-thiocholines were affected more than those for iPrMP-thiocholine, indicating that Arg at the rim of the gorge impedes the rates of reaction for the bulkier alkyl-substituted OPs more than with the smaller isopropyl methylphosphonate. Furthermore, the changes in rate constants observed for the W286R mutation are conserved between enantiomers which is consistent with the cationic substitution restricting diffusional entry.

The rate constants for uncharged phosphonates were either maintained or enhanced with the W286A and W286R mutations (Table 2b), also suggesting that the 286 residue does not influence reaction rates through stabilization of the complex but rather may contribute through steric hindrance by the large indole ring of bulky ligands entering the gorge.

Influence on Diffusion of Ligands Entering the Gorge. The *meta*-substituted trifluoromethyl acetophenones (TFK) (Fig-

Table 3: Bimolecular Association Rate Constants (10^9 M^{-1} min^{-1})[a] Determined for the Inhibition of Mouse Wild-Type and Mutant AChEs by *m*-Trimethylammonio Trifluoromethyl Acetophenones (TFK^+) and *m-tert*-Butyl Trifluoromethyl Acetophenones (TFK^o)

enzyme	TFK^+	TFK^o
MAChE	180 ± 20	4.0 ± 0.5
D74N	5.1 ± 0.4	5.1 ± 0.1
E202Q	94 ± 4	4.5 ± 0.3
W286A	120 ± 10	2.6 ± 0.2
W286R	34 ± 2	2.3 ± 0.5
MAChE[b]	210 ± 20	3.0 ± 0.4
W86A[b]	19 ± 9	2.6 ± 0.8

[a] Values corrected for the ratios of hydrated to nonhydrated compound according to Nair et al. (1994). [b] Data of Radić et al. (1995).

ure 1), whose conjugates behave as transition state analogs to ATC, exhibit a diffusion-controlled association with bimolecular constants in the range of 10^9–10^{11} M^{-1} min^{-1} (Nair et al., 1993, 1994; Radić et al., 1995). In order to dissect the influence of residue substitutions on diffusion from the specific interactions that give rise to OP specificity, inhibition of AChE mutants at Asp 74, Trp 86, Glu 202, and Trp 286 by *meta*-substituted trimethylammonio and *tert*-butyl TFKs (TFK^+ and TFK^o, respectively) was analyzed (Table 3).

Mutations of anionic residues to neutral isosteres at the rim of the gorge and at the base of the gorge both resulted in decreases in the k_{on} of TFK^+; however, D74N exhibited a 35-fold reduction, whereas with E202Q, only a 2-fold reduction in the association rate constant was observed. The magnitude of these reductions is considerably less than that observed with the S_p and R_p CHMP-thiocholines. As for the uncharged *tert*-butyl-substituted TFK, the D74N and E202Q mutations essentially were without influence, a result which parallels that seen for uncharged CHMP-thioates with the D74N mutation but not for the E202Q mutation which reduces the OP reaction rate constant. Through comparison of on-rate constants for the cationic and uncharged analogs, it becomes apparent that among these residues Asp at position 74 solely accounts for the 50-fold faster association rate constant for the TFK^+ with AChE compared to that for TFK^o.

The most influential mutation from the choline subsite on inhibition rate constants for the cationic OPs, W86A, was reported previously to reduce the association rate constant of the TFK^+ analog with AChE while not altering that with the TFK^o analog (Radić et al., 1995). As with the mutations D74N and E202Q, the 11-fold reduction of k_{on} for trimethylammonio-substituted TFK with the W86A mutation is 3–4-fold less than that of the cationic CHMP-thiocholine compounds, suggesting that the rates of reaction of the cationic phosphonates have a greater dependence on Asp 74, Trp 86, and Glu 202 than does the cationic TFK^+ analog.

Substitution of an Arg for Trp at position 286 revealed that introducing a positive charge at the rim of the gorge reduced the bimolecular association rate constant of TFK^+ to a similar extent as that for S_p and R_p CHMP-thiocholines. However, the uncharged TFK analog was less affected with this mutation, indicating that TFK^+ association is hindered by electrostatic repulsive forces at the mouth of the gorge. The W286A mutation further supports this contention since Ala substitution slightly affects the association rate constant of the charged and uncharged TFKs to the same degree.

Effect of the Mutations on the Catalysis of Carboxyl Ester Hydrolysis. The changes in catalytic parameters for the hydrolysis of acetylthiocholine (ATC) were compared with data for the above substrates (Radić et al., 1993; Hosea et al., 1995). Velocities of hydrolysis for various ATC concentrations were fit according to Radić et al. (1993), and the resulting kinetic constants are given in Table 4. Related mutant ChEs reported previously have been included to allow for direct comparisons.

Table 4: Kinetic Constants[a] Calculated for the Catalysis of Acetylthiocholine by Mutant and Wild-Type AChEs

enzyme	K_m (μM)	k_{cat}[b] (10^3 min^{-1})	k_{cat}/K_m (10^6 M^{-1} min^{-1})
MAChE[c]	46 ± 3	140 ± 10	3000
D74N[d]	1300 ± 140	84 ± 11	65
E202Q[e]	130 ± 10	85 ± 13	650
E450Q[f]	140 ± 10	3.4 ± 0.4	24
W86A[g]	66 ± 19	2.8 ± 0.2	42
Y337A[h]	110 ± 20	52 ± 16	470
Y337F[i]	53 ± 5	68 ± 26	1300
W286A[j]	64 ± 3	140 ± 20	2200
W286R[k]	420 ± 60	160 ± 30	380

[a] Values are shown as the mean from three measurements ± the standard error of the mean. [b] k_{cat} was determined from titrations of the inhibition assay with MEPQ. Values for K_m, K_{ss}, and b were calculated using nonlinear regression to fit according to $v = [V_{max}(1 + b[S]/K_{ss})]/[(1 + K_m/[S])(1 + [S]/K_{ss})]$ (Webb, 1963) using Sigma Plot. [c] K_{ss} = 15 ± 2 mM, b = 0.23 ± 0.01; data of Radić et al. (1993). [d] K_{ss} = 530 ± 170 mM, b = 0; data of Radić et al. (1993). [e] K_{ss} = 103 ± 3 mM, b = <0.2. [f] K_{ss} = 59 ± 22 mM, b = 1.8 ± 0.1. [g] K_{ss} = 20 ± 9 mM, b = 8.2 ± 1.0; data of Radić et al. (1995). [h] K_{ss} = 29 ± 21 mM, b = 0.59 ± 0.08; data of Radić et al. (1993). [i] K_{ss} = 10 ± 2 mM, b = 0.42 ± 0.03; data of Radić et al. (1993). [j] K_{ss} = 46 ± 12 mM, b = 0.26 ± 0.13. [k] K_{ss} = 23 ± 8 mM, b = 0.24 ± 0.06; data of Radić et al. (1993).

The mutation, D74N, significantly affected the K_m value, unlike removing the charges located at the base of the gorge as with the E202Q and E450Q mutations (Table 4). E450Q however substantially reduced the maximum rate of turnover, k_{cat}, of ATC, whereas removing the negative charges at positions 202 and 74 had very little effect on k_{cat}. The combination of the reduced k_{cat} with E450Q and the increased K_m with D74N results in enzymes less efficient in catalyzing the hydrolysis of ATC as seen by comparing k_{cat}/K_m of the mutants and wild-type AChEs. Comparatively, the anionic character of Glu 202 seems to contribute less to binding and turnover of ATC since both the k_{cat} and the K_m are only slightly modified with the E202Q mutation. Replacement of Glu 202 with Gln in TAChE (Glu 199) resulted in a near 50-fold reduction in k_{cat}/K_m (Radić et al., 1992), while in human AChE, the mutation showed an 18-fold reduction in k_{cat}/K_m (Shafferman et al., 1992), revealing that species differences exist in the magnitude of influence of this conserved anionic residue.

Mutations in the choline binding domain (Sussman et al., 1991) that we examined are W86A, Y337A, and Y337F. As shown in Table 4, mutations at Tyr 337 and the W86A mutation have essentially no effect on the K_m, while substitutions at these two positions have very different effects on the maximum turnover of ATC since mutating the Tyr 337 slightly reduced the k_{cat} and W86A shows a 50-fold reduction in the maximum turnover and, consequently, in the efficiency of the catalytic hydrolysis of ATC. From these data, it was suggested that the aromaticity of Trp 86 stabilizes the positively charged choline group for the most efficient hydrolysis (Ordentlich et al., 1993a; Radić et al., 1993, 1995), but the effective removal of an indole side chain with this substitution will also create a substantial volume difference and may rather significantly perturb local structure and polarity in this region.

The third region of analysis at position 286 reveals that introducing a positively charged residue at the rim of the gorge as in W286R significantly increases K_m, whereas replacing the Trp with Ala has no effect. Additionally, the reduced k_{cat}/K_m value for W286R, but not for W286A, indicates that Trp 286 in AChE does not influence the catalysis of ATC hydrolysis by stabilization of the quaternary group but, as seen with the TFKs, may gate entry of cationic ligand passing into the gorge.

DISCUSSION

The chemical diversity of substrates catalyzed by AChE can be used advantageously to delineate distinct steps in the catalytic pathway and, in turn, residues governing the specificity of the component steps. The trifluoromethyl acetophenones conjugate with the active center serine to form a hemiketal without departure of a leaving group. The organophosphonates rapidly acylate the enzyme with loss of a leaving group, but subsequent deacylation is typically slow. The carboxyl esters show rapid acylation and deacylation rates. Of these three chemical classes, only the organophosphonates possess an asymmetric center at the point of nucleophilic attack by the enzyme, thus adding another dimension to the analysis of specificity. In this study, we employ charged and uncharged congeners of enantiomeric phosphonates and trifluoromethyl acetophenones with specific mutations in AChE to examine residues that influence substrate diffusion to and association with the AChE active center.

Recognition versus Phosphonylation. The absolute stereochemistry of the enantiomeric organophosphonates is known (Berman & Leonard, 1989), and substantial evidence has emerged from experimental data (Cygler et al., 1994; Hosea et al., 1995) and theoretical considerations (Sussman et al., 1991; Harel et al., 1991, 1996; Barak et al., 1992) to show that their rapid acylation of the enzyme requires insertion of the phosphonyl oxygen in the oxyanion hole. Our findings that the D74N mutated enzyme loses reactivity with the cationic phosphonates, but not with the uncharged agents (Table 1), implicate the importance of an electrostatic interaction in orientation of the phosphonate. Moreover, that reactions with the enantiomers are equally altered with the D74N mutation indicates that the cationic groups of the R_p and S_p enantiomers and D74 are separated by the same distances in their initial docking positions. We conclude, therefore, that the docking orientation of the tetrahedral phosphonate is such that the leaving group (thiocholine) is directed toward the mouth of the gorge. Of significance is that this orientation is achieved for both (R_p)- and (S_p)-methylphosphonyl thiocholines. With the positions of the P=O and the thiocholine groups identified, the differences in reactivity of the enantiomeric phosphonylthiocholines can now be seen to depend on the relative orientation of the remaining two substituents: the methyl and alkoxyl groups. Accordingly, the reduced reactivity of the R_p enantiomer relative to that of the S_p enantiomer must therefore reflect respective differences primarily in steric restrictions encountered by each enantiomer with proximal side chains in the active center gorge. In fact, the 230-fold preference for the S_p enantiomers arises from the steric constraints precluding the optimal fit of the more bulky alkoxyl group in the acyl pocket, an apparent requirement for efficient phosphonyl transfer (Hosea et al., 1995).

Scheme 1

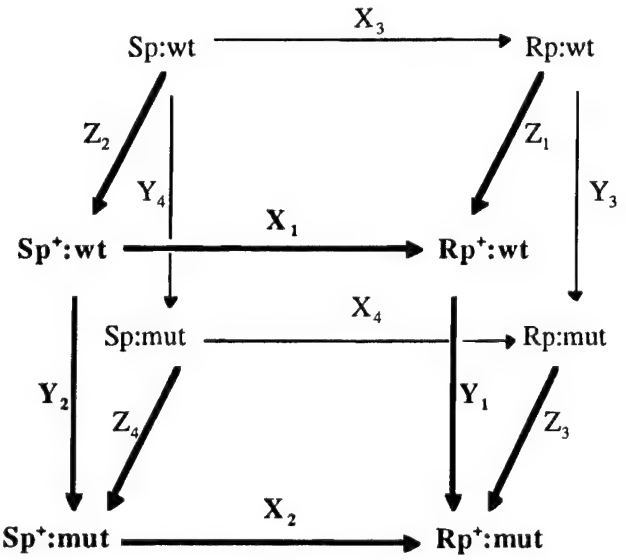

Mutant Cycle Analysis and Orientation of the Phosphonates. Our data of AChE mutagenesis in relation to the charge on the leaving group of the organophosphonate may be combined with previous data on acyl pocket mutations and enantiomer selectivity (Hosea et al., 1995) to analyze the linkages between ligand structure and the mutations by a mutant cycle analysis (Scheme 1) (Wolfenden, 1978; Carter et al., 1984; Hidalgo & MacKinnon, 1995; Schreiber & Fersht, 1995). In Scheme 1, enantiomeric selectivities of the bimolecular rate constants for organophosphonate reaction with AChE [i.e. $k(S_p{:}wt)$] in relation to the mutations (*XY* planes) are defined by

$$\psi_+ = \frac{S_p}{R_p^+} = \frac{X_1}{X_2} = \frac{Y_2}{Y_1} = \frac{k(S_p^+{:}wt)k(R_p^+{:}mut)}{k(R_p^+{:}wt)k(S_p^+{:}mut)} \quad (1)$$

$$\psi_o = \frac{S_p}{R_p} = \frac{X_3}{X_4} = \frac{Y_4}{Y_3} = \frac{k(S_p{:}wt)k(R_p{:}mut)}{k(R_p{:}wt)k(S_p{:}mut)} \quad (2)$$

The electrostatic influence of charge on the leaving group with respect to the mutations (*ZY* planes) is defined by

$$\phi_S = \frac{S_p}{S_p^+} = \frac{Z_2}{Z_4} = \frac{Y_4}{Y_2} = \frac{k(S_p{:}wt)k(S_p^+{:}mut)}{k(S_p^+{:}wt)k(S_p{:}mut)} \quad (3)$$

$$\phi_R = \frac{R_p}{R_p^+} = \frac{Z_1}{Z_3} = \frac{Y_3}{Y_1} = \frac{k(R_p{:}wt)k(R_p^+{:}mut)}{k(R_p^+{:}wt)k(R_p{:}mut)} \quad (4)$$

These values are represented as absolute values without reference to sign. They may be converted to the change in free energy of activation for the corresponding reactions, $\Delta\Delta G^{\ddagger}$, where

$$\psi_+^{\ddagger} = RT \ln \psi_+ \quad (5)$$

$$\psi_o^{\ddagger} = RT \ln \psi_o \quad (6)$$

$$\phi_S^{\ddagger} = RT \ln \phi_S \quad (7)$$

$$\phi_R^{\ddagger} = RT \ln \phi_R \quad (8)$$

and $R = 1.99 \times 10^{-3}$ kcal mol^{-1} K^{-1} and $T = 298$ K.

Analysis of the coupling between enantiomer selectivity of cycloheptyl methylphosphonyl thiocholine and mutations

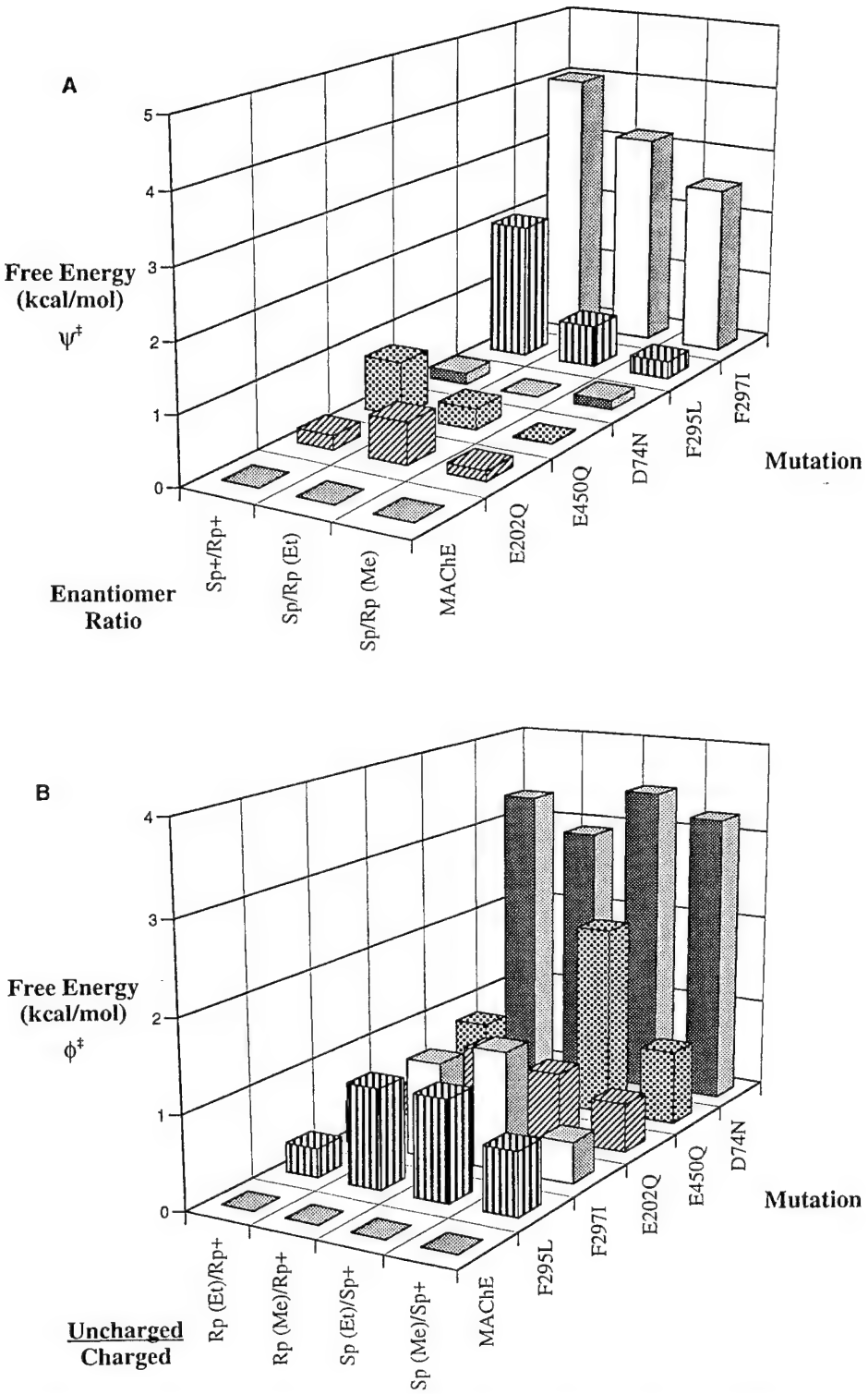

FIGURE 2: Relationship between the change in free energy of activation, selected mutations in acetylcholinesterase, and structures of cycloheptyl methylphosphonyl thioates. (A) Selectivity for the S_p and R_p enantiomers. (B) Selectivity for charged and uncharged phosphonates: +, cationic cycloheptyl methylphosphonyl thiocholine; Me, uncharged cycloheptyl methylphosphonyl thiomethane; and Et, uncharged cycloheptyl methylphosphonyl thioethane. The scheme for the analysis is shown in Scheme 1, and equations are detailed in the text.

is shown in Figure 2A. The dominant influence of the acyl pocket, and in particular residue 297, is evident. It is also apparent that the influence of residues 295 and 297 is greatest with the larger thiocholine leaving group, but the influence of the 297 residue prevails irrespective of the charge on the leaving group. The influence of mutating the charged residues or other residues in the choline binding site (not shown) is of relatively small consequence. Analysis of coupling between the charge on the leaving group and the mutations is shown in Figure 2B. We observe that, despite large influences of charge on the reactivity of the cationic and uncharged phosphonates, Asp 74 has the dominant influence on altering relative selectivity for the phosphonates containing a charged leaving group. This phenomenon prevails irrespective of whether the R_p or S_p enantiomers are employed.

Hence, analysis of the linkage between residue mutations and enantiomeric specificity in one dimension and between charge on the leaving group in a second dimension shows a distinct dependence on residue location. Moreover, the

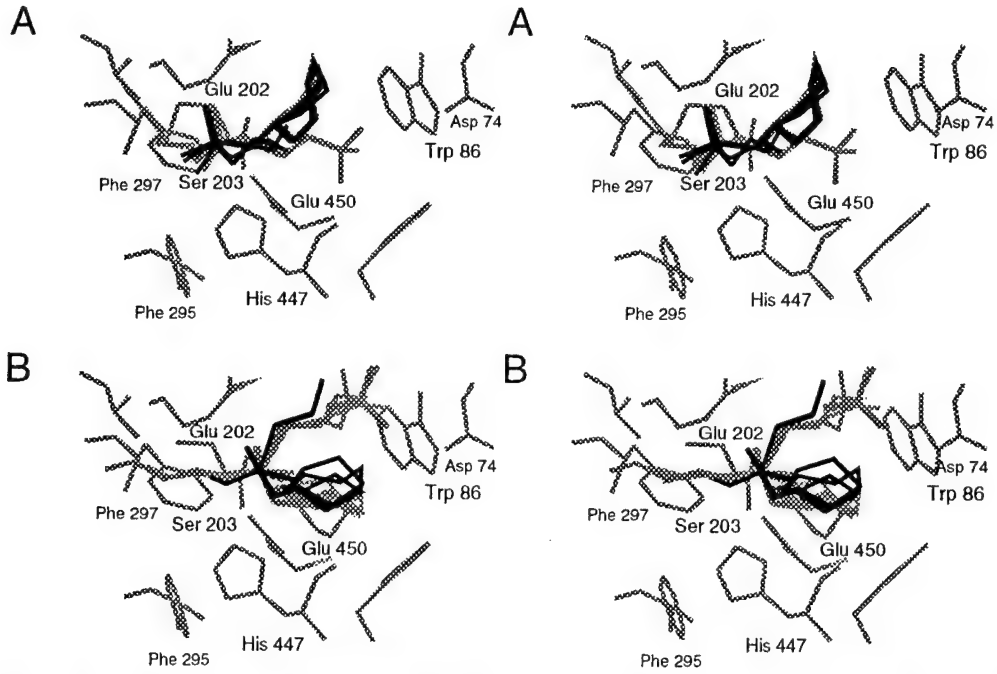

FIGURE 3: Stereoviews of the computational docking using molecular dynamics (see Materials and Methods) of (A) S_p and (B) R_p cycloheptyl methylphosphonyl thiocholines (gray) and cycloheptyl methylphosphonyl thioethylates (black) showing the spatial arrangement of the substituents about the phosphate.

proposed orientation of the organophosphonate in its transition state (Figure 3) is completely consistent with the positions of the residues on AChE dictating specificity.

Figure 3 shows the docking orientation achieved for the two enantiomers using molecular dynamics. With the phosphonyl oxygen directed toward the oxyanion hole (amide backbone nitrogens of Gly 121, Gly 122, and Ala 204 as hydrogen bond donors) and the leaving groups of both R_p and S_p isomers directed toward Asp 74, the cycloheptyl and methyl substituents remain fixed in space with respect to the enzyme coordinates. Previous studies showed that the bimolecular inhibition constants for uncharged and cationic OPs differ by up to 3 orders of magnitude. Analysis of the kinetics shows that 2 orders of magnitude are attributable to affinity and 1 order of magnitude is attributable to unimolecular phosphonylation (Berman & Leonard, 1989). The present study indicates a role for D74 in establishing the orientation of the cationic OPs prior to reaction and further suggests that the interaction of the thiocholine moiety with D74 further stabilizes the transition state. The uncharged phosphonothioates, since they cannot derive electrostatic stabilization energy through ion-pair formation with D74, bind with lower affinity than the cationic OPs. Consequently, they are less likely to be oriented by D74, and free diffusion of these agents into the gorge has a higher probability of resulting in nonproductive orientations (Berman & Leonard, 1989).

Reductions in inhibition constants with increasing chain length of substituted alkylphosphonylthiocholines have been shown to result mostly from reduction in phosphorylation rate while with identically substituted alkyl phosphonylfluoridates to result mostly from reduction in affinity (greater K_d) (Berman, 1995). This phenomenon is thought to arise from constraints imposed on the alkylphosphonylthiocholines, but not the fluoridates, which impede rotation for optimal reaction of phosphonylation, allowing one to conclude that the fate of the orientation for the cationic alkyl phosphonates is determined near the rim of the gorge. Our data on the D74N mutation suggest that this Asp residue at this location likely serves to dock the phosphonate inhibitor prior to and during formation of the transition state, thus dictating the orientation of cationic ligands in the active center.

Results of ligand docking of the reversible complex of AChE with CHMP congeners using molecular dynamics show that initial docking of the S_p enantiomer occurs with the leaving group thiocholine approximating an apical position 180° from the apical position of the γ-oxygen of Ser 203. At the same time, the phosphonyl oxygen resides within hydrogen-bonding distance (3−4 Å) of the hydrogen bond donors of the oxyanion hole (Figure 4). This orientation, in that the attacking nucleophile and the leaving group adapt apical positions and the P═O bond is polarized through hydrogen bonding in the oxyanion hole, represents a productive configuration allowing for facile direct in-line attack by the γ-oxygen of Ser 203 and facile displacement of the thioate moiety. The dynamics for the less reactive, R_p enantiomers, however, show that either positioning of the P═O bond or apical positioning of the leaving group is possible; but one cannot obtain the two positions simultaneously (Figure 4). The primary reason for such exclusion is that the positioning of the thiocholine moiety toward D74 requires positioning of the cycloheptyl moiety in the acyl pocket, where it encounters steric hindrance with Phe 295 and 297 (Hosea et al., 1995). Thus, the reduced reaction rate constants for the R_p enantiomers in comparison with the S_p enantiomers are due to steric hindrance within the acyl pocket, as shown previously (Hosea et al., 1995).

Orientation of Tetrahedral Phosphonates Compared to That of Trigonal Carboxyl Esters. With the position of the leaving group directed out of the gorge and the phosphonyl oxygen in the oxyanion hole, the more energetically favorable in-line attack by γ-oxygen of Ser 203 on one face of the tetrahedron of the S_p and R_p isomers would then give rise to choline subsite occupation by the alkoxyl substituent of the S_p isomer and the methyl substituent of the R_p isomer (Hosea et al., 1995). Evidence for such a spatial arrangement derives from kinetic analysis of the aging profiles of the final

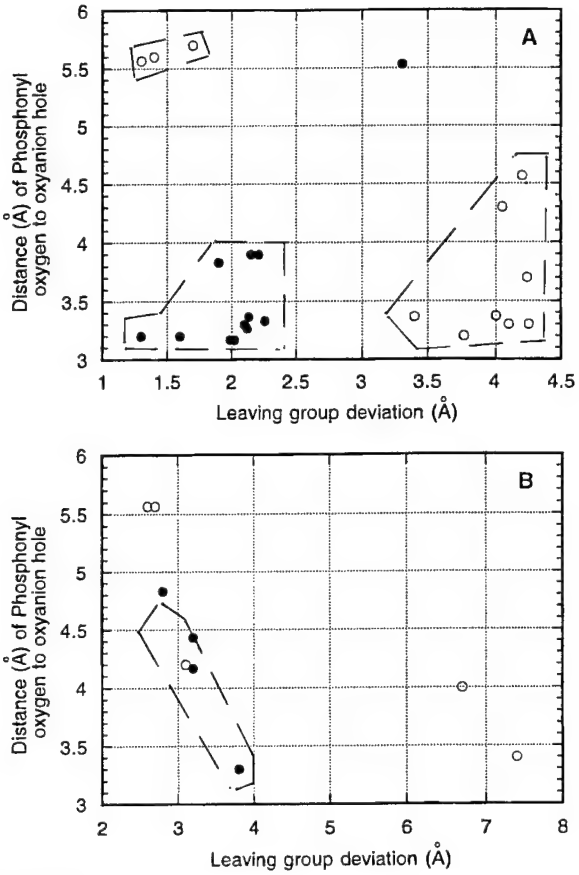

FIGURE 4: Relationship between phosphonyl oxygen location and leaving group orientation for (A) S_p (closed circles) and R_p (open circles) cycloheptyl methylphosphonyl thiocholines and for (B) S_p (closed circles) and R_p (open circles) cycloheptyl methylphosphonyl thioethylates in reversible complexes with TAChE. Each circle represents one conformer. Productivity is assumed to require insertion of the phosphonyl oxygen of CHMP congeners into the oxyanion hole (formed by the amide backbone hydrogens of Gly 121, Gly 122, and Ala 204), where the phosphonyl oxygen mean distance is measured from the three potential hydrogen bond donors. Leaving group deviation refers to the distance of the quaternary nitrogen (for the charged thiocholine complexes) or the β-carbon (for the neutral thioethylate complexes) of the leaving group from that of a conformer in the pentavalent complex which most closely resembles the ideal leaving group position of 180° from the γ-oxygen of Ser 203, for an S_N2 concerted mechanism which would give apical positions of the γ-oxygen and leaving group (Westheimer, 1968). The ideal conformer was approximated by S_p CHMP-thiocholine, which kinetically is most reactive.

cycloheptyl methylphosphonyl (CHMP) AChE conjugates. Upon dealkylation during aging of the conjugate of S_p CHMP-AChE (reaction with S_p CHMP thiocholine), the fluorescent bisquaternary inhibitor decidium exhibits enhanced affinity with the conjugated enzyme, a phenomenon not present with conjugates formed by reactions with the R_p isomer (Berman & Decker, 1986, 1989). In that decidium likely occupies the choline subsite with one of the quaternary ammonium groups in the nonacylated enzyme, the differences observed between the reactions with S_p and R_p enantiomers provide evidence for choline subsite occupation by the alkoxyl group of the S_p enantiomer which departs through dealkylation during aging. Furthermore, the reduced aging rates with the conjugates formed through reactions with the R_p enantiomer suggest that the alkoxyl substituent resides elsewhere while positioning the methyl substituent in the choline subsite. Molecular modeling further supports this spatial arrangement of the substituents and shows, during the pentavalent intermediate, occupation of the choline subsite by the alkoxyl moiety of the S_p isomer and the methyl substituent of the R_p isomer for both the uncharged and cationic CHMP congeners (Figure 3).

Examination of the crystal structure of TAChE conjugated with TFK^+ allows for a comparison of distances between critical anionic and aromatic residues in AChE and the quaternary ammonium groups of TFK^+ (Harel et al., 1996) and the two organophosphonate enantiomers (Figure 3). The cationic, quaternary ammonium moiety in the tetrahedral conjugate of TFK^+ with AChE is 3.7 Å from Trp 86 $(84)^2$ and nearly 9 Å away from Asp 74 $(72)^2$. Therefore, the decrease in the association rate constant of TFK^+ with the D74N mutated enzyme (Table 3) likely arises through diminishing the diffusion rate of the ligand into the gorge. By contrast, in the pentavalent intermediate formed from the tetrahedral phosphonates, the quaternary ammonium moiety appears equidistant from Asp 74 and Trp 86. The type of interaction that can be expected from the Trp 86 is cation–π, whereas that from Asp 74 is ion-pair, both of which are suggested to be Coulombic in nature where the energy of the interaction is inversely proportional to the distance between the charges (Dougherty, 1996). That Trp 86 contributes negative charge from the center above and below the face of the ring and possesses a positive charge on the perimeter of the ring [cf. Creighton (1993) and Dougherty (1996)] suggests Coulombic interactions involving cation–π interactions would be strongest when the cation resides in-line with the quadrupole moment perpendicular to the face of the aromatic ring (Dougherty, 1996). On the other hand, the strength of interaction between the cationic quaternary ammonium moiety and Asp 74, possessing a negative charge, should not be dependent on the angle of the substituent orientation. Thus, the leaving group position directed toward D74 and along side W86 represented in Figure 3 indicates that Asp 74 would contribute more to electrostatic stabilization of the OP–AChE complex than Trp 86 and is consistent with D74N having a more dramatic affect on rates with cationic phosphonates than Trp 86.

Distinct Activation Barriers for the Organophosphonates and Trifluoromethyl Acetophenones. The trifluoromethyl acetophenones and organophosphonates can be expected to have distinct activation barriers for their reactions with AChE. Hence, Asp 74 will affect different steps in the two overall reactions. In the case of TFK^+, the activation barrier arises from diffusion of the ligand through the restricted gorge dimensions. Accordingly, the D74N mutation exerts its influence on the diffusional step of TFK^+ entry. At the base of the gorge, Trp 86 stabilizes the cationic moiety (Harel et al., 1996), and the diffusion-limited reaction rate constant (1.8×10^{11} M^{-1} min^{-1}) suggests that TFK^+ conjugation with the active site serine occurs without traversing through an additional, limiting activation barrier. Association of TFK^+ with the W86A mutant enzyme has a decreased association rate constant and increased dissociation rate constant (Radić et al., 1995). This reflects not only formation of a less stable conjugate but also the imposition of a second activation barrier for association. The latter may arise from the multiple orientations of TFK^+ in the mutant AChE gorge when the indole ring is removed, many of which may be unproductive.

The alkyl phosphonates exhibit reaction rates below the diffusion limitation, which suggest that an activation barrier is encountered with acylation by the phosphonate. Whether this arises in the formation of a pentavalent intermediate or in the dissociation of the leaving group is not resolved.

However, it is likely that the charge on Asp 74 influences this activation barrier either through facilitating the positioning of the charged organophosphonate with the thiocholine directed out of the gorge or in facilitating the loss of the thiocholine leaving group. The dissection of bimolecular rate constants using stopped-flow methods into components of affinity and phosphonylation should further elucidate determinants which dictate productive versus nonproductive binding.

REFERENCES

Aldridge, W. N., & Reiner, E. (1972) in *Enzyme Inhibitors as Substrates* (Neuberger, A., & Tatum, E. L., Eds.) North-Holland Publishing Co., Amsterdam, London, and American Elsevier Publishing Co., Inc., New York.

Ashani, Y., Radić, Z., Tsigelny, I., Vellom, D. C., Pickering, N. A., Quinn, D. M., Doctor, B. P., & Taylor, P. (1995) *J. Biol. Chem. 270,* 6370−6380.

Ausubel, F. M., Brent, R., Kingston, R. E., Moore, D. D., Seidman, J. G., Smith, J. A., & Struhl, K. (1994) in *Current Protocols in Molecular Biology*, p 9.1.1, Green Publishing Associates, Inc., and John Wiley and Sons, Inc., New York.

Barak, D., Ariel, N., Velan, B., & Shafferman, A. (1992) in *Multidisciplinary Approaches to Cholinesterase Functions* (Shafferman, A., & Velan, B., Eds.) pp 195−199, Plenum Press, New York and London.

Barak, D., Bromberg, A., Ordentlich, A., Kronman, C., Marcus, D., Lazar, A., Ariel, N., Velan, B., & Shafferman, A. (1994) *J. Biol. Chem. 269,* 6296−6305.

Barak, D., Ordentlich, A., Bromberg, A., Kronman, C., Marcus, D., Lazar, A., Ariel, N., Velan, B., & Shafferman, A. (1995) *Biochemistry 34,* 15444−15452.

Berman, H. A. (1995) in *Enzymes of the Cholinesterase Family* (Quinn, D. M., Balasubramanian, A. S., Taylor, P., & Doctor, B. P., Eds.) pp 177−182, Plenum Press, New York.

Berman, H. A., & Decker, M. M. (1986) *J. Biol. Chem. 261,* 10646−10652.

Berman, H. A., & Decker, M. M. (1989) *J. Biol. Chem. 264,* 3951−3956.

Berman, H. A., & Leonard, K. (1989) *J. Biol. Chem. 264,* 3942−3950.

Bourne, Y., Taylor, P., & Marchot, P. (1995) *Cell 83,* 503−512.

Carter, P. J., Winter, G., Wilkison, A. J., & Fersht, A. R. (1984) *Cell 38*, 835−840.

Creighton, T. E. (1993) *Protein: Structure and Molecular Properties*, 2nd ed., pp 142−144, W. H. Freeman and Company, New York.

Cygler, M., Schrag, J. D., Sussman, J. L., Harel, M., Silman, I., Gentry, M. K., & Doctor, B. P. (1993) *Protein Sci. 2*, 366−382.

Cygler, M., Grochulski, P., Kazlauskas, R. J., Schrag, J. D., Bouthillier, F., Rubin, B., Serreqi, A. N., & Gupta, A. K. (1994) *J. Am. Chem. Soc. 116*, 3180−3186.

Dougherty, D. A. (1996) *Science 271,* 163−168.

Dougherty, D. A., & Stauffer, D. A. (1990) *Science 250,* 1558−1560.

Ellman, G. C., Courtney, K. D., Andres, V., Jr., & Featherstone, R. M. (1961) *Biochem. Pharmacol. 7,* 88−95.

Fersht, A. R. (1985) *Enzyme Structure and Mechanism*, 2nd ed., pp 150−152, W. H. Freeman and Company, New York.

Fersht, A. R. (1988) *Biochemistry 27*, 1577−1580.

Froede, H. C., & Wilson, I. B. (1971) in *The Enzymes* (Boyer, P. D., Ed.) Vol. 5, pp 87−114, Academic Press, New York and London.

Gentry, M. K., & Doctor, B. P. (1995) in *Enzymes of the Cholinesterase Family* (Quinn, D. M., Balasubramanian, A. S., Taylor, P., & Doctor, B. P., Eds.) pp 493−501, Plenum Press, New York.

Harel, M., Su, C.-T., Frolow, F., Ashani, Y., Silman, I., & Sussman, J. L. (1991) *J. Mol. Biol. 221*, 909−918.

Harel, M., Schalk, I., Ehret-Sabattier, L., Bouet, F., Goeldner, M., Hirth, C., Axelsen, P., Silman, I., & Sussman, J. L. (1993) *Proc. Natl. Acad. Sci. U.S.A. 90*, 9031−9035.

Harel, M., Quinn, D. M., Nair, H. K., Silman, I., & Sussman, J. L. (1996) *J. Am. Chem. Soc. 118,* 2340−2346.

Hidalgo, P., & MacKinnon, R. (1995) *Science 268*, 307−310.

Hosea, N. A., Berman, H. A., & Taylor, P. (1995) *Biochemistry 34*, 11528−11536.

Levy, D., & Ashani, Y. (1986) *Biochem. Pharmacol. 35,* 1079−1085.

Mecozzi, S., West, A. P., Jr., & Dougherty, D. A. (1996) *J. Am. Chem. Soc. 118,* 2307−2308.

Michel, H. O., Hackley, B. E., Jr., Berkowitz, G. L., Hackley, E. B., Gillilan, W., & Pankau, M. (1967) *Arch. Biochem. Biophys. 121*, 29−34.

Nair, H. K., Lee, K., & Quinn, D. M. (1993) *J. Am. Chem. Soc. 115,* 9939−9941.

Nair, H. K., Seravalli, J., Arbuckle, T., & Quinn, D. M. (1994) *Biochemistry 33*, 8566−8576.

Nolte, H.-J., Rosenberry, T. L., & Neumann, E. (1980) *Biochemistry 19*, 3705−3711.

Oosterbaan, R. A., & Cohen, J. A. (1964) In *Proceedings of the 1st FEBS Meeting, London* (Goodwin, T. W., Harris, J. I., & Hartley, B. S., Eds.) Vol. 1, pp 87−95, Academic Press, London and New York.

Ordentlich, A., Barak, D., Kronman, C., Flashner, Y., Leitner, M., Segall, Y., Ariel, N., Cohen, S., Velan, B., & Shafferman, A. (1993a) *J. Biol. Chem. 268,* 17083−17095.

Ordentlich, A., Kronman, C., Barak, D., Stein, D., Ariel, N., Marcus, D., Velan, B., & Shafferman, A. (1993b) *FEBS Lett. 334* (2), 215−220.

Ordentlich, A., Barak, D., Kronman, C., Ariel, N., Segall, Y., Velan, B., & Shafferman, A. (1995) *J. Biol. Chem. 270,* 2082−2091.

Qian, N., & Kovach, I. M. (1993) *FEBS Lett. 336* (2), 263−266.

Quinn, D. M. (1987) *Chem. Rev. 87*, 955−979.

Quinn, D. M., Servalli, J., Nair, H. K., Medhekar, R., Husseini, B., Radić, Z., Vellom, D. C., Pickering, N., & Taylor, P. (1995) in *Enzymes of the Cholinesterase Family* (Quinn, D. M., Balasubramanian, A. S., Taylor, P., & Doctor, B. P., Eds.) pp 203−207, Plenum Press, New York.

Radić, Z., Gibney, G., Kawamoto, S., MacPhee-Quigley, K., Bongiorno, C., & Taylor, P. (1992) *Biochemistry 31*, 9760−9767.

Radić, Z., Pickering, N. A., Vellom, D. C., Camp, S., & Taylor, P. (1993) *Biochemistry 32,* 12074−12084.

Radić, Z., Duran, R., Vellom, D. C., Li, Y., Cervenansky, C., & Taylor, P. (1994) *J. Biol. Chem. 269,* 11233−11239.

Radić, Z., Quinn, D. M., Vellom, D. C., Camp, S., & Taylor, P. (1995) *J. Biol. Chem. 270,* 20391−20399.

Ripoll, D. R., Faerman, C. H., Axelsen, P. H., Silman, I., & Sussman, J. L. (1993) *Proc. Natl. Acad. Sci. U.S.A. 90,* 5128−5132.

Rosenberry, T. L. (1975) *Adv. Enzymol. 43*, 103−218.

Saxena, A., Doctor, B. P., Maxwell, D. M., Lenz, D. E., Radić, Z., & Taylor, P. (1993) *Biochem. Biophys. Res. Commun. 197*, 343−349.

Schreiber, G., & Fersht, A. R. (1995) *J. Mol. Biol. 248*, 478−486.

Shafferman, A., Velan, B., Ordentlich, A., Kronman, C., Grosfeld, H., Leitner, M., Flashner, Y., Cohen, S., Barak, D., & Ariel, N. (1992) *EMBO J. 11*, 3561−3568.

Sussman, J. L., Harel, M., Frolow, F., Oefner, C., Goldman, A., Toker, L., & Silman, I. (1991) *Science 253*, 872−878.

Sussman, J. L., Harel, M., Raves, M., Quinn, D. M., Nair, H. K., & Silman, I. (1995) in *Enzymes of the Cholinesterase Family* (Quinn, D. M., Balasubramanian, A. S., Taylor, P., & Doctor, B. P., Eds.) pp 59−65, Plenum Press, New York.

Tan, R. C., Truong, T. N., McCammon, J. A., & Sussman, J. L. (1993) *Biochemistry 32,* 401−403.

Taylor, P., & Radić, Z. (1994) *Annu. Rev. Pharmacol. Toxicol. 34*, 281−320.

Webb, J. L. (1963) *Enzyme and Metabolic Inhibitors*, Vol. 1, pp 45−47, Academic Press, New York and London.

Westheimer, F. H. (1968) *Acc. Chem. Res. 1*, 70−78.

Wolfenden, R. (1978) in *Transition States of Biochemical Processes* (Gandour, R. D., & Schowen, R. L., Eds.) pp 555−578, Plenum Press, New York.

BI9611220

DETERMINING LIGAND ORIENTATION AND TRANSPHOSPHONYLATION MECHANISMS ON ACETYLCHOLINESTERASE BY Rp, Sp ENANTIOMER SELECTIVITY AND SITE-SPECIFIC MUTAGENESIS

Palmer Taylor[1], Natilie A. Hosea[1], Igor Tsigelny[1],
Zoran Radić[1] and Harvey A. Berman[2]

[1]Department of Pharmacology, 0636
University of California, San Diego
La Jolla, CA 92093

[2]Department of Biochemical Pharmacology
State University of New York at Buffalo
Buffalo, NY 14260

Running Title: Enantiomer Selectivity and Mutagenesis

Key Words: acetylcholinesterase, phosphonates, enantiomeric inhibitors, site-specific mutagenesis, serine phosphonylation

Supported by USPHS and DAMD Grants: GM 18360, ES 03085 and 17-95-1-5027

SUMMARY:

Acetylcholinesterase, an enzyme of the serine hydrolase family, catalyzes the rapid hydrolysis of certain carboxyl esters. Other acyl esters efficiently transacylate the enzyme with a subsequent, slow deacylation step. Of these, the phosphoryl and phosphonyl esters are perhaps of greatest mechanistic interest since individual enantiomers of known absolute stereochemistry can be isolated and their interactions with the dissymmetric enzyme active site examined. We describe here studies of a series of enantiomeric Rp- and Sp-alkylphosphonates interacting with acetylcholinesterase from mouse. Since the acetylcholinesterase is generated by recombinant DNA methods, mutant enzymes can be made with specific replacements of individual amino acid side chains. Individual amino acid replacements in the acyl pocket, the choline subsite and at the active center gorge entry have been generated, and the reaction kinetics of the mutant enzymes analyzed. These studies have shown that substitution of aliphatic amino acids for phenylalanines 295 and 297 in the acyl pocket diminishes, and in some cases, actually inverts chiral preferences. The combined structure-activity approach, where both ligand and enzyme are modified systematically, has enabled us to show that the restricted dimensions of the acyl pocket in the active center dictate enantiomeric selectivity. Moreover, the reactions of compounds of known absolute stereochemistry show three requirements for efficient transphosphonylation: (a) apposition of the phosphate with the γ-oxygen on Serine 203 to form a pentavalent, presumed trigonal bipyramidal intermediate, (b) polarization of the phosphonyl oxygen bond by its positioning in the oxyanion hole, and (c) positioning the leaving group towards the gorge exit.

INTRODUCTION:

Cloning and sequence determination of the cholinesterases have shown that these enzymes belong to a large family of serine hydrolases (1,2) whose tertiary structure is characterized by an α,β hydrolase fold (3,4). Included within this family are not only a large number of serine hydrolases, but several proteins that appear to serve non-hydrolytic functions. The first identified homologous protein, thyroglobulin (1) serves as a precursor for thyroid hormone. Subsequently, a series of proteins which appear to be involved in heterologous cell contacts and synaptogenesis (the glutactins, neurotactins, gliotactins and neuroligins) have been identified. The proteins with hydrolase activity contain a serine, glutamate (occasionally aspartate) and histidine forming a catalytic triad, with the residues found in that sequence order. The glutamate and histidine residues render the catalytic serine nucleophilic. The proteins of this family also contain at least two characteristic disulfide loops. Figure 1 details the sequence identities and residue positions in this family of proteins.

The determination of the three-dimensional structure of first the *Torpedo* (4), and then the mammalian acetylcholinesterase (AChE) (5), provided essential structural templates for the analysis of catalytic mechanism. The catalytic triad resides at the base of a narrow gorge, 18-20Å in depth, which is heavily lined with aromatic residues. The active center containing this catalytic triad is located nearly centrosymmetric to the subunit.

The cholinesterases show considerable diversity in the catalysis of hydrolytic reactions and are well known for their high catalytic efficiency (k_{cat} approaching 10^4 molecules of acetylcholine

per molecule of enzyme per sec). In addition to hydrolysis of carboxyl esters, such as in the natural substrate and neurotransmitter-acetylcholine, phosphoryl, phosphonyl, sulfonyl and carbamoyl esters or halides also react with the enzyme to form the corresponding acyl enzymes. With the latter compounds enzyme deacylation is slow, and hence they may be thought of as hemisubstrates. Since the hemisubstrates block access of acetylcholine to AChE, they are effective inhibitors of the enzyme and are employed therapeutically for this purpose (cf: 2). Trifluoroacetophenones also conjugate with the active center serine, leading to the formation of hemiketals (6, 7).

The carboxyl esters, the carbamoyl esters and the trifluoroacetophenones are all planar, with the moieties attached to the electrophilic carbon in a trigonal geometry. Hence substrate enantiomers at the reactive carbon do not exist, and the planar configuration confers minimal steric constraints for the exit of a leaving group in a gorge of limited dimensions. By virtue of their tetrahedral configuration, the phosphonates contain an asymmetric phosphorus atom when it is surrounded by chemically different groups. Such asymmetry, and the observation of a measurable chiral preference in reaction with AChE, permits direct inferences on the nature (steric; electrostatic charge) of amino acid residues within the active center of the enzyme. Moreover, the capacity to alter structure in a precise manner through site-directed mutagenesis, allowed us to manipulate not only the structure of the organic moiety undergoing reaction with the enzyme, but selected amino acid residues within the reactive pocket of the enzyme.

The studies that we describe employ enantiomeric methylphosphonates containing organic residues surrounding the asymmetric phosphorus. These agents were synthesized through reaction of *1*-(-)-ephedrine with methylphosphonothioic dichloride to form separable diastereomers, (2Rp,4S,5R) - and (2Sp,4S,5R)-2,3,4-trimethyl-5-phenyl-1,3,2-oxazaphospholidine-2-thione (Scheme 1; 1a,b) (10-12). These individual diastereomers were resolved through column chromatography, and were then subjected to reaction with an alcohol, subsequent hydrogenolysis, and then final reaction with an appropriate alkyl halide. Each chemical step in this procedure yields a predictable stereochemical outcome. This factor, coupled with resolution of a common precursor (1a,b) during an early step in the synthetic scheme, afforded unambiguous assignment of configuration of the final products.

Three families of agents were synthesized: enantiomeric cycloheptyl-, isopropyl- , and 3,3-dimethylbutyl methylphosphonothioates containing thiomethyl-, thioethyl-, and thiocholine leaving groups (see Table I). The phosphonyl ester moieties, comprising cyclic and acyclic branched alkyl groups, are seen to differ in their hydrophobicity and the steric properties with which they interact with the enzyme surface. Of particular interest are the enantiomeric 3,3-dimethylbutyl methylphosphonyl thiocholines. For these agents, since the space-filling properties of the leaving group and the alkyl ester are similar, inversion of configuration is not expected to engender substantial steric interference to binding.

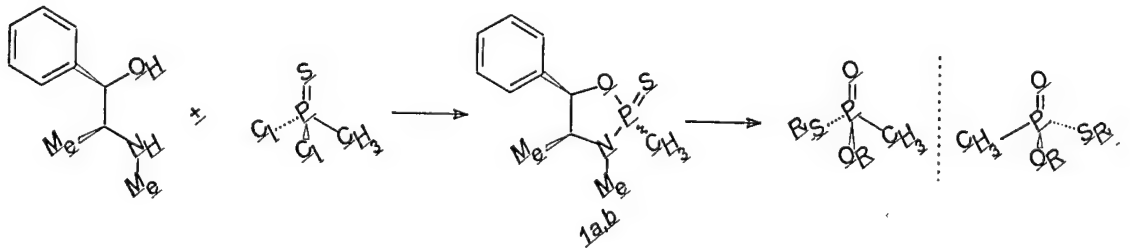

Scheme 1 - Original

Thus, analysis of the reaction of tetrahedral phosphonates with the cholinesterases adds another dimension to structure-activity considerations of ligands interacting at a target site. Herein, we examine the specificity for AChE of Rp and Sp enantiomeric phosphonates containing uncharged and charged leaving groups.

METHODS:

The procedures for site-specific mutagenesis, transfection of expression plasmids containing the cDNA of interest, selection of stable transfectants, expression of mouse AChE in human embryonic kidney cells, isolation and purification of the recombinant wild-type and mutant enzymes, and kinetic analyses have been presented previously (8, 9). The synthesis, modeling and characterization of the enantiomeric phosphonates (Table I) have also been documented previously (10-12).

RESULTS:

Studies on ligand specificity for the cholinesterases, when coupled with the recent findings from x-ray crystallography (4, 5) and site-specific mutagenesis (13-15), reveal three distinct domains on the enzyme: (a) the acyl pocket of the active center, (b) the choline binding site in the active center, and (c) a peripheral anionic site residing near the rim of the gorge. Ligands interacting with these sites and the residues that have an important involvement at these sites are detailed below (13-16).

AChE has phenylalanines at positions 295 and 297 which extend towards the substrate binding site and, as such, delimit the dimensions of this site. Butyrylcholinesterase contains leucine and isoleucine at the corresponding positions, and this accounts for its capacity to catalyze the hydrolysis of the larger substrate butyrylcholine as rapidly as acetylcholine (Fig. 2). Mutation of Phe's 295 and 297 in AChE to Leu and Ile, respectively, results in an enzyme with butyrylcholinesterase specificity (13-16), as well as substrate activation, a characteristic of butyrylcholinesterase (15). Examination of the chiral preference of a series of Rp- and Sp-alkylmethylphosphonyl thiocholines, containing cycloheptyl, isopropyl or 3, 3-dimethylbutyl ester moieties shows that up to a 230-fold enantiomeric selectivity is achieved (Table II). The chiral preference appears greater for the more bulky alkyl groups and for secondary rather than primary alkyl groups. Replacement of the Phe with Leu and Ile at these positions results in a loss of enantiomeric selectivity and, in fact, upon replacement at the 297 position, the 230-fold preference for the Sp enantiomer reverts to a slight preference for the Rp enantiomer.

Since the absolute stereochemistry of the phosphonates is known (10), the Rp and Sp enantiomers of the phosphonates can be positioned within the active center, either by docking as an initial tetrahedral complex or as a pentavalent, trigonal bipyramidal intermediate; the latter would simulate the putative transition state for an associative mechanism. In addition to the apposition of the γ-oxygen of the catalytic serine (Ser 203) with the phosphorus, there is substantial evidence for the placement of the phosphonyl oxygen in the oxyanion hole as a requirement for transphosphonylation (6, 17-19). In particular, the crystal structure of a phosphonylated intermediate with a *Candida* lipase, an enzyme homologous to AChE, shows the

insertion of its phosphonyl oxygen in the oxyanion hole (20). Upon positioning the phosphorus in bonding distance with the serine and the phosphonyl oxygen in the oxyanion hole, neither the leaving group nor the bulky alkoxyl groups can fit into the acyl pocket of limited dimensions; only the methyl group on the phosphonate should be devoid of steric hindrance in the acyl pocket. Accordingly, the orientation permits the Sp enantiomer to have the thiocholine leaving group pointed out towards the gorge entrance; whereas in the Rp enantiomer, the thiocholine is oriented behind the cycloheptyl group. Consequently, the cycloheptyl moiety is directed out of the gorge with the respective orientations of the alkoxyl and thioalkyl groups interchanged. In this configuration the leaving group would suffer from two orientational constraints: (a) the leaving group is pointed in the wrong direction and it must traverse around the bulky cycloheptyl group for exit from the gorge, (b) an apical positioning of the serine and leaving group would be limited by dimensional constraints of the gorge wall. Hence the higher reactivity of the Sp enantiomer can be explained on these grounds. However, the data are less informative regarding the reactive orientation of the less active, Rp enantiomer during the transphosphonylation reaction.

To shed further light on this issue, we have expanded our structural considerations to include uncharged thioates, as well as examined additional mutations in the enzyme. Although the uncharged thioates with methanethiol and ethanethiol as leaving groups are about 1000-fold less reactive with both the *Torpedo* (10, 12) and mouse AChE's (Tables II and III), the enantiomeric selectivities for the wild-type and mutant AChE's are virtually the same as the charged compounds. This would suggest, but not prove, that the additional charge and volume of the thiocholine have little influence on the reactive orientations of the Rp and Sp

phosphonates. In addition, the comparison of reaction rates for charged and uncharged phosphonates shows residues in the acyl pocket do not account for their reactivity differences.

Having established the above principles on ligand position, we have gone on to modify charge within the active center gorge at the positions of Glu 202, Glu 450, and Asp 74 by isosteric replacement to form the corresponding carboxamides. Glu 202 and Glu 450 reside deep within the gorge and may be involved in facilitating the polarization of the phosphonyl oxygen. Their influence on the transphosphonylation reaction shows no preference for the charged or uncharged leaving group. Moreover, these mutations do not affect appreciably the chiral preference (Table IV). However, the isosteric mutation of Asp 74 to the neutral Asn, results in a marked reduction of transphosphonylation for the charged phosphonates but not the uncharged compounds. In fact, there appears to be a slight increase in the rate of transphosphonylation for the uncharged compounds (Table IV).

Despite the great reductions in rate of phosphonates of the cationic enantiomers, enantiomeric preference for the Rp and Sp phosphonylation does not change with the Asp74Asn mutation. This suggests that the trimethylammonio moieties in the Rp and Sp enantiomers reside at similar distances from Asp 74 in the transition state; otherwise, it is unlikely that the Coulombic influence would be virtually identical for the two enantiomers.

DISCUSSION:

The findings reviewed here show two distinct linkage relationships. Chiral preference is

dependent on the dimensions of the acyl pocket which are governed by the amino acid side chains directed towards the active center. Thus, chiral selectivity is largely independent of the charge and apparent dimensions of the leaving group. By contrast, the anionic side chain (Asp 74) near the gorge entry is linked to the charge on the leaving group and the enhanced reactivity of the cationic alkylphosphonates is eliminated by the isosteric substitution of an Asn at this position. Although this substitution affects rates of reaction markedly, chiral selectivity is largely unaffected.

The diminished reactivity of the Rp enantiomer results from steric constraints precluding the simultaneous: (a) positioning of the phosphorus to enable attack by the γ-oxygen of the serine, (b) insertion of the oxygen in the oxyanion hole, and (c) positioning the leaving group to extend out the gorge exit. Mutation of Phe 297 to Ile eliminates the apparent steric hindrance, and this would account for the greatly increased reactivity of the Rp compound.

Recently, it was shown that the boundary region to the active center contains a rather thin wall and a conformational change might yield a "back door" opening suitable for product removal (21). This region outlines a portion of the choline binding site. Should such an alternative portal exist, it would be better situated for the thiocholine exit of the Rp enantiomers, yet we find the Rp enantiomers acylate some 230-fold more slowly than the Sp enantiomers. Hence, the transphosphonylation rates do not lend support to a "back door" hypothesis for removal of a thiocholine moiety.

Over sixty years ago, Eason and Stedman proposed that stereospecificity in drug action and in catalytic processes was a consequence of a three-point attachment between the chiral compound and a dissymmetric macromolecular surface (22). Although the original binding site was often modeled on a planar surface, the hypothesis has withstood the tests of time to explain stereospecificity of drug action. Even with the addition of three-dimensional structures as templates for the interaction of small ligands, the principle of a *minimal* three-point attachment can be shown to be applicable to chiral ligands and AChE.

Shown in Figure 5 is an analysis of docking of a pentavalent transition state for the Rp and Sp enantiomers of cycloheptyl methylphosphonothiocholine using molecular dynamics with further minimization to achieve a low energy conformation of the docked ligand (9). Three dimensions can be considered here. The first is in the reaction bond distance and is displayed in the Z-axis direction; this becomes fixed for the γ oxygen on serine 203 attacking the phosphorus. Although the precise transition state cannot be described, it is assumed that the attacking serine and the leaving group adopt apical positions. In turn, the three remaining groups would be equatorially disposed around the phosphorus. Hence the plane of phosphorus and the three equatorial groups define the Z dimension. A fixed optimal reaction distance should hold irrespective of whether we consider the transition state for transphonylation to be associative or dissociative in nature. The remaining two positions, the oxygen in the oxyanion hole and the leaving group directed out of the gorge, are then analyzed in the docked low energy conformations minimized following molecular dynamics. Clearly, only the Sp enantiomer reproducibly yields the simultaneous optimization of positions for the phosphonyl oxygen and the

leaving group. In the case of the oxyanion hole, interaction is dependent on hydrogen bonding distances between the three candidate donor hydrogens (amide hydrogens on Gly121, Gly122 and Ala201) and the phosphonyl oxygen. Data in Figure 5 are represented as an average of the three distances for these potential hydrogen bonds. For the thiocholine leaving group, we show the data as a deviation from the apical position which would be 180° from the γ-oxygen of the serine. Hence, this analysis and the positioning of the three critical groups are compatible with the overall kinetics.

Our examination of enantiomeric selectivity is part of a larger investigation of ligand interactions with the active center of the cholinesterases. Site-specific mutations have been made at other positions on AChE and the kinetics analyses for three classes of charged and uncharged congeneric ligands have been examined (8, 9). The trifluoroketones conjugate directly with the active center serine to form a hemiketal (6, 7) without loss of a leaving group. Their reaction with AChE approaches the diffusion limitation. Second, the alkylphosphonates, sulfonates and carbamoyl esters form relatively stable phosphonyl, sulfonyl and carbamoyl esters with the active center serine with the loss of a leaving group. The stability of the newly formed acyl serine intermediate typically allows for direct study of the acylation step. Third, the carboxyl esters show rapid turnover because of the near diffusion controlled acylation step and a rapid deacylation. Under physiologic concentrations it is thought that the acylation and deacylation steps are of comparable magnitude allowing for a fractional build up of acylenzyme intermediate (23). Only steady-state kinetics for catalysis of the carboxyl esters can be readily monitored, and the characterization of intermediate species has proven more elusive.

Enantiomeric selectivity of the alkylphosphonates is of considerable practical significance. The toxic nerve gas soman contains two chiral centers, one on the phosphorus and one on the attached carbon substituent yielding four diastereomers. The four diastereomers have very different rates of reaction and overall stability in the body (24). Similarly, the widely used insecticide malathion possesses a chiral center on a carbon side chain. By virtue of rearrangement around the phosphorus, it can form diastereomers possessing distinct toxicities (25).

Such enantiomeric or diastereomeric selectivity can be understood on the basis of fundamental steric and electrostatic properties of the groups surrounding the asymmetric phosphorus, and the interactions they encounter with the side chains of amino acids in spatial proximity with the reactive serine. As seen here, the chemistry of organophosphorus agents in combination with techniques of site-directed mutagenesis allow one not only to estimate the prevalent physical interactions at play but the identity of the individual amino acids that govern such interactions.

REFERENCES:

1. Schumacher, M., Camp, S., Maulet, Y., Newton, M., MacPhee-Quigley, K., Taylor, S.S., Friedmann, T. and Taylor, P. Primary structure of *Torpedo californica* acetylcholinesterase deduced from cDNA sequence. *Nature* 319: 407-409 (1986).

2. Taylor, P. and Radić, Z. The cholinesterases: from genes to proteins. *Ann. Rev. Pharmacol. & Toxicol.* 34: 281-320 (1994).

3. Cygler, M., Schrag, J.D., Sussman, J.L., Harel, M., Silman, I., Gentry, M.K. and Doctor, B.P. Relationship between sequence conservation and three-dimensional structures in a large family of esterases, lipases and related proteins. *Protein Science* 2: 366-382 (1993).

4. Sussman, J.L., Harel, M., Frolow, F., Oefner, C., Goldman, A., Toker, L. and Silman, I. Atomic structure of acetylcholinesterase from *Torpedo californica*: a prototypic acetylcholine-binding protein. *Science* 253: 872-879 (1991).

5. Bourne, Y., Taylor, P. and Marchot, P. Acetylcholinesterase inhibition by fasciculin: crystal structure of the complex. *Cell* 83: 503-512 (1995).

6. Nair, H.K., Seravalli, J., Arbuckle, T. and Quinn, D.M. Molecular recognition in acetylcholinesterase catalysis: free-energy correlations for substrate turnover and inhibition by trifluoroketone transition state analogs. *Biochemistry*: 33, 8566-8576 (1994).

7. Harel, M., Quinn, D.M., Nair, H.K., Silman, I. and Sussman, J.L. The x-ray structure of a transition state analog complex reveals the molecular origins of catalytic power and substrate specificity of the cholinesterases. *J. Am. Chem. Soc.*118: 2340-2346 (1996).

8. Hosea, N.A., Berman, H.A. and Taylor, P. Specificity and orientation of trigonal carboxyl esters and tetrahedral alkylphosphonyl esters in cholinesterases. *Biochemistry* 34: 11528-11536 (1995).

9. Hosea, N.A., Radić, Z., Tsigelny, I., Berman, H.A., Quinn, D.M. and Taylor, P. Aspartate 74 as a primary determinant in acetylcholinesterase governing specificity to cationic organophosphonates. *Biochemistry* 35: 10995-11004 (1996).

10. Berman, H.A. and Leonard, K. Chiral reactions of acetylcholinesterase probed with enantiomeric methylphosphonothioates: non-covalent determinants of enzyme chirality. *J. Biol. Chem.* 264: 3942-3950 (1989).

11. Berman, H.A. and Decker, M.M. Kinetic, equilibrium and spectroscopic studies on dealkylation of alkylorganophosphonyl acetylcholinesterase. *J. Biol. Chem.* 261: 10646-10652 (1986).

12. Berman, H.A. and Decker, M.M. Chiral nature of covalent methylphosphonyl conjugates of acetylcholinesterase. *J. Biol. Chem.* 264: 3951-3956 (1989).

13. Vellom, D.C., Radić, Z., Li, Y., Pickering, N.A., Camp, S, and Taylor, P. Amino acid residues controlling acetylcholinesterase and butyrylcholinesterase specificity. *Biochemistry* 32: 12-17 (1993).

14. Ordentlich, A., Barak, D., Kronman, C., Flashner, Y., Leitner, M., Segall, Y., Ariel, N., Cohen, S., Velan, B. and Shafferman, A. Dissection of the human acetylcholinesterase active center determinants of substrate specificity. *J. Biol. Chem.* 268: 17083-17095 (1993).

15. Radić, Z., Pickering, N.A., Vellom, D.C., Camp, S. and Taylor, P. Three distinct domains in the cholinesterase molecule confer selectivity for acetyl- and butyrylcholinesterase inhibitors. *Biochemistry* 32: 12074-12084 (1993).

16. Harel, M., Sussman, J.L., Krejci, E., Bon, S., Chanal, P., Massoulié, J., Silman, I. Conversion of acetylcholinesterase to butyrylcholinesterase, modeling and mutagenesis. *Proc. Natl. Acad. Sci. USA.* 89: 10827-10831 (1992).

17. Taylor, P. and Jacobs, N.M. Interaction between *bis*-quaternary ammonium ligands and acetylcholinesterase---complex formation studies by fluorescence quenching. *Mol. Pharmacol.* 10: 93-107 (1974).

18. Grochulski, P., Bouthillier, F., Kazlauskas, R.J., Serreqi, A.N., Schrag, J.D., Ziomek, E. and Cygler, M. Analogs of reaction intermediates identify a unique substrate binding sites in *Candida rugosa*. *Biochemistry* 33: 3494-3500 (1994).

19. Zhao, Q., Kovach, I.M., Bencsura, A. and Papathanassia, A. Enantioselective and reversible inhibition of trypsin and alpha-chymotrypsin by phosphonate esters. *Biochemistry* 33: 8128-8138 (1994).

20. Cygler, M., Grochulski, P., Kazlauskas, R.J., Schrag, J.D., Bouthillier, F., Rubin, B., Serreqi, A.N. and Gupta, A.K. A structural basis for the chiral preferences of lipases. *J. Am. Chem. Soc.* 116: 3180-3186 (1994).

21. Gilson, M.K., Straatsma, J.P., McCammon, J.A., Ripoll, D.R., Faerman, C.H., Axelsen, P.H., Silman, I., Sussman, J.L. Open "back door" in a molecular dynamics simulation of acetylcholinesterase. *Science* 263: 1276-1278 (1994).

22. Eason, L.M. and Stedman, E. Studies on the relation between chemical constitution and physiological action. *Biochem. J.* 27: 1257-1266 (1933).

23. Froede, H.C. and Wilson, I.B. Direct determination of acetyl enzyme intermediate in the acetylcholinesterase-catalyzed hydrolysis of acetylcholine and acetylthiocholine. *J. Biol. Chem.* 259: 11010-11013 (1984).

24. de Jong, L.P., van Dijk, C., Berhitoe, D., and Benschop, H.P. Hydrolysis and binding of a toxic stereoisomer of soman in plasma and tissue homogenates. *Biochem. Pharm.* 46: 1413-1419 (1993).

25. Berkman, C.E., Thompson, C.M. and Perrin, S.R. Synthesis, absolute configuration and analysis of malathion, malaoxon and isomalathion enantiomers. *Chem. Res. Toxicol.* 6: 718-723 (1993).

26. Auld, V.J., Fetter, R.D., Broadie, K. and Goodman, C.S. Gliotactin, a novel transmembrane protein on peripheral glia, is required to form the blood-brain barrier in Drosophila. *Cell* 81: 757-767 (1995).

27. Ichtchenko, K., Nguyen, T. and Sudhof, T.C. Structures, alternative splicing and neurexin binding of multiple neuroligins. *J. Biol. Chem.* 271: 2676-2682 (1996).

Figure Legends:

Figure 1: The cholinesterase superfamily is composed of an expanding number of proteins with documented homology in sequence but diverse and eclectic functions. Shown by the various hatch and stippled markings are the regions of sequence identity and specialized and/or alternatively spliced regions of sequence. The bars above each linear sequence denote conserved cysteines and intra-subunit disulfide bonds. The S, E (D) and H symbols denote the essential serine, glutamate (aspartate) and histidine in each catalytic triad. Note that the glutactins, neurotactins, gliotactins, thyroglobulins and neuroligins do not contain all three essential residues, consistent with their lack of catalytic activity. (cf: 1, 26, 27).

Figure 2: Positions of acetylcholine in native (A) and in Phe295Leu; Phe297Ile (B) acetylcholinesterases; Structures were developed from the crystallographic coordinates of *Torpedo* AChE (4) and are based on the probable positioning of the substrate.

Figure 3: Stereoviews of Sp- and Rp-cycloheptyl methylphosphonothiocholine docked in the active center of native (A) and Phe297Ile (B) acetylcholinesterase. Residues of the acyl pocket (Phe 295 and 297), choline binding subsite (Trp 86, Tyr 337, Glu 202) are shown (cf: ref. 8 for details).

Figure 4: Sp-cycloheptyl methylphosphonothiocholine docked in the active center of acetylcholinesterase. The view is a 90° side view from figure 3 to show the orientation of the thiocholine moiety with respect to the gorge exit and Asp 74. A portion of the cholinesterase molecule is cut away in order to show an unobstructed view of the inhibitor (cf: refs. 8, 9 for details).

Figure 5: Molecular dynamics simulation followed by energy minimization of a docked Sp (closed circles) and Rp (open circles) cycloheptyl methylphosphonothiocholine in a reversible complex with acetylcholinesterase. The phosphorus group is docked within bonding distance with the γ-oxygen of serine 203 in the enzyme. This position along the Z-axis then becomes defined by the plane X,Y. A productive conformation is assumed to require: (a) the appropriate Ser-O-P distance on the

Z axis, (b) insertion of the phosphonyl oxygen in the oxyanion hole (Y axis): a mean hydrogen bonding distance of 3-4 Å from the amide backbone hydrogens of Gly 121, Gly 122 and Ala 204 and (c) an orientation of the leaving group directed towards gorge entrance. The ideal position is assumed to be 180 degrees from the attacking serine oxygen placing the serine oxygen and the leaving group in apical positions and the remaining three groups in equatorial positions. The deviations reflect the difference in distances for the quaternary nitrogen between the energy minimized position and that expected for apical positioning (180°) of the serine γ-oxygen and the leaving group (9).

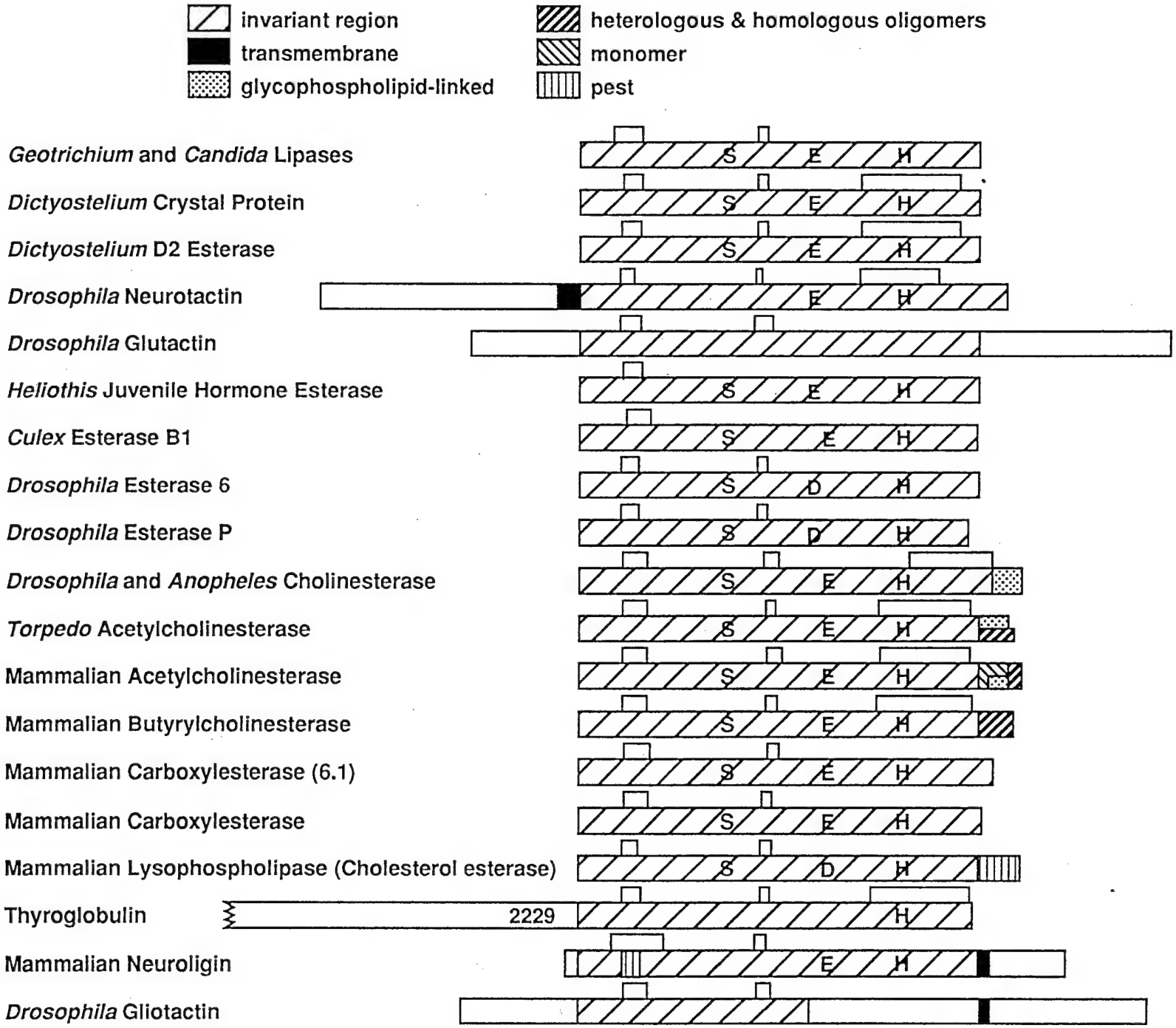

TayloPpha7893*DI1/111593dme

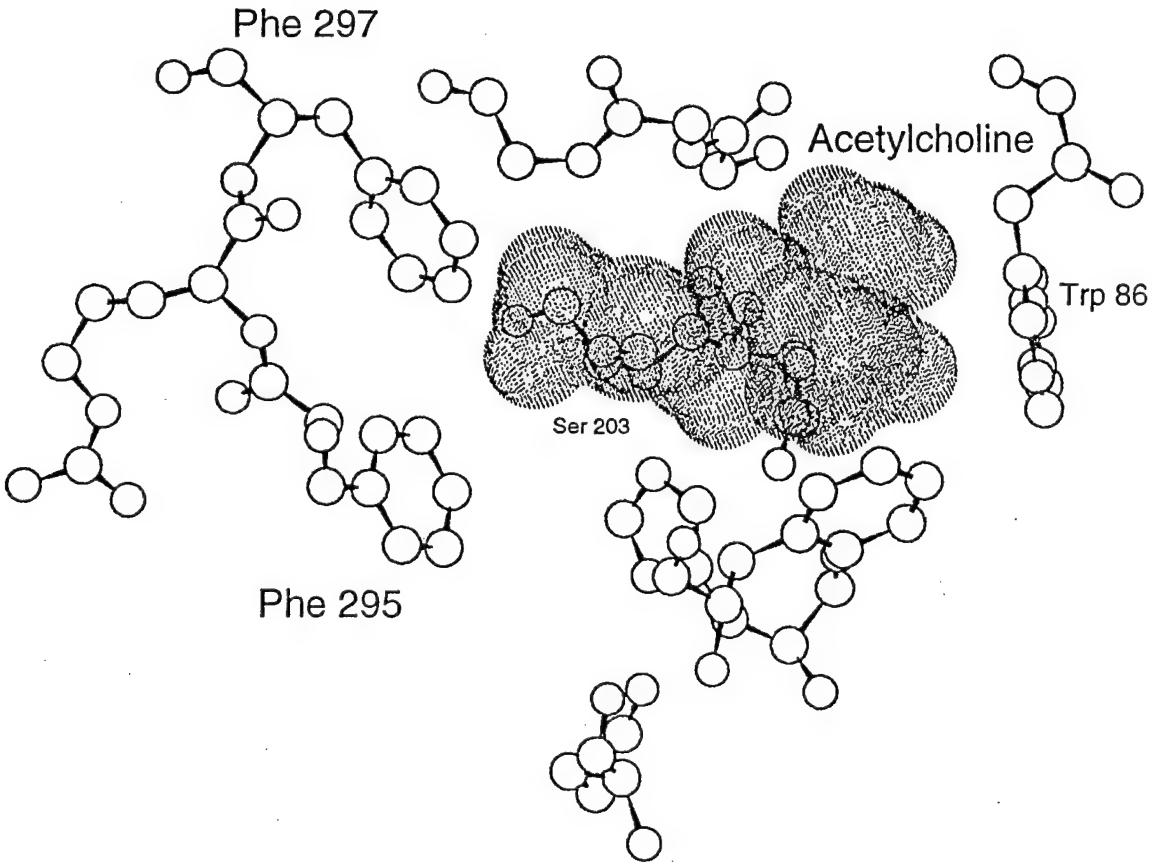
Phe 297
Acetylcholine
Trp 86
Ser 203
Phe 295

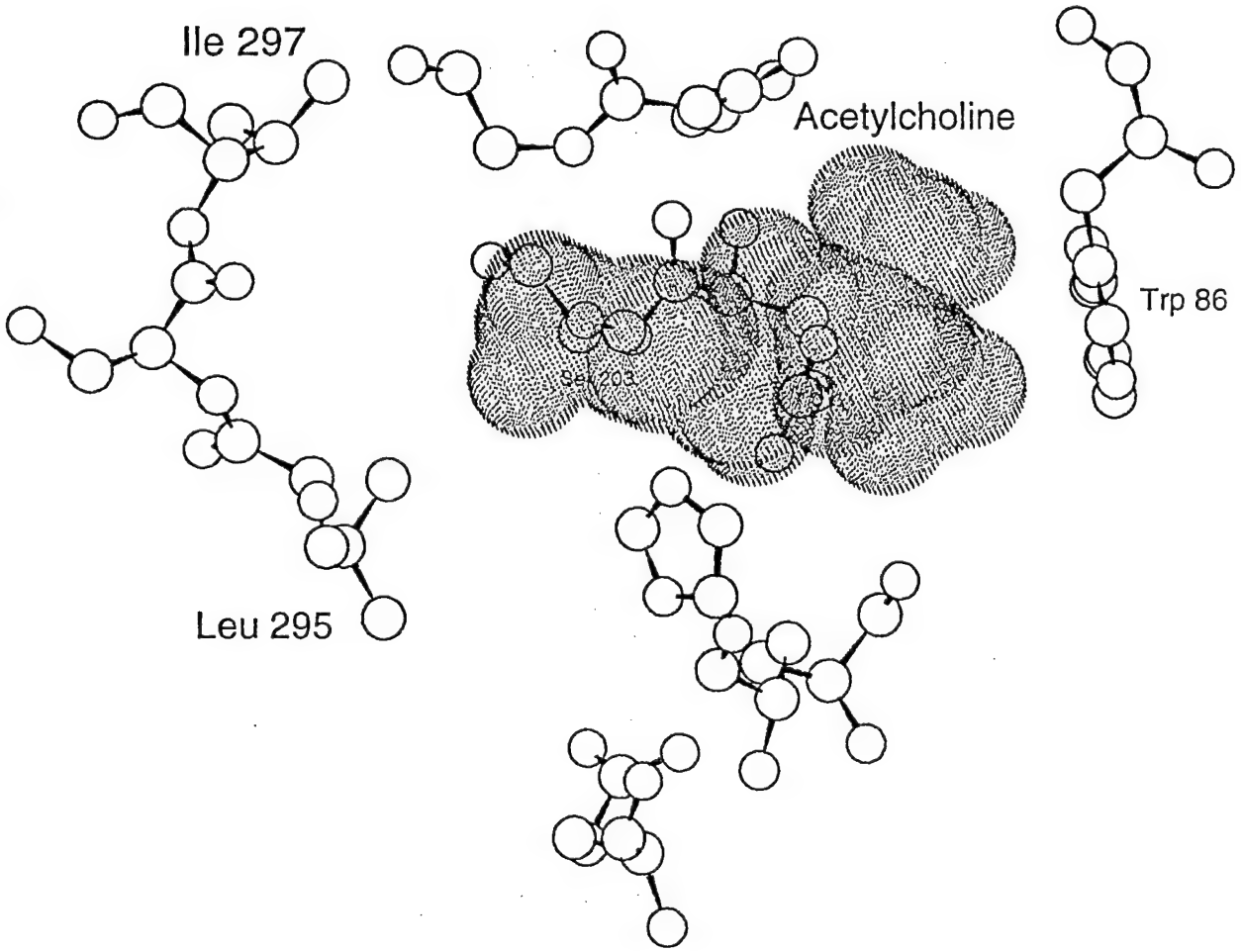
Ile 297
Acetylcholine
Trp 86
Leu 295

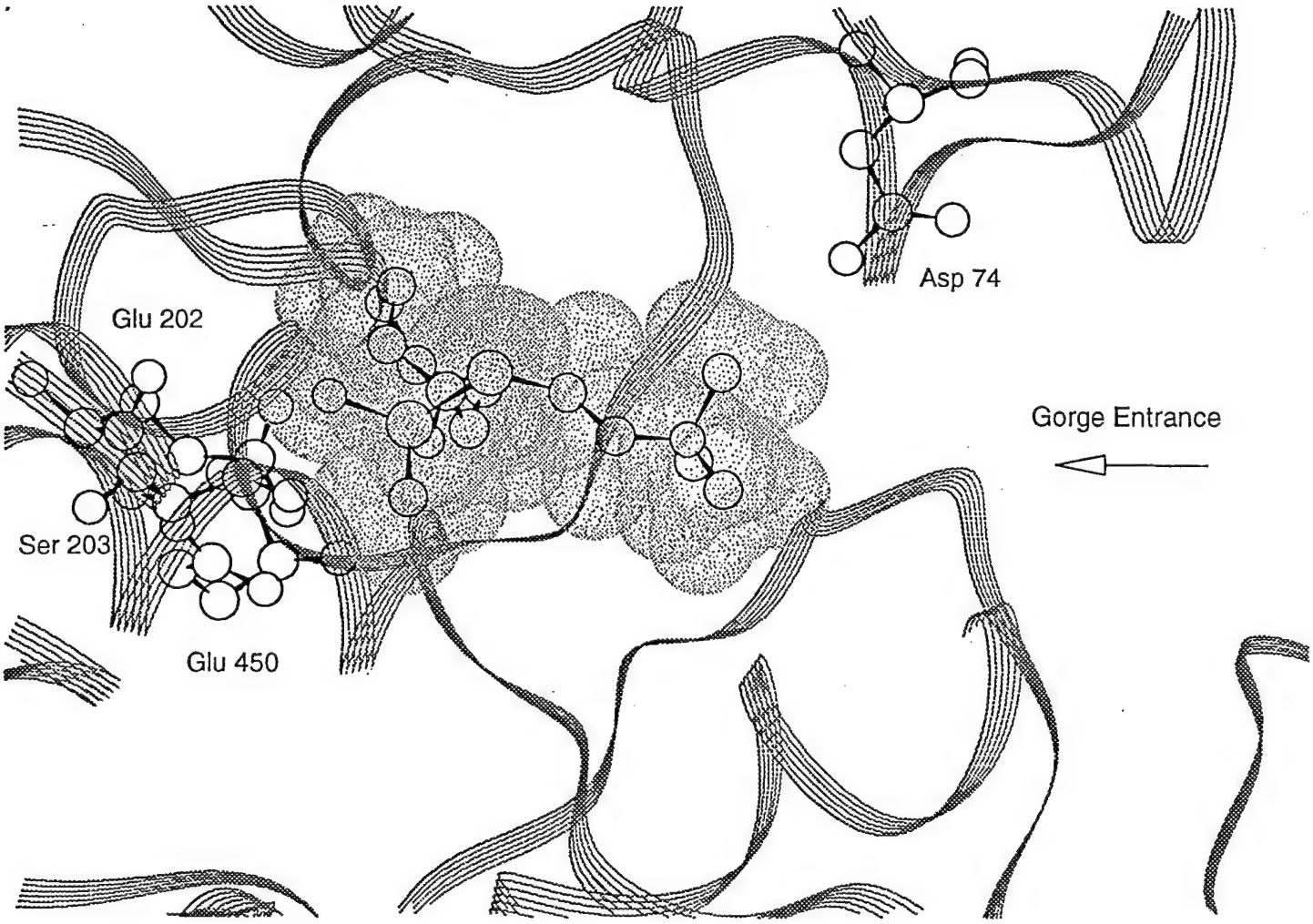
Asp 74
Glu 202
Gorge Entrance
Ser 203
Glu 450

Sp-Cycloheptyl Methylphosphonyl Thiocholine

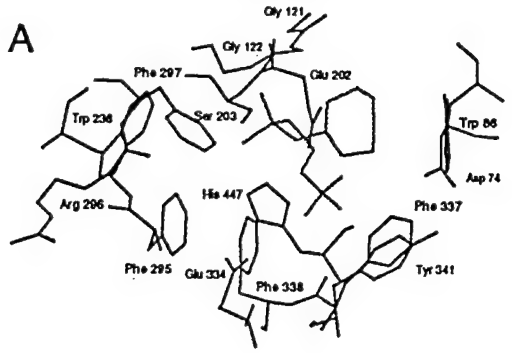

Sp-Cycloheptyl Methylphosphonyl Thiocholine

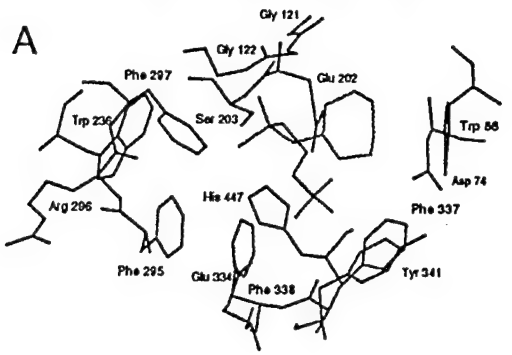

Rp-Cycloheptyl Methylphosphonyl Thiocholine

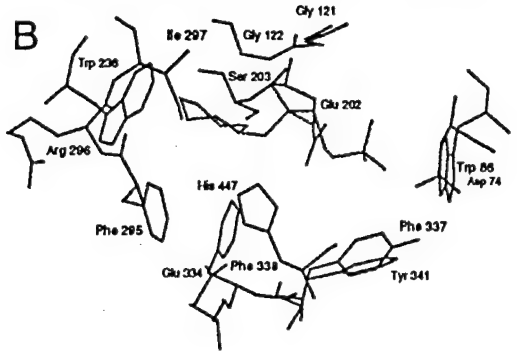

Rp-Cycloheptyl Methylphosphonyl Thiocholine

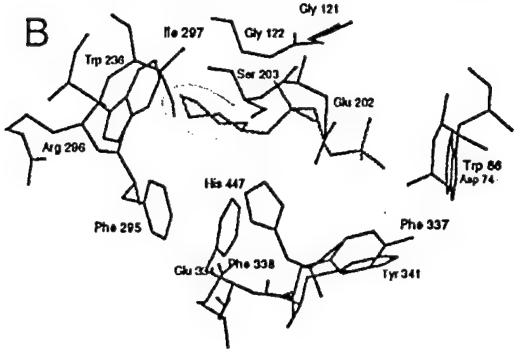

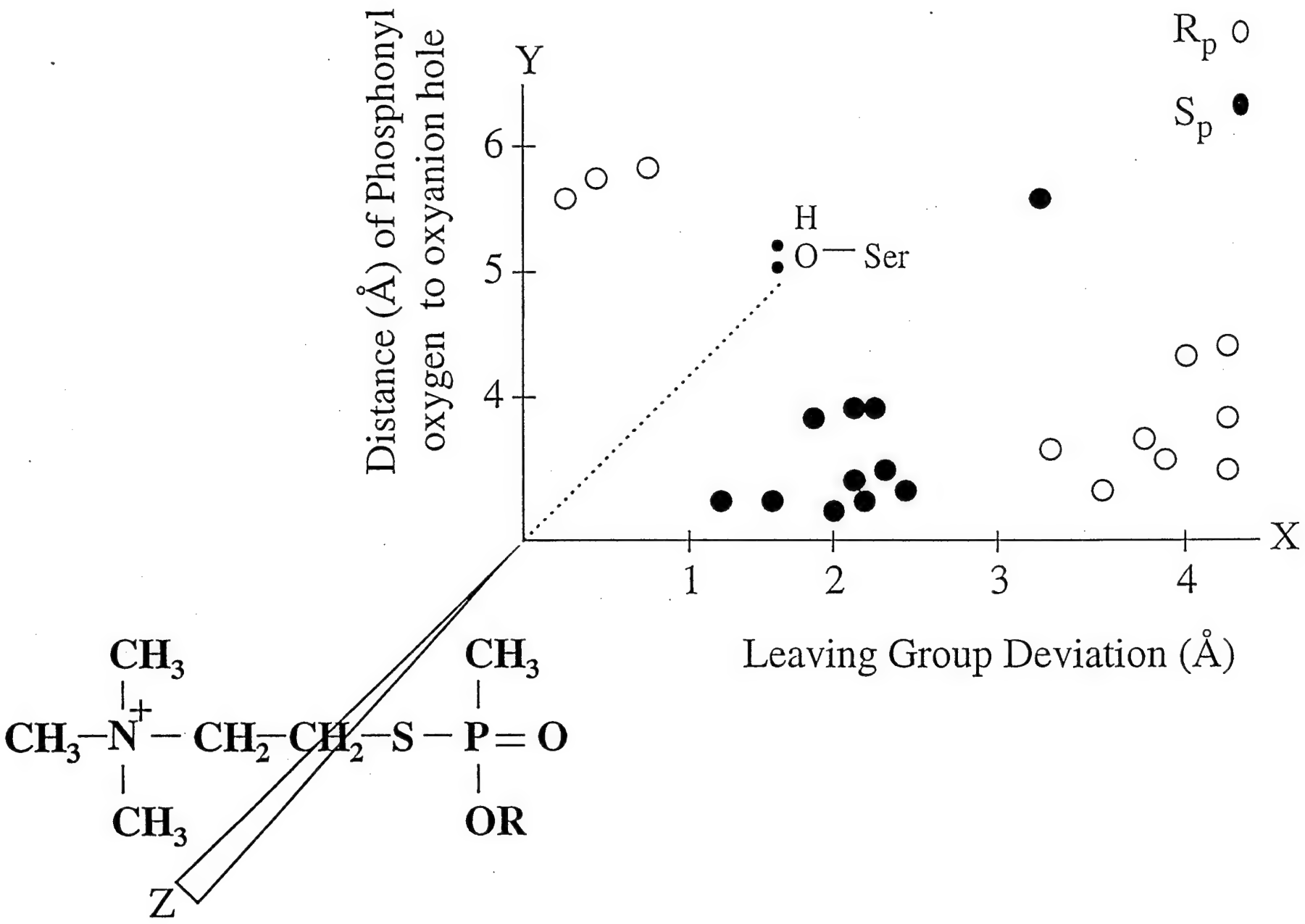
Distance (Å) of Phosphonyl oxygen to oxyanion hole
Y
6
5
4
H
O — Ser
R_p
S_p
1
2
3
4
X
Leaving Group Deviation (Å)
CH_3
$CH_3—N^+—CH_2—CH_2—S—P=O$
CH_3
OR
Z

Table I: Structures of compounds employed. CHMP, iPrMP and DMBMP refer to cycloheptyl-, isopropyl- and 3,3-dimethylbutyl- methylphosphonyl.

	Sp	Rp
CHMP thiocholine	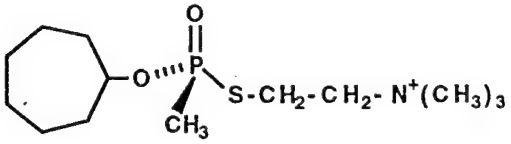	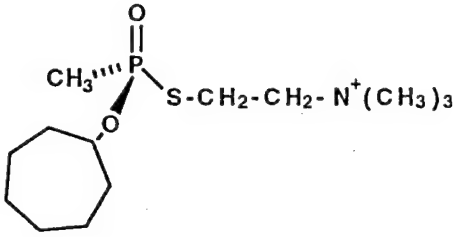
iPrMP thiocholine	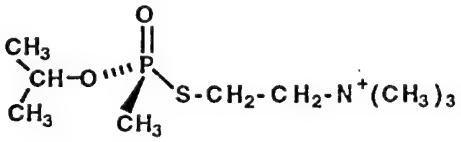	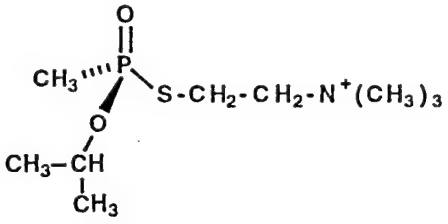
DMBMP thiocholine	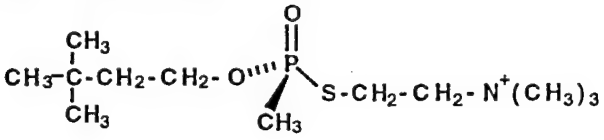	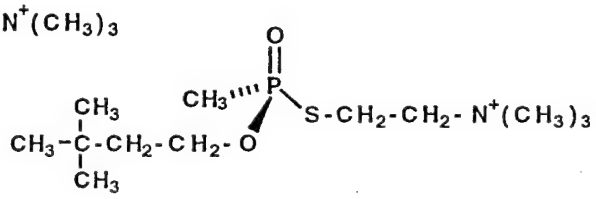
CHMP thiomethylate	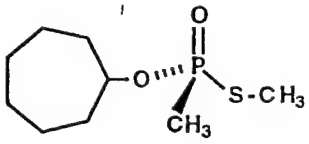	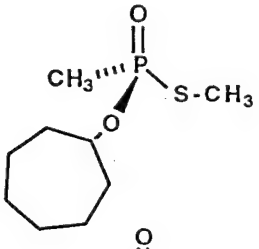
CHMP thioethylate	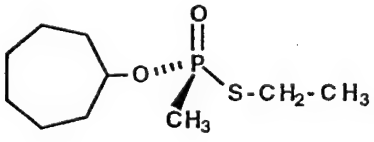	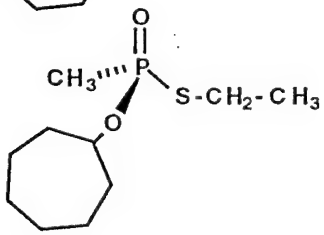

Table II: Rates[a] of Transphosphonylation by Rp- and Sp- Alkyl Methylphosphonyl Thiocholine with Wild-type and Acyl Pocket Mutations of Mouse Acetylcholinesterase

Enzyme	Alkyl Group								
	Cycloheptyl			Isopropyl			3,3-Dimethylbutyl		
	Sp	Rp	Sp/Rp	Sp	Rp	Sp/Rp	Sp	Rp	Sp/Rp
AChE (Wild-type)	190,000	820	230	16,000	140	110	360,000	19,000	19
Phe 295 Leu	66,000	8,700	7.6	3,400	1,200	3	140,000	10,000	14
Phe 297 Ile	16,000	62,000	0.3	950	1,200	0.8	56,000	12,000	5

[a]Rate constants given as 10^3/Mmin; the standard error of the mean from typically three experiments was 10-15%. Data were obtained from reference 8.

Table III: Rates[a] of Transphosphonylation by Rp- and Sp-Cycloheptyl Methylphosphonyl Thioate Possessing Charged Leaving Groups

Enzyme	Leaving Group					
	-S-CH_3			-S-CH_2-CH_3		
	Sp	Rp	Sp/Rp	Sp	Rp	Sp/Rp
AChE (Wild-type)	310	1.7	180	74	0.16	460
Phe 295 Leu	340	2.9	120	160	1.0	160
Phe 297 Ile	55	22	2.5	55	26	2.1

[a]Rate constants are given as 10^3/Mmin; the standard error the mean from typically three experiments was 10-15%. Data was obtained from reference 8.

Table IV: Rates[a] of Transphosphonylation by Rp- and Sp-Cycloheptyl Methylphosphonyl Thioate Possessing Charged and Uncharged Leaving Groups

Enzyme	Leaving Group								
	$-S-CH_2-CH_2-N^+(CH_3)_3$			$-S-CH_3$			$-S-CH_2-CH_3$		
	Sp	Rp	Sp/Rp	Sp	Rp	Sp/Rp	Sp	Rp	Sp/Rp
AChE (Wild-type)	190,000	820	230	310	1.7	180	74	0.16	460
Asp 74 Asn	1,400	8.0	180	530	2.3	230	190	0.41	460
Glu 202 Gln	21,000	130	160	14	0.060	230	2.3	0.014	160
Glu 450 Gln	1,400	23	61	9	0.050	180	14	0.018	780

[a]Rate constants are given as 10^3/Mmin; the standard error the mean from typically three experiments was 10-15%. Data were obtained from reference 9.

THE CHOLINESTERASES AT ATOMIC RESOLUTION: APPLICATION OF STRUCTURAL STUDIES TO MECHANISMS OF INHIBITION

Palmer Taylor[1], Natilie Hosea[1], Pascale Marchot[1], Zoran Radic[1] and Harvey A. Berman[2]

[1]Dept. of Pharm., 0636, UCSD, La Jolla, CA 92093; [2]Dept. of Biochem. Pharm., St. U. of NY at Buffalo,Buffalo, NY 14210

Structural studies of the cholinesterases over the last decade have provided a template for the family of enzymes at atomic resolution. These studies began with determination of sequence, proceeded with molecular cloning and expression by recombinant DNA methods and culminated with crystallographic studies of three-dimensional structure. Not only has this approach yielded structures suitable for a detailed analysis of the mechanism of catalysis and inhibition, but it also lead to new directions in which the cholinesterases themselves or their mutuant forms can be expressed in large amounts and become prophylatic modalities or antidotes. Since the cholinesterases were found to define a large superfamily of proteins, the structural relationships between these proteins have important implications for other fields of biology as well.

This work was supported by the U.S. Army Medical Research and Material Command under Grant DAMD 17-95-1-5027.

Introduction

The primary structure of the first cholinesterase was reported only a decade ago (1). Five years ago a high resolution crystal structure of *Torpedo* cholinesterase was solved (2), and in the past year, the first mammalian cholinesterase structure was reported (3). The sequence and the three dimensional structural information that has emerged from protein sequencing, recombinant DNA techniques and x-ray crystallography, has not only brought structural resolution from the molecular to an atomic level, but it has also enabled investigators to produce substantial quantities of the cholinesterases from recombinant DNA sources and to study systematically the influence of particular residues on enzyme catalysis and inhibition.

Details have been presented in review articles (4;5) and in recent conference proceedings (6;7). Presentations of Drs. Sussman, Shafferman, Soreq, Lockridge and Broomfield in this series will amplify these points and provide the appropriate detail. Moreover, studies of Drs. Lockridge and Broomfield (8) and those from Dr. B.P. Doctor's group (9) illustrate some of the practical applications that these techniques are providing in the use of recombinant DNA-derived enzymes as potential prophylactic agents, antidotes and *in vitro* detoxificants. Investigations involving recombinant DNA and high resolution structural techniques require a long term investment, and the USAMDC leadership at Edgewood and Fort Detrick deserve considerable credit for their foresight and unwaivering commitment to this area of research.

The potential benefits for society are likely to extend even beyond the area of cholinesterases for the structure of these enzymes has defined a large superfamily of proteins, only some of which have hydrolase activity. This was evident in the initial discovery which showed that thyroglobulin (the precursor of thyroid hormone) was homologous to cholinesterase (1), but has taken on increasing importance with the finding that the tactin (10) and the neuroligin (11) families of proteins fall into the cholinesterase superfamily. These families of proteins represent more recent discoveries, but may be as extensive in their diversity as the members of the superfamily which have serine hydrolase activity. Gliotactin appears to play a role in the formation of a proper blood-brain barrier, while the neuroligins are intimately involved in the selectivity of formation of synaptic contacts through interactions with neurexins. Hence, research into cholinesterases structure has yielded important dividends in unanticipated areas of developmental neurobiology.

Figure 1 shows the sequence relationships between the cholinesterase superfamily as well as the regions where alternative splicing of the newly formed pre-mRNA occurs; the latter mechanism appears pivotal in contributing to the diversity of this family of proteins. The conserved sequence

gives rise to a three dimensional structural motif known as the α,β hydrolase fold (12). Interestingly, this motif is even found in proteins, such as certain carboxypeptidases, diene lactone hydrolase and a haloalkane dehalogenase where the sequence homology is not evident. This further attests to the importance and eclectic nature of this protein matrix in biology.

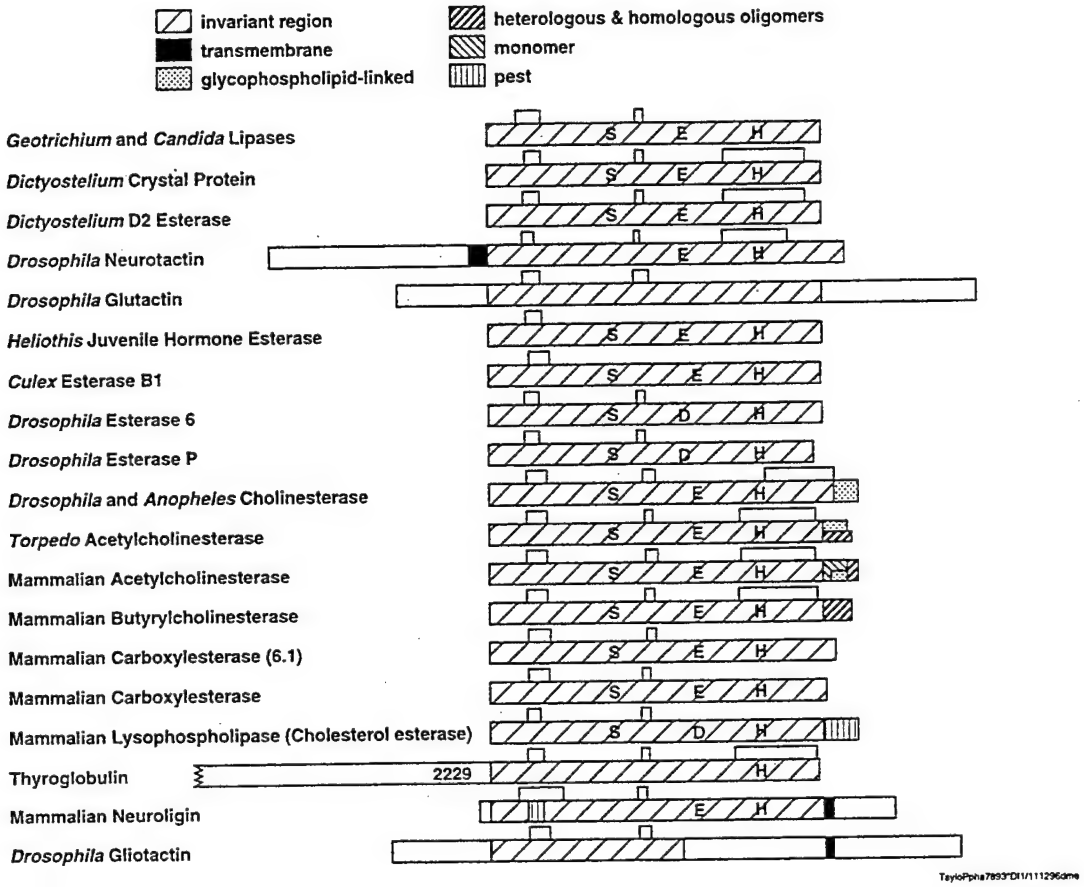

Figure 1: The cholinesterase superfamily is composed of an expanding number of proteins with documented homology in sequence but diverse and eclectic functions. Shown by the various hatch and stippled markings are the regions of sequence identity and specialized and/or alternatively spliced regions of sequence. The bars above each linear sequence denote conserved cysteines and intra-subunit disulfide bonds. The S, E (D) and H symbols denote the essential serine, glutamate (aspartate) and histidine in each catalytic triad. Note that the glutactins, neurotactins, gliotactins, thyroglobulins and neuroligins do not contain all three essential residues, consistent with their lack of hydrolase activity. (cf: 5, 10,11).

Inhibition Selectivity for the Cholinesterases

Studies on ligand specificity for the cholinesterases, when coupled with the recent findings from x-ray crystallography (2,3,12) and site-specific mutagenesis (13-16),

reveal three distinct domains on the enzyme: (a) the acyl pocket of the active center, (b) the choline binding site in the active center, and (c) a peripheral anionic site residing near the rim of the gorge. Ligands interacting with these sites and the residues that have an important involvement at these sites are detailed below and in previous reviews (4-7).

AChE has phenylalanines at positions 295 and 297 which extend towards the substrate binding site and, as such, delimit the dimensions of this site. Butyrylcholinesterase (BuChE) contains leucine and isoleucine at the corresponding positions, and this accounts for its capacity to catalyze the hydrolysis of the larger substrate butyrylcholine as rapidly as acetylcholine. Mutation of Phe's 295 and 297 in AChE to Leu and Ile, respectively, results in an enzyme mimicking BuChE specificity (13-16), as well as substrate activation, a characteristic of BuChE (14). Moreover, certain BuChE selective inhibitors such as isoOMPA lose their selectivity upon mutation of the phenylalanines (13-16). Hence it is well established that acyl pocket size is a primary determinant of selectivity.

The second site constitutes the aromatic and electronegative region around the choline binding site (15-17). This is the area when the Alzheimer drug, tacrine (tetrahydroaminoacridine) binds, and π bonding and steric constraints, respectively, dictate specificity of huperzine for AChE (18) and ethopropazine for BuChE (16), two agents which show selectivity for this site. Residues such as Trp 86, Tyr 337 and Glu 202 are major contributors to binding at this site.

Finally, it has long been known that AChE contains a peripheral anionic site, physically removed from the active center and exhibiting a distinct inhibitor specificity (19; 20). This site is also the location of binding of the peptide inhibitor fasciculin (21). The selectivity of fasciculin for AChE arises largely from three aromatic residues (Trp 284, Tyr 72 and Tyr 124) that lie at the lip of the gorge. Their mutation results in close to a 10^8 fold reduction in affinity with dissociation constants increasing from ~2pM to 0.2mM (22).

Catalytic Specificity of the Cholinesterases

The cholinesterases show considerable diversity in the catalysis of hydrolytic reactions and are well known for their catalytic efficiency (k_{cat} approaching 10^4 moles of acetylcholine per mole of enzyme per sec). In addition to hydrolysis of carboxyl esters, such as with the natural neurotransmitter-acetylcholine, phosphoryl, phosphonyl, sulfonyl and carbamoyl esters or halides also react with the enzyme to form the corresponding acyl enzymes. With the latter compounds enzyme deacylation is slow, and hence they may be thought of as hemisubstrates. Since the hemisubstrates block access of acetylcholine to AChE, they are effective inhibitors of the enzyme and are employed thera-

peutically for this purpose. Trifluoroacetophenones conjugate with the active center serine, leading to the formation of hemiketals without loss of a leaving group (23).

Carboxyl esters, carbamoyl esters and trifluoroacetophenones are all planar, with the moieties attached to the electrophilic carbon in a trigonal geometry. Hence substrate enantiomers at the reactive carbon do not exist, and the planar configuration confers minimal steric constraints for the exit of a leaving group in a gorge of limited dimensions. By contrast, the phosphonates are tetrahedral, show chirality and impose additional steric constraints in the reaction mechanism.

Stereospecificity of Organophosphate and Oxime Action

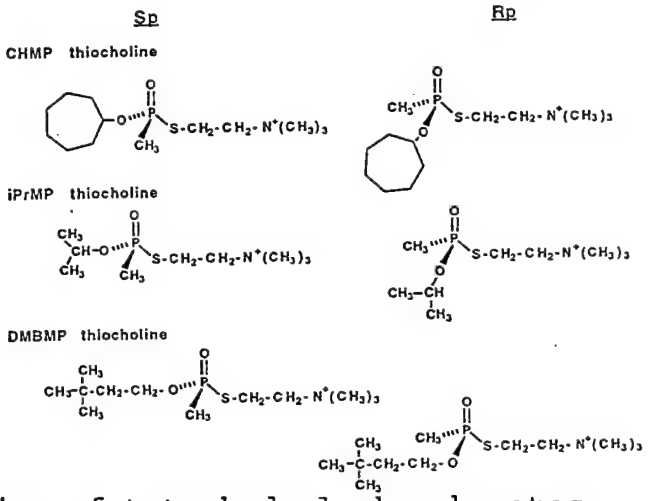

Fig. 2:Structures of the cationic compounds employed. CHMP, iPrMP and DMBMP refer to cycloheptyl-, isopropyl- and 3,3-dimethylbutyl-methylphosphonyl.

Analysis of the reaction of tetrahedral phosphonates with the cholinesterases adds another dimension to structure-activity considerations of ligands interacting at a target site.

Examination of the enantiomeric specificity of a series of Rp- and Sp-alkoxylmethylphosphonyl thiocholines, where the alkoxyl group is cycloheptyl, isopropyl or 3,3-dimethylbutyl (fig. 2), shows as much as a 230-fold enantiomeric selectivity (Table I). The selectivity appears greater for the more bulky alkoxyl groups and for secondary rather than primary alkoxyl groups. Replacement of the Phes with Leu and Ile at these positions results in a loss of enantiomeric selectivity and, in fact, with replacement at the 297 position, the 230-fold preference for the Sp enantiomer reverts to a slight preference for the Rp enantiomer (Table Ia).

Since the absolute stereochemistry of these phosphonates is known (24), the Rp and Sp enantiomers of the phosphonates can be positioned within the active center, either by docking as an initial tetrahedral complex or as a pentavalent, trigonal bipyramidal intermediate; the latter would simulate the putative transition state for an associative mechanism

Table Ia.: Rates[a] of Transphosphonylation by Rp- and Sp Alkyl Methylphosphonyl Thiocholine with Wild-type and Acyl Pocket Mutations of Mouse Acetylcholinesterase

	Alkyl Group								
	Cycloheptyl			Isopropyl			3,3-Dimethylbutyl		
Enzyme	Sp	Rp	Sp/Rp	Sp	Rp	Sp/Rp	Sp	Rp	Sp/Rp
AChE (Wild-type)	190,000	820	230	16,000	140	110	360,000	19,000	19
Phe 295 Leu	66,000	8,700	7.6	3,400	1,200	3	140,000	10,000	14
Phe 297 Ile	16,000	62,000	0.3	950	1,200	0.8	56,000	12,000	5

Table Ib: Rates[a] of Transphosphonylation by Rp- and Sp-Cycloheptyl Methylphosphonyl Thioate Possessing Uncharged Leaving Groups

	Leaving Group					
	$-S-CH_3$			$-S-CH_2-CH_3$		
Enzyme	Sp	Rp	Sp/Rp	Sp	Rp	Sp/Rp
AChE (Wild-type)	310	1.7	180	74	0.16	460
Phe 295 Leu	340	2.9	120	160	1.0	160
Phe 297 Ile	55	22	2.5	55	26	2.1

Table Ic: Rates[a] of Transphosphonylation by Rp- and Sp-Cycloheptyl Methylphosphonyl Thioate Possessing Charged and Uncharged Leaving Groups

	Leaving Group								
	$-S-CH_2-CH_2-N^+(CH_3)_3$			$-S-CH_3$			$-S-CH_2-CH_3$		
Enzyme	Sp	Rp	Sp/Rp	Sp	Rp	Sp/Rp	Sp	Rp	Sp/Rp
AChE (Wild-type)	190,000	820	230	310	1.7	180	74	0.16	460
Asp 74 Asn	1,400	8.0	180	530	2.3	230	190	0.41	460
Glu 202 Gln	21,000	130	160	14	0.060	230	2.3	0.014	160
Glu 450 Gln	1,400	23	61	9	0.050	180	14	0.018	780

[a]Rate constants are given as 10^3/Mmin; the standard error the mean from typically three experiments was 10-15%. Data were obtained from reference 9.

(fig. 3). In addition to the apposition of the γ-oxygen of the catalytic serine (Ser 203) with the phosphate, there is substantial evidence for the placement of the phosphonyl oxygen in the oxyanion hole as a requirement for transphos-

phonylation (25-27). In particular, the crystal structure of a phosphonylated intermediate with a *Candida* lipase, an enzyme homologous to AChE, shows the insertion of its phosphonyl oxygen in the oxyanion hole (28). Upon positioning the phosphorus in bonding distance with the serine and the oxygen in the oxyanion hole, neither the leaving group nor the bulky alkoxyl groups can fit into the acyl pocket of limited dimensions; only the methyl group on the phosphonate should be devoid of steric hindrance in the acyl pocket. Accordingly, the orientation permits the Sp enantiomer to have the thiocholine leaving group pointed out towards the gorge entrance (cf fig. 4); whereas in the Rp enantiomer, the thiocholine is oriented behind the cycloheptyl group. Consequently, the cycloheptyl moiety is directed out of the gorge. In this configuration the leaving group would suffer from two orientational constraints: (a) it is pointed in the wrong direction and must traverse around the bulky cycloheptyl group for exit from the gorge, (b) an

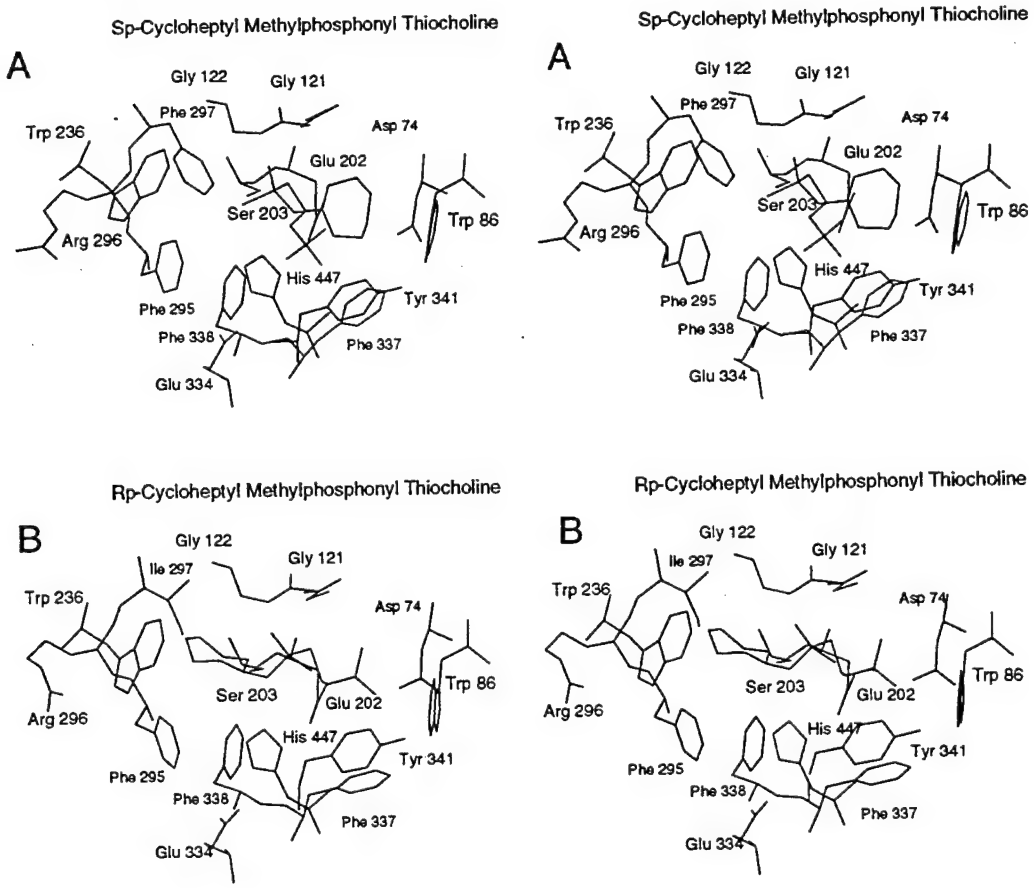

Figure 3: Stereoviews of Sp- and Rp-cycloheptyl methylphosphonothiocholine docked in the active center of native (A) and Phe297Ile (B) acetylcholinesterase. Residues of the acyl pocket (Phe 295 and 297), choline binding subsite (Trp 86, Tyr 337, Glu 202) are shown (cf: 30,31).

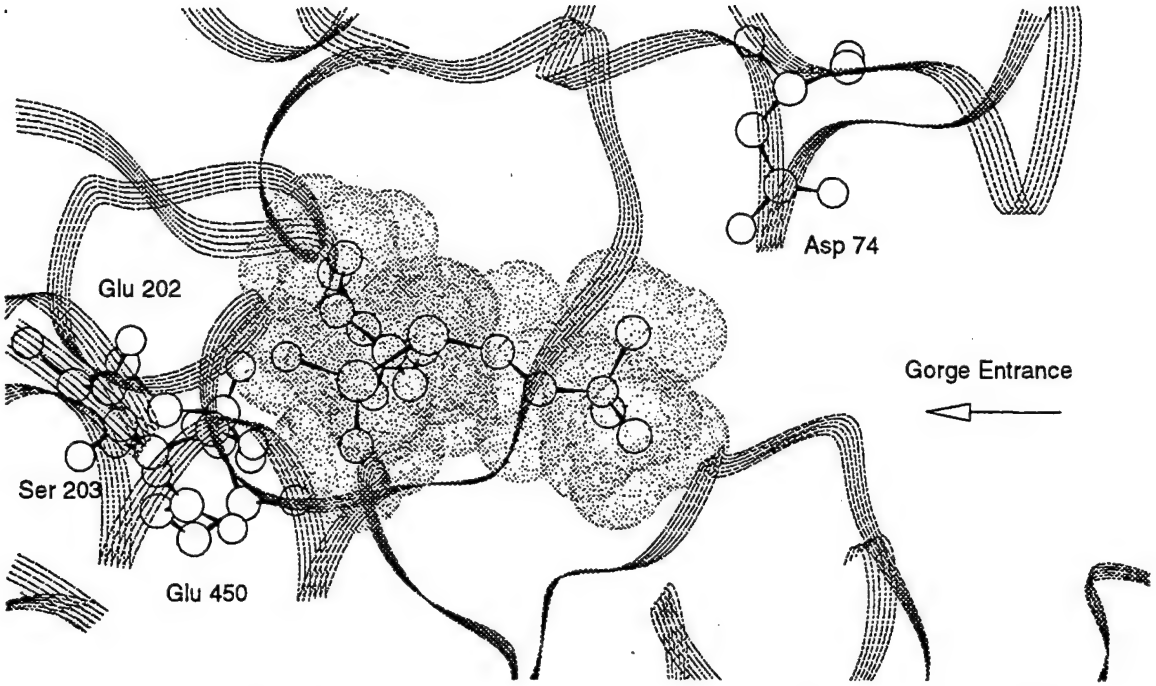

Figure 4: Sp-cycloheptyl methylphosphonothiocholine docked in the active center of acetylcholinesterase. The view is a 90° side view from figure 3 to show the orientation of the thiocholine moiety with respect to the gorge exit and Asp 74. A portion of the cholinesterase molecule is cut away to show an unobstructed view of the inhibitor (cf: 30,31).

apical positioning of the serine and leaving group would be limited by dimensional constraints of the gorge wall. Although the higher reactivity of the Sp enantiomer can be explained on these grounds, the data are less informative regarding the reactive orientation of the less active, Rp enantiomer during the transphosphonylation reaction.

To shed further light on this issue, we expanded our structural considerations to include uncharged thioates, as well as examined additional mutations in the enzyme. Although the uncharged thioates with methane thiol and ethane thiol as leaving groups are about 1000-fold less reactive with both the *Torpedo* (24, 29) and mouse AChE's (Tables Ib and Ic), the enantiomeric selectivities for the wild-type and mutant AChE's are virtually the same as the charged compounds. This would suggest, but not prove, that the additional charge and volume of the thiocholine have little influence on the reactive orientations of the Rp- and Sp-phosphonates. In addition, a comparison of reaction rates for charged and uncharged phosphonates shows residues in the acyl pocket do not account for their reactivity differences.

Having established the above principles on ligand position, we have gone on to modify charge within the active center gorge at the positions of Glu 202, Glu 450, and Asp 74

by isosteric replacement to form the corresponding carboxamides. Glu 202 and Glu 450 reside deep within the gorge and may facilitate polarization of the phosphonyl oxygen. Their influence on the transphosphonylation reaction shows no preference for the charged or uncharged leaving group. Moreover, these mutations do not affect appreciably chiral preference (Table Ic). However, isosteric substitution of Asp 74 to the neutral Asn, results in a marked reduction of transphosphonylation for the charged phosphonates, but not for the uncharged compounds. In fact, there is a slight increase in rate of transphosphonylation for the uncharged compounds (Table Ic).

Despite large reductions in rate of reaction for the cationic phosphonates, enantiomeric preference for the Rp and Sp phosphonylation does not change with the Asp74Asn mutation. This suggests that the trimethylammonio moieties in the Rp and Sp enantiomers reside at similar distances from Asp 74 in the transition state; otherwise, it is unlikely that its Coulombic influence would be virtually identical for the two enantiomers.

The findings reviewed here show two distinct linkage relationships. Chiral preference is dependent on the dimensions of the acyl pocket which are governed by the phenylalanine side chains directed towards the active center. This chiral selectivity is largely independent of the charge and apparent dimensions of the leaving group. By contrast, the anionic side chain (Asp 74) near the gorge entry is linked to the charge on the leaving group, and the enhanced reactivity of the cationic alkylphosphonates is eliminated by the isosteric substitution of an Asn at this position. Chiral selectivity is largely unaffected by this substitution. The diminished reactivity of the Rp- enantiomer results from steric constraints precluding simultaneous (a) positioning of the phosphorus to enable attack by the γ-oxygen of the serine, (b) insertion of the oxygen in the oxyanion hole, and (c) positioning the leaving group to extend out the gorge exit. Mutation of Phe 297 to Ile eliminates the apparent steric hindrance, and this would account for the greatly increased reactivity of the Rp compound.

Over sixty years ago, Easson and Stedman proposed that stereospecificity in drug action and in catalytic processes was a consequence of a three-point attachment between the chiral compound and a dissymmetric macromolecular surface (32). Although the original binding site was modeled on a planar surface, their hypothesis has withstood the tests of time to explain stereospecificity of drug action. Even with the resolution of three-dimensional structures as templates for the interaction of small ligands, the principle of a *minimal* three-point attachment can be shown to be applicable to chiral ligands and AChE.

Our examination of enantiomeric selectivity is part of a

larger investigation of ligand interactions with the active center of the cholinesterases. Site-specific mutations at other positions on AChE and the kinetics analyses for three classes of charged and uncharged congeneric ligands have been examined (31). The trifluoroketones conjugate directly with the active center serine to form a hemiketal (23) without loss of a leaving group. Their reaction with AChE approaches the diffusion limitation. Second, the alkylphosphonates, sulfonates and carbamoyl esters form relatively stable phosphonyl, sulfonyl and carbamoyl esters with the active center serine accompanied by the loss of a leaving group. The stability of the newly formed acyl serine intermediate typically allows for direct study of the acylation step. Third, the carboxyl esters show rapid turnover because of the near diffusion controlled acylation step and a rapid deacylation. Under physiologic concentrations, the acylation and deacylation steps appear of comparable magnitude allowing for a fractional build up of acyl enzyme intermediate (34). Only steady-state kinetics for catalysis of the carboxyl esters can be readily monitored, and the characterization of intermediate species has proven more elusive. Finally, oxime reactivation of the chiral phosphonate conjugates (which are effectively diastereomers) shows a enantiomer preference which can be modified by active center mutations (N. Hosea, unpublished).

Enantiomeric selectivity of the alkylphosphates is of considerable practical significance. The toxic nerve agent soman contains two chiral centers, one on the phosphorus and one on the attached carbon substituent yielding four diastereomers. The four diastereomers have very different rates of reaction and overall stability in the body (34). Similarly, the widely used insecticide malathion possesses a chiral center on a carbon side chain. By virtue of rearrangement around the phosphorus, it spontaneously forms diastereomers possessing distinct toxicities (35).

REFERENCES:

1. Schumacher, M., Camp, S., Maulet, Y., Newton, M., MacPhee-Quigley, K., Taylor, S.S., Friedmann, T. and Taylor, P. *Nature* 319: 407-409 (1986).
2. Sussman, J.L., Harel, M., Frolow, F., Oefner, C., Goldman, A., Toker, L. and Silman, I. *Science* 253: 872-879 (1991).
3. Bourne, Y., Taylor, P. and Marchot, P. *Cell* 83: 503-512 (1995).
4. Massoulié, Pezzementi, L., Bons, S., Krejei, E. and Vallete, F-M. Prog. Neurobiol. 41, 39-91 (1993).
5. Taylor, P. and Radić, Z. *Ann. Rev. Pharmacol. & Toxicol.* 34: 281-320 (1994).
6. Shafferman, A. and Velan, B. eds. Multidisciplinary Approaches to Cholinesterase Functions. Plenum New York (1992).

7. Quinn, D.M., Balasubramanian, A.S., Doctor, B.P and Taylor, P. eds. Enzymes of the Cholinesterase Family, Plenum, New York, 534 pp. (1995).
8. Millard, C.B., Lockridge, O. and Broomfield, C.A. Biochemistry 34, 15925-15933 (1995).
9. Maxwell, D.M., Brecht, K.M., Saxena, A., Taylor, P. and Doctor, B.P. in Enzymes of the Cholinesterase Family, D.M. Quinn et al, eds. Plenum N.Y. pp. 353-360 (1995).
10. Auld, V.J., Fetter, R.D., Broadie, K. and Goodman, C.S. *Cell* 81: 757-767 (1995).
11. Ichtchenko, K., Nguyen, T. and Sudhof, T.C. *J. Biol. Chem.* 271: 2676-2682 (1996).
12. Cygler, M., Schrag, J.D., Sussman, J.L., Harel, M., Silman, I., Gentry, M.K. and Doctor, B.P. *Protein Science* 2: 366-382 (1993).
13. Harel, M., Sussman, J.L., Krejci, E., Bon, S., Chanal, P., Massoulié, J., Silman, I. *Proc. Natl. Acad. Sci. USA.* 89: 10827-10831 (1992).
14. Vellom, D.C., Radić, Z., Li, Y., Pickering, N.A., Camp, S, and Taylor, P. *Biochemistry* 32: 12-17 (1993).
15. Ordentlich, A., Barak, D., Kronman, C., Flashner, Y., Leitner, M., Segall, Y., Ariel, N., Cohen, S., Velan, B. and Shafferman, A. *J. Biol. Chem.* 268: 17083-17095 (1993).
16. Radić, Z., Pickering, N.A., Vellom, D.C., Camp, S. and Taylor, P. *Biochemistry* 32: 12074-12084 (1993).
17. Ordentlich, O.,Barak, D., Kronman, C., Ariel, N., Segall, Y., Velan, B. and Shafferman, A. J. Biol. Chem. 52, 2082-2091 (1995).
18. Saxena, A., Quian, N., Kovach, I.M., Kozikowski, A.P., Pang, Y.P., Vellom, D.C., Radic, Z., Quinn, D.M., Taylor, P. and Doctor, B.P. Protein Sci. 3, 1770-1778 (1992).
19. Changeux, J.P. Mol. Pharmacol. 2, 369-392 (1966).
20. Taylor, P. and Lappi, S. Biochemistry 14, 1989-1997 (1975).
21. Karlsson, E., Mbuguo, P.M. and Rodriguez-Ihurralde, D. J. Physiol. (Paris) 79, 234-240 (1984).
22. Radic, Z., Quinn, D.M., Vellom, D.C., Camp, S. and Taylor, P. J. Biol. Chem. 270, 20391-20399 (1995).
23. Harel, M., Quinn, D.M., Nair, H.K., Silman, I. and Sussman, J.L. *J. Am. Chem. Soc.*118: 2340-2346 (1996).
24. Berman, H.A. and Leonard, K. *J. Biol. Chem.* 264: 3942-3950 (1989).
25. Taylor, P. and Jacobs, N.M. *Mol. Pharmacol.* 10: 93-107 (1974).
26. Grochulski, P., Bouthillier, F., Kazlauskas, R.J., Serreqi, A.N., Schrag, J.D., Ziomek, E. and Cygler, M. *Biochemistry* 33: 3494-3500 (1994).
27. Zhao, Q., Kovach, I.M., Bencsura, A. and Papathanassia, A. *Biochemistry* 33: 8128-8138 (1994).

28. Cygler, M., Grochulski, P., Kazlauskas, R.J., Schrag, J.D., Bouthillier, F., Rubin, B., Serreqi, A.N. and Gupta, A.K. *J. Am. Chem. Soc.* 116: 3180-3186 (1994).
29. Berman, H.A. and Decker, M.M. *J. Biol. Chem.* 264: 3951-3956 (1989).
30. Hosea, N.A., Berman, H.A. and Taylor, P. *Biochemistry* 34: 11528-11536 (1995).
31. Hosea, N.A., Radić, Z., Tsigelny, I., Berman, H.A., Quinn, D.M. and Taylor, P. *Biochemistry*, In press, (1996).
32. Eason, L.M. and Stedman, E. *Biochem. J.* 27: 1257-1266 (1933).
33. Froede, H.C. and Wilson, I.B. *J. Biol. Chem.* 259: 11010-11013 (1984).
34. de Jong, L.P., van Dijk, C., Berhitoe, D., and Benschop, H.P. *Biochem. Pharm.* 46: 1413-1419 (1993).
35. Berkman, C.E., Thompson, C.M. and Perrin, S.R. *Chem. Res. Toxicol.* 6: 718-723 (1993).

THE JOURNAL OF BIOLOGICAL CHEMISTRY

Vol. 272, No. 6, Issue of February 7, pp. 3502–3510, 1997
Printed in U.S.A.

Expression and Activity of Mutants of Fasciculin, a Peptidic Acetylcholinesterase Inhibitor from Mamba Venom*

(Received for publication, July 15, 1996, and in revised form, October 8, 1996)

Pascale Marchot‡§, Claudine N. Prowse‡, Joan Kanter‡, Shelley Camp‡, Elizabeth J. Ackermann‡, Zoran Radić‡, Pierre E. Bougis§, and Palmer Taylor‡¶

From the ‡Department of Pharmacology, University of California at San Diego, La Jolla, California 92093-0636 and §CNRS, Unité de Recherche Associée 1455, Institut Fédératif de Recherche Jean Roche, Université de la Méditerranée, Faculté de Médecine Secteur Nord, 13916 Marseille Cedex 20, France

Fasciculin, a selective peptidic inhibitor of acetylcholinesterase, is a member of the three-fingered peptide toxin superfamily isolated from snake venoms. The availability of a crystal structure of a fasciculin 2 (Fas2)-acetylcholinesterase complex affords an opportunity to examine in detail the interaction of this toxin with its target site. To this end, we constructed a synthetic fasciculin gene with an appropriate leader peptide for expression and secretion from mammalian cells. Recombinant wild-type Fas2, expressed and amplified in Chinese hamster ovary cells, was purified to homogeneity and found to be identical in composition and biological activities to the venom-derived toxin. Sixteen mutations at positions where the crystal structure of the complex indicates a significant interfacial contact point or determinant of conformation were generated. Two mutants of loop I, T8A/T9A and R11Q, ten mutants of the longest loop II, R24T, K25L, R27W, R28D, H29D, ΔPro^{30}, P31R, K32G, M33A, and V34A/L35A, and two mutants of loop III, D45K and K51S, were expressed transiently in human embryonic kidney cells. Inhibitory potencies of the Fas2 mutants toward mouse AChE were established, based on titration of the mutants with a polyclonal anti-Fas2 serum. The Arg^{27}, Pro^{30}, and Pro^{31} mutants each lost two or more orders of magnitude in Fas2 activity, suggesting that this subset of three residues, at the tip of loop II, dominates the loop conformation and interaction of Fas2 with the enzyme. The Arg^{24}, Lys^{32}, and Met^{33} mutants lost about one order of magnitude, suggesting that these residues make moderate contributions to the strength of the complex, whereas the Lys^{25}, Arg^{28}, Val^{34}-Leu^{35}, Asp^{45}, and Lys^{51} mutants appeared as active as Fas2. The Thr^{8}-Thr^{9}, Arg^{11}, and His^{29} mutants showed greater ratios of inhibitory activity to immunochemical titer than Fas2. This may reflect immunodominant determinants in these regions or intramolecular rearrangements in conformation that enhance the interaction. Of the many Fas2 residues that lie at the interface with acetylcholinesterase, only a few appear to provide substantial energetic contributions to the high affinity of the complex.

Fasciculins, selective inhibitors of acetylcholinesterase (AChE),[1] but not butyrylcholinesterase, are 7-kDa peptides with four disulfide bridges isolated from mamba venoms. They belong to the family of three-fingered snake toxins that includes the selective nicotinic receptor blockers, α-neurotoxins (1–3) and κ-neurotoxins (4, 5), the subtype-specific muscarinic receptor agonists (6, 7), the L-type calcium channel blockers, calciseptine and FS2 (8, 9), the GPIIb-IIIa antagonist and platelet aggregation inhibitor, RGD-containing dendroaspin (or mambin) (10, 11), and the cell membrane lytic cardiotoxins (or cytotoxins) (12, 13). Despite a highly conserved structural motif, the toxins in this family are directed to diverse targets, yet their individual modes of action are highly selective. The three-finger scaffold, that is also found in proteins isolated from sources other than snake venoms and devoid of toxic activity (14–17), constitutes a structural motif which accomplishes a plethora of precise, but eclectic, functions.

Fasciculins selectively inhibit mammalian and electric fish AChEs with K_i values in the pico- to nanomolar range (18–22). Several kinetic studies have shown that the fasciculin-AChE complex, despite its high affinity and extremely slow rate of dissociation, possesses residual catalytic activity (20, 23–26): in the complex, both substrate and catalytic site inhibitors are able to access the active center of the enzyme, located at the bottom of a deep and narrow gorge (27). On the other hand, fasciculin is competitive with propidium (18, 20, 24), a peripheral site inhibitor of AChE (28) which binds at an allosteric site presumed to be at the rim of the gorge (*cf.* Ref. 29). Three aromatic residues, that lie at the gorge rim, were found to be critical for fasciculin binding to AChE by site-directed mutagenesis of the enzyme (21).

The recently solved x-ray structures of the Fas2-mouse AChE and Fas2-*Torpedo* AChE complexes revealed that three domains of Fas2 anchor it to the enzyme, and delineated a large contact area consistent with the low dissociation constant of the complex; the Fas2 and AChE residues participating in the binding interface were unambiguously established, and major hydrophobic interactions were identified (30, 31). The structural analyses, however, did not reveal to what extent each contact between Fas2 and AChE contributes to the overall binding energy. In addition, the central loop of Fas2 was found to fit snugly at the gorge entrance so that the entry of other molecules, even as small as water, should be precluded. The mode of inhibition of fasciculin therefore appeared to be total

* This work was supported by CNRS and NATO (to P. M.) and by United States Public Health Service Grant GM18360 and DAMD Grant 17–95-I 5027 (to P. T.). The costs of publication of this article were defrayed in part by the payment of page charges. This article must therefore be hereby marked "*advertisement*" in accordance with 18 U.S.C. Section 1734 solely to indicate this fact.

¶ To whom correspondence should be addressed. Tel.: 619-534-1366; Fax: 619-534-8248.

[1] The abbreviations used are: AChE, acetylcholinesterase; BSA, bovine serum albumin; CHO, Chinese hamster ovary; CPK, Corey-Pauling-Koltun; Fas2, natural venom-derived fasciculin 2; FPLC, fast pressure liquid chromatography; HEK, human embryonic kidney; mAChE, recombinant acetylcholinesterase from mouse; NH_4Ac, ammonium acetate; PAGE, polyacrylamide gel electrophoresis; rFas2, recombinant wild-type fasciculin 2; RIA, radioimmunoassay.

occlusion of substrate entry at the mouth of the active-site gorge. To reconcile the disparity in the kinetic and structural data, either a second portal for entry of substrate and catalytic site inhibitors in the complex or a conformational change in the enzyme, not obvious in the crystal structure, opening a gap between the gorge wall and the bound peptide, have been proposed (30).

Complete understanding of the chemistry of the Fas2-AChE association requires a functional map of the binding surfaces. By site-directed mutagenesis of a synthetic Fas2 gene, we have generated new probes aimed at analyzing the individual contributions of the fasciculin residues to complex formation and conformation. In a mammalian system, we expressed a fully processed recombinant fasciculin, rFas2, that is undistinguishable from the natural, venom-derived Fas2. Fourteen mutants, encompassing 16 amino acid residues distributed among the three loops (fingers) of Fas2, were designed based on both the kinetic and structural data. We show that common determinants are identified by the structural and the mutagenesis approaches, but only a few of the many Fas2 residues residing at the binding interface provide the critical contacts required for enzyme inhibition.

EXPERIMENTAL PROCEDURES

Materials—HEK-293 and CHO-K1 cells were obtained from American Type Culture Collection. Ultraculture and serum-free Ultra-CHO cell culture media were from BioWhittaker, and serum-free Dulbecco's modified Eagle's cell culture medium from Life Technologies, Inc. L-Methionine sulfoximine, polyethylene glycol 8000, protease-free BSA, 5,5′-dithiobis-(2-nitrobenzoic acid), acetylthiocholine iodide, and the gel-filtration molecular weight markers (Mw-GF-70 Kit) were products of Sigma. The prepacked FPLC columns, Mono S HR 5/5 and Superose-12 HR 10/30, were from Pharmacia Biotech Inc. Dialysis tubing (Spectra/Pore6) was from Spectrum Medical Industries. The BCA kit for protein assays was from Pierce. Prestained protein molecular weight standards for SDS-PAGE were from Life Technologies, Inc. ^{125}I-Na (2100 Ci mmol^{-1}) was from Amersham. Complete and incomplete Freund's adjuvants were from Difco Laboratories. Normal rabbit serum and goat anti-rabbit whole serum were from Jackson ImmunoResearch Laboratories. All buffers were made with deionized water from a Millipore MilliRO/MilliQ system.

Biological Materials—The pGS expression vector was a gift from Scios Nova Inc. (Mountain View, CA). Purification of Fas2 from *Dendroaspis angusticeps* venom has been described previously (32). Concentrations of stock solutions were determined from their UV spectra ($\epsilon_{276\ nm}$ = 4900 M^{-1} cm^{-1}). Wild-type AChE from mouse recombinant DNA was expressed, concentrated, and titrated as described previously (33, 34). The polyclonal anti-Fas2 serum was obtained by immunization of a Blanc du Bouscat Evic rabbit with subcutaneous multi-site injections of purified Fas2 (100–150 μg). Primary and booster injections were made with complete and incomplete Freund's adjuvants, respectively (35).

Design of Synthetic Genes Encoding Wild-type and Mutant Fas2—A cDNA encoding rFas2 and the leader peptide from erabutoxin a (36) was synthesized as two sets of complementary oligonucleotides of ~130 base pairs in length, that were annealed, ligated together, and cloned into the expression vector pGS. rFas2 was expressed from the cytomegalovirus promoter while glutamine synthetase under the control of the Rous sarcomal virus-long terminal repeat was used as a dominant selectable marker conferring resistance to a low level of methionine sulfoximine. The pGS-rFas2 plasmid was transfected into CHO-K1 cells by calcium phosphate co-precipitation with glycerol shock. Individual cell colonies which successfully integrated the rFas2 and adjacent GS genes were selected in glutamine-free Ultraculture medium in the presence of 25 μM methionine sulfoximine and grown to confluence. Clones which produced the highest Fas2 activity were then further amplified using either 250 μM or 500 μM methionine sulfoximine.

Mutagenic oligonucleotides (usually 18 mers) were used in generating Fas2 mutants according to Kunkel *et al.* (37). Mutations were done on either M13 or single-stranded pBluescript templates. The entire nucleotide sequences of the mutated plasmids were verified using dideoxy sequencing. Transient transfections into HEK-293 cells employed the pGS plasmid and coprecipitation with calcium phosphate and glycerol shock. To ascertain transfection efficiencies, 5 μg of a pcDNA-3 expression vector containing the *Escherichia coli lacZ* gene were cotransfected (38). The cells were rinsed and placed in serum-free medium 24 h after transfection. Secreted fasciculin activity was examined 48 to 72 h later.

Chromatography—Ultraculture medium containing the expressed rFas2 (10 ml/10-cm plate) was harvested every 3–4 days, centrifuged (4 °C, 10 min) to remove cell debris, extensively dialyzed against 50 mM NH_4Ac, pH 7.5, 0.01% (w/v) NaN_3, and filtered through 0.22-μm cellulose acetate filters. rFas2 was purified by cation-exchange and size-exclusion FPLC (Pharmacia) performed at 4 °C in NH_4Ac, pH 7.5, with flow rates of 0.5 ml min^{-1}. The dialyzed and filtered cell culture medium (up to 500 ml) was loaded on a Mono S column previously equilibrated with 50 mM NH_4Ac, then the column was washed extensively with the same buffer. Elution of the rFas2 fraction was performed with a 50–200 mM NH_4Ac gradient over 60 min, followed by an isocratic step at 200 mM NH_4Ac. The eluted rFas2 fraction was lyophilized, redissolved in 100 mM NH_4Ac, and loaded as a 200-μl sample on a Superose-12 column equilibrated in 100 mM NH_4Ac. For the final cation-exchange step, the pooled rFas2-containing fractions emerging from successive gel filtrations were diluted twice and loaded on the Mono S column equilibrated in 50 mM NH_4Ac. Elution of rFas2 was performed under isocratic conditions with 100 mM NH_4Ac.

All Fas2 mutants were concentrated and partially purified from the culture medium through the first ion-exchange step, then further concentrated by ultrafiltration. To prevent cross-contamination, separate Mono S columns were used for rFas2 and the Fas2 mutants, and the columns were fully regenerated after each use.

Electrophoresis—SDS-PAGE under reducing conditions used the discontinuous system of Laemmli (39) with a 20% resolving/5% stacking gel. Samples were denatured in 500 mM Tris-HCl, pH 6.8, in the presence of 5% (v/v) β-mercaptoethanol and 4% SDS, at 90 °C for 2 min, then loaded onto the gel in the presence of 10% (v/v) glycerol and 0.01% bromphenol blue. Isoelectric focusing was performed with pH 3–10 precast gels (Novex) as specified by the manufacturer. Staining was by silver nitrate.

Peptide Analyses—Amino acid analysis of rFas2 (5 nmol), previously hydrolyzed with 6 M HCl and 1% (w/v) phenol for 20 h *in vacuo*, was carried out on a ABS Auto Analyzer. Automated Edman analysis of rFas2 (250 pmol) was conducted on a ABS sequenator. Equivalent samples of venom-derived Fas2 were analyzed in parallel.

Liquid-phase Radioimmunoassay (RIA)—Lactoperoxidase-catalyzed radioiodination of Fas2 to a specific radioactivity of ~1200 Ci mmol^{-1} has been detailed elsewhere (20). The titer of the anti-Fas2 serum, defined as the serum dilution which binds 50% of the ^{125}I-Fas2 added to the sample, was determined as a 316,000-fold dilution. For standard RIAs, ^{125}I-Fas2 (10,000 cpm) was incubated at 37 °C for 90 min with the anti-Fas2 serum at its titer in 200 μl of 50 mM NaH_2PO_4/Na_2HPO_4, pH 7.5, 0.1 mg ml^{-1} BSA, and then the samples were diluted with buffer to 500 μl and incubated overnight at 4 °C. Double immunoprecipitation of the antigen-antibody complexes was performed at 4 °C with successive additions of normal rabbit serum (50 μl of a 1/50 dilution), goat anti-rabbit serum (50 μl of a 1/20 dilution), and polyethylene glycol (400 μl of a 20% (w/v) solution). Samples were centrifuged (10,000 × *g*, 25 min, 4 °C), and the radioactivity of the pellets was determined. Titration of the unlabeled rFas2 and Fas2 mutants by RIA was based on competition with ^{125}I-Fas2 for complexation with anti-Fas2 serum and comparison to a Fas2 standard curve.

Assay for AChE Inhibition—Relative AChE activities (40) were recorded at room temperature by microtitration on a V_{max} kinetic microplate reader (Molecular Devices Corp.) at 405 nm, in the presence of 0.5 mM acetylthiocholine iodide and 0.3 mM 5,5′-dithiobis-(2-nitrobenzoic acid), in 50 mM $NaPO_4$ buffer, pH 8.0, 0.1 mg ml^{-1} BSA (20). The activities of purified rFas2 and of the Fas2 mutants were monitored by inhibition of 5–10 pM AChE after a 1-h incubation at 37 °C and 14–18 h at room temperature.

Characterization of the Mutants—Culture media, 72 h after transfection, were screened for immunoreactivity and inhibitory activity directly or after 10–20-fold concentration by ultrafiltration. The Fas2 mutants were titrated by RIA, and their inhibitory activities were quantitated by AChE inhibition assay after partial purification and concentration by cation exchange of the media (100–200 ml) and ultrafiltration of the chromatographic fractions. The Fas2 mutants were submitted to at least two independent transfection-chromatography-assay sequences.

```
                HindIII    [→ Leader peptide →
                  ][          -20
                AAG CTT ATG AAA ACT CTG CTC CTG ACC
                        M   K   T   L   L   L   T

                                                ScaI
                    -10                          ][
CTG GTG GTC GTG ACA ATC GTG TGC CTG GAC CTG GGA TAC AGT
 L   V   V   V   T   I   V   C   L   D   L   G   Y   S

[→ Mature Fas2 →
 1                                  10
ACT ATG TGT TAC TCT CAC ACC ACT ACC TCT CGC GCT ATC CTG
 T   M   C   Y   S   H   T   T   T   S   R   A   I   L

                    20
ACC AAC TGT GGC GAG AAT TCT TGT TAC CGC AAA TCT CGC CGC
 T   N   C   G   E   N   S   C   Y   R   K   S   R   R

    30                                          40
CAC CCG CCG AAA ATG GTG CTG GGC CGC GGC TGT GGC TGT CCA
 H   P   P   K   M   V   L   G   R   G   C   G   C   P

                        50
CCG GGT GAC GAC AAC CTG GAA GTG AAA TGT TGT ACC TCT CCG
 P   G   D   D   N   L   E   V   K   C   C   T   S   P

                                    NotI
            60                       ][
GAC AAA TGT AAC TAC TAA GGA TCC GCG GCC GC
 D   K   C   N   Y   -
```

FIG. 1. **Nucleotide and amino acid sequences of the chemically synthesized cDNA encoding rFas2.** The nucleotide sequence was designed from frequent mammalian codon usage and flanked on the 5′ end by the sequence encoding the signal peptide of erabutoxin a (36). Positive numbering of the encoding amino acid sequence starts at the first residue of the processed rFas2. Initiation and termination codons are *underlined*, and relevant restriction sites are indicated.

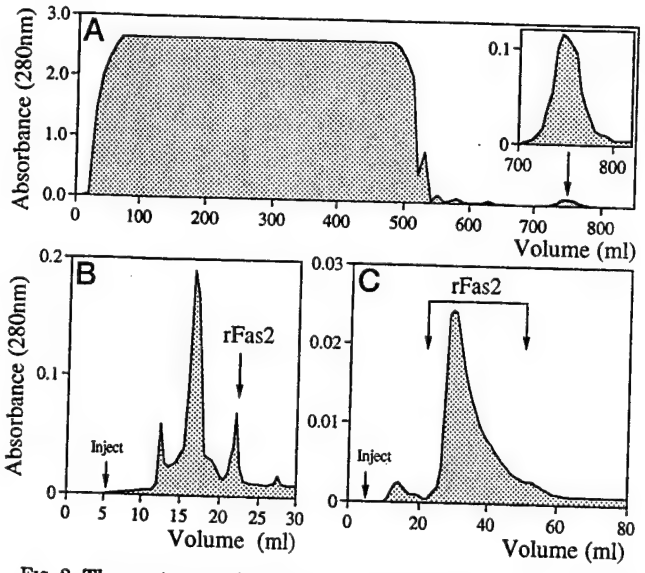

FIG. 2. **Three-step purification of rFas2 by FPLC.** *A*, rFas2 was concentrated and partially purified from the cell culture medium using cation exchange and elution with a NH_4Ac concentration gradient. Note the amounts of proteins (including rFas2) that are retained *versus* not retained by the column; *inset*, magnification of the rFas2 elution peak. *B*, the rFas2 fraction was further purified by gel filtration; rFas2 elutes in the included peak. *C*, final purification of rFas2 from trace contaminants was achieved by cation exchange under isocratic conditions, which accounts for the skewed peak.

RESULTS

Recombinant Wild-type Fasciculin

Expression of rFas2 in CHO Cells and Purification—Synthesis of the oligonucleotides encoding rFas2 enabled us to use codons of high usage frequency for mammalian cells and place restriction sites at convenient locations within the open reading frame and flanking regions. To ensure secretion and processing, a sequence encoding the leader peptide of a structurally related three-fingered toxin, erabutoxin a (36), was joined at the 5′ end (Fig. 1). A *ScaI* site was generated at the linkage between the two sequences by replacing Thr at position −1 by Ser.

Selected clonal cells at confluence secreted up to 1.7 $\mu g\ ml^{-1}$ (0.25 μM) of rFas2 in the 3-day intervals between medium changes; this rate continued for up to 10 weeks. Purification employed three steps on 500-ml batches of media (Fig. 2). Initial cation exchange led to removal of most medium proteins with a 440-fold enrichment (in pmol of Fas2 per mg of total protein) in rFas2, with more than 90% of recovery (Fig. 2*A*). A gel-filtration step purified rFas2 1500-fold (Fig. 2*B*). Final removal of trace contaminants was achieved by a second cation-exchange chromatography performed in isocratic conditions (Fig. 2*C*). rFas2 migrated in the same positions as the venom-derived Fas2 in the second and third chromatographic steps. An overall purification of 2200-fold was achieved in ~50% yield.

Physical and Biological Characterization of rFas2—SDS-PAGE in reducing conditions (Fig. 3, *inset*) and isoelectric focusing analysis (not shown) each revealed a single, sharp band that migrated at a position identical to the venom-purified Fas2. Parallel runs on the amino acid analyzer yielded identical compositions for rFas2 and Fas2. Amino-terminal sequencing of native rFas2 yielded a single sequence, TMXY-SHTTTS, identical to that of Fas2, with a blank third step (noted as *X*) for non-reduced Cys[3]. UV absorbance of natural Fas2 was used to estimate concentration of rFas2 stocks. Radioimmuno- and AChE-inhibition assays showed equivalent

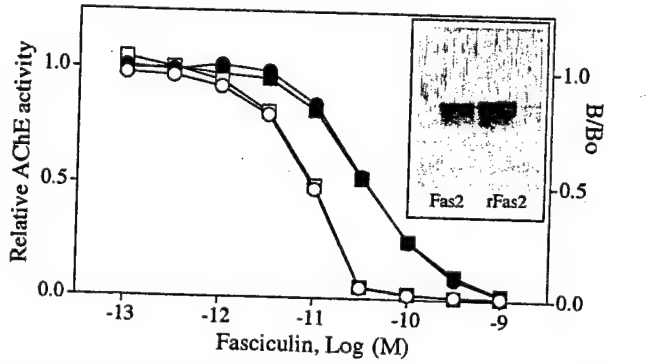

FIG. 3. **Biological and physical characterization of purified rFas2, compared to the venom-derived Fas2.** The concentrations of the Fas2 and rFas2 stock solutions were calculated from their UV spectra ($\epsilon_{276\ nm} = 4900\ M^{-1}\ cm^{-1}$). In this inhibition assay, Fas2 (○) and rFas2 (□) were incubated with ~20 pM mouse AChE; a similar superimposition of the Fas2 and rFas2 curves was also observed when 5 pM AChE was used. In this RIA, Fas2 (●) and rFas2 (■) were incubated with ^{125}I-Fas2 (10,000 cpm) and a 100,000-fold dilution of the anti-Fas2 serum; *B* and B_o denote amounts of ^{125}I-Fas2 specifically bound by the anti-Fas2 serum in the presence and in the absence of competing ligand, respectively. Data points correspond to the average value of quadruplicates that differed by less than 5%. *Inset*, SDS-PAGE of rFas2 and Fas2 under denaturing conditions.

potencies for rFas2 and venom-derived Fas2 for inhibiting mouse AChE and competing with ^{125}I-Fas2 for binding to a polyclonal anti-Fas2 serum (Fig. 3 and Table I). Hence fully processed and correctly folded rFas2 is directly produced in mammalian cells.

Mutant Fasciculins

Selection of Positions for Mutation of Fas2—The overall net positive charge (+4 at neutral pH) of Fas2, coupled with its association at a peripheral anionic site on AChE, suggested an electrostatic attractive component with the cationic amino acids on Fas2 (Fig. 4). Cationic positions unique to the fasciculins were considered first. Hence, Arg^{11}, Arg^{24}, Lys^{25}, Arg^{27}, Arg^{28}, Lys^{32}, and Lys^{51} were mutated, but Arg^{37} and Lys^{58}, being

TABLE I

Relative inhibitory activities and apparent dissociation constants (K_i') of the recombinant wild-type and mutant fasciculins for mouse AChE

The relative inhibitory activity of the purified rFas2 was determined in the presence of 5 pM AChE (*cf.* legend to Fig. 3). The relative inhibitory activities of the transiently expressed rFas2 and mutants, monitored with 5 or 10 pM AChE, were calculated from ratios of dilutions for 50% inhibition and competition in the inhibition and radioimmunoassay titrations, respectively (*cf.* Fig. 6); the values were normalized to ratios with the venom-derived Fas2. Apparent K_i' values are expressed relative to the K_i value of Fas2 for mouse AChE (2.3 pM) (21). Data are from the major peak when more than a single peak appeared on the cation-exchange resin (*cf.* Fig. 5); *n*, number of independent experiments.

Fasciculin	Relative inhibitory activity[a] (normalized to Fas2)	Apparent K_i'
		pM
Wild-type		
rFas2 (purified)	1.00 ± 0.05 (n = 4)	2.3 ± 0.1
rFas2 (transient)	0.98 ± 0.26 (n = 5)	2.3 ± 0.6
Loop I mutations		
T8A/T9A	18 ± 13 (n = 3)	≤2.3
R11Q	6.3 ± 3.1 (n = 2)	≤2.3
Loop II mutations		
R24T	0.080 ± 0.003 (n = 2)	29 ± 1
K25L	1.08 ± 0.06 (n = 5)	2.1 ± 0.1
R27W	0.021 ± 0.017 (n = 3)	112 ± 91
R28D	1.10 ± 0.05 (n = 3)	2.1 ± 0.9
H29D	73 ± 21 (n = 3)	≤2.3
ΔP30	0.0052 ± 0.0065 (n = 4)	440 ± 550
P31R	0.0016 ± 0.0002 (n = 2)	1440 ± 180
K32G	0.32 ± 0.12 (n = 3)	7.2 ± 2.7
M33A	0.13 ± 0.05 (n = 2)	17.7 ± 6.8
V34A/L35A	0.93 ± 0.60 (n = 2)	2.5 ± 1.6
Loop III mutations		
D45K	0.7 ± 0.1 (n = 3)	3.3 ± 0.5
K51S	1.08 ± 0.01 (n = 2)	2.1 ± 0.02

[a] Values are shown as average ± the variation (n = 2) and means ± S.D. (n > 2).

invariant among the three-fingered toxins and with their sidechains only partly solvent-accessible (41, 42), were not studied. Second, His^{29}, supposedly unprotonated at neutral pH, is located at the tip of loop II, a position corresponding to the critical Asp^{31} in erabutoxin a (43). Third, Pro^{31}, whose *cis* configuration constrains the conformation of the tip of loop II (30, 41), was modified to Arg, a residue and position essential for the α-neurotoxin activity (43, 44). Fourth, a doublet of anionic residues, Asp^{45}-Asp^{46}, at the tip of loop III, is found only in the fasciculins and "synergistic-type" toxins, all from mamba venoms (45). All α-neurotoxins have a positively charged residue at position 45. Finally, the recently solved structures of two Fas2-AChE complexes (30, 31) revealed that several neutral residues participate in the interaction of Fas2 to AChE. Hence, Thr^{8}-Thr^{9}, Pro^{30}, Met^{33}, and Val^{34}-Leu^{35}, were also mutated.

By substituting residues found in homologous toxins, perturbations in secondary structure might be minimized. Based on sequence homology and superimposition of crystal structures in the members of the three-fingered peptide family, Fas2, erabutoxin b, α-cobratoxin, α-bungarotoxin, and cardiotoxin VII4 (Fig. 4*A*), we mutated $Arg^{11} \rightarrow$ Gln (R11Q), $Arg^{24} \rightarrow$ Thr (R24T), $Lys^{25} \rightarrow$ Leu (K25L), $Arg^{27} \rightarrow$ Trp (R27W), $Arg^{28} \rightarrow$ Asp (R28D), $His^{29} \rightarrow$ Asp (H29D), $Pro^{31} \rightarrow$ Arg (P31R), $Lys^{32} \rightarrow$ Gly (K32G), $Asp^{45} \rightarrow$ Lys (D45K), and $Lys^{51} \rightarrow$ Ser (K51S) (Fig. 4*B*). The close fit and potential for hydrogen bonding of certain residues at the binding interface of the Fas2-AChE complex suggested that side chains on Thr^{8}, Thr^{9}, Met^{33}, Val^{34}, and Leu^{35} be minimally perturbed. Accordingly, we changed them into Ala (T8A/T9A, M33A, and V34A/L35A mutants). Finally, to shorten loop II and possibly create a gap between the bound Fas2 and the entrance of the gorge of the enzyme, we deleted Pro^{30} (ΔP30 mutant).

Transient Expression of Fas2 Mutants in HEK Cells—Expression from transiently transfected cells enabled direct analysis of activity and/or peptide production in the cell culture media. Analysis of AChE inhibition and RIA titer allowed an initial classification of the Fas2 mutants. Class I comprised the T8A/T9A, K25L, R28D, H29D, D45K, V34A/L35A, and K51S mutants, which displayed significant AChE inhibition and immunoreactivity. Class II comprised the R24T, R27W, ΔP30, P31R, K32G, and M33A mutants, which displayed significant immunoreactivity but less AChE inhibition. Class III comprised only the R11Q mutant, which displayed AChE inhibition but in complete curves immunoreactivity curves. Production yields, determined by RIA titration of rFas2 and the Fas2 mutants secreted into the media, ranged between 0.5 and 5 pmol ml^{-1} in a 3-day period.

Chromatography of the Fas2 Mutants—Elution positions of the Fas2 mutants on the cation-exchange resin were monitored by RIA and AChE inhibition assay for the class I and class III mutants and by RIA for the class II mutants. Representative profiles are shown in Fig. 5. Compared to rFas2 (*top panels*), 10 of the 14 mutants showed elution positions consistent with their net charge. Mutants T8A/T9A, ΔP30, M33A, and V34A/L35A, all possessing the same net charge as rFas2, eluted at the same ionic strength as rFas2. Mutants K25L, R27W, K32G, and K51S, which lost one net positive charge, eluted at lower ionic strength than rFas2. Mutants P31R and D45K, which gained one and two net positive charge(s), eluted at higher ionic strengths than rFas2. In contrast, mutants R11Q, R24T, R28D, and H29D, which lost either one or two positive charge(s), eluted at a similar ionic strength as rFas2, suggesting that the initial and newly introduced side chains at positions 11, 24, 28, and 29 are not solvent-accessible and/or do not interact with the anionic matrix of the column. Two mutants, R24T and R27W, eluted as several peaks, but calculation of concentrations based on a simple reversible equilibrium for ligand binding revealed that the additional peaks are minor components. Whether these peaks reflect incomplete processing or folding of the peptides, or slow conformational equilibria, has not been ascertained.

Analysis of the Apparent Dissociation Constants (K'_i) of the Fas2 Mutants—The Fas2 mutants, enriched in purity and concentrated by cationic exchange and ultrafiltration, were titrated by RIA and analyzed for inhibitory activity (Fig. 6). The RIA profiles were generally consistent with the amounts of peptide expected based on transfection efficiency and purification yields. In contrast, the concentration dependences of the AChE inhibition curves, relative to those of immunoreactivity, varied widely, illustrating significant differences in the affinities of the Fas2 mutants for AChE. The transiently expressed rFas2 sample, enriched and concentrated, yielded the same AChE inhibition potency as the stably expressed and fully purified rFas2 (*cf.* Fig. 3). Compared to rFas2, no significant differences in inhibition potency were found for mutants K25L, R28D, K32G, V34A/L35A, D45K, and K51S. In contrast, significant differences were found for mutants T8A/T9A, R11Q, R24T, R27W, H29D, ΔP30, P31R, and M33A. The inhibitory activities of the Fas2 mutants toward mouse AChE, calculated from the dilutions for 50% inhibition in the inhibition assays and 50% competition in the RIA titrations, and normalized to Fas2, are reported in Table I. The apparent K'_i values that are also reported are expressed relative to a K_i value of 2.3 pM for Fas2 (21). Because of the limitations that may arise from slow equilibration, from the disparity between added and free ligand, and from using immunoreactivity to reflect peptide concentration, the mutants with low dissociation constants are specified only by an upper limit.

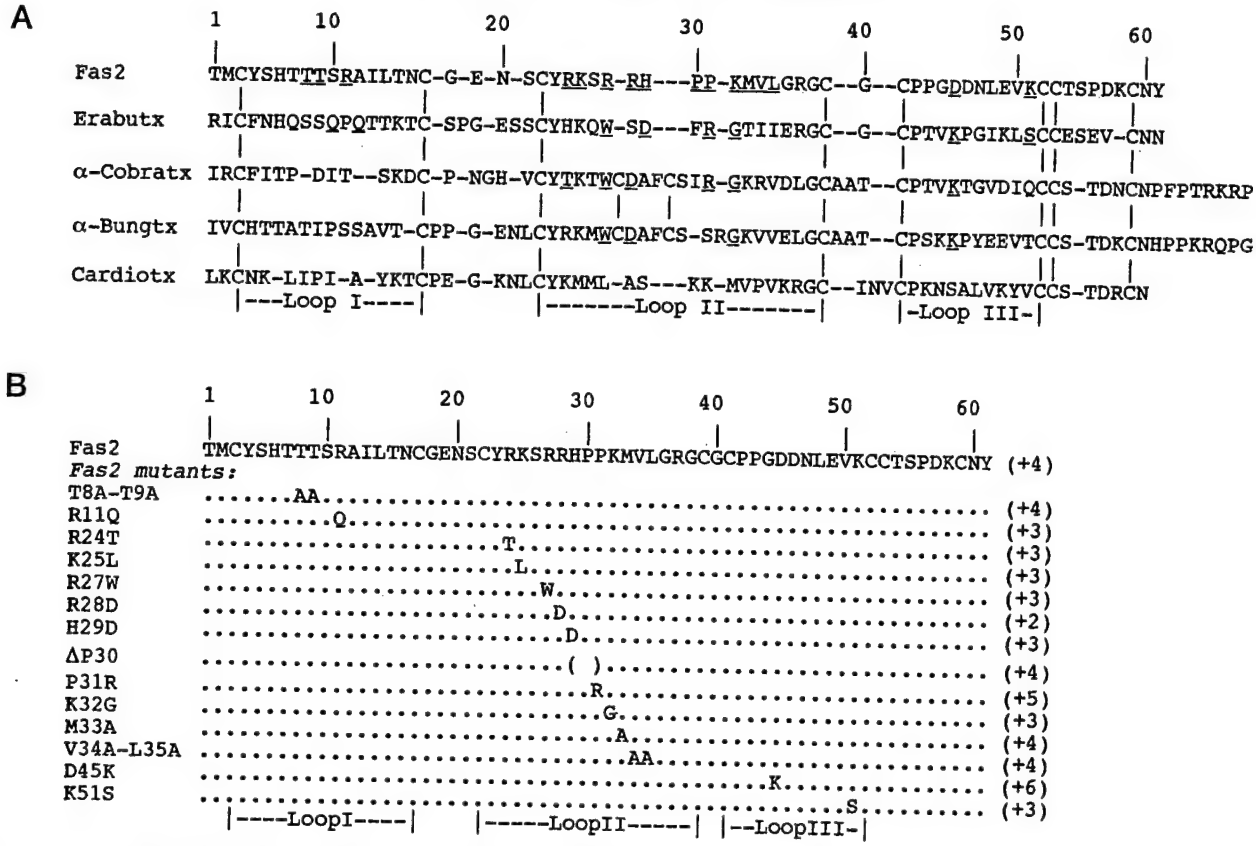

FIG. 4. **Sequence alignments.** *A*, alignment of three-fingered toxins of known three-dimensional structure was generated with HOMOLOGY (Biosym Technologies, Inc., 1994) by optimization of the superimposition of the crystal structures of Fas2 (entry code, 1FSC), erabutoxin b (3EBX), α-cobratoxin (1CTX), α-bungarotoxin (2ABX), and cardiotoxin V^{II}_4 (1CDT) according to their backbone atoms. The amino acid numbering corresponds to Fas2 numbering. The *bars* between the sequences indicate the conserved disulfide bridges; note the extra bridge within loop II of the two long neurotoxins. The residues *underlined* in the Fas2 sequence have been mutated. The residues *underlined* in the other toxin sequences correspond to some of the studied substitutions (see text). *B*, amino acid sequences of the wild-type and mutant fasciculins. For clarity, only the substitutions made on the Fas2 sequence are displayed. The values on the *right* indicate the theoretical net charge of the proteins at neutral pH, with the His residues assumed to be unprotonated.

Residue Contributions to Fas2 Inhibition Based on Mutagenesis Studies—Based on the relative inhibitory activities of the rFas2 mutants (Table I), the mutations can be classified in four categories: (i) those which cause little or no apparent effect on Fas2 activity, as seen for mutants K25L, R28D, V34A/L35A, D45K, K51S (no change), or K32G (3-fold decrease), (ii) those which cause a decrease by about one order of magnitude in the Fas2 activity, as seen for mutants R24T (13-fold) and M33A (8-fold), (iii) those which cause a decrease by two or more orders of magnitude, as seen for mutants R27W (49-fold), ΔP30 (192-fold), and P31R (625-fold), and (iv) those which cause an apparent increase in the Fas2 inhibitory activity, as seen for mutants T8A/T9A, R11Q, and H29D (18-, 6-, and 73-fold, respectively).

The contribution of the mutated residues to activity, relative to their location in the three-dimensional structure of Fas2 bound to mouse AChE (30), is shown in Fig. 7. The three residues that dominate the AChE-inhibitory activity of Fas2, Arg^{27}, Pro^{30}, and Pro^{31}, form a subset located at the tip of loop II. The surface area of this subset, 261 Å^2, represents only 6% of the total accessible surface area of Fas2 but 25% of the Fas2 area buried in the Fas2-mAChE complex. Fas2 residues Thr^8, Thr^9, and Arg^{11}, mutation of which resulted in an apparent increase in Fas2 activity, form a second subset located at the tip of loop I. The surface area of this subset, 300 Å^2, represents 7% of the total accessible surface area of Fas2 but 29% of the Fas2 area buried in the complex. Hence, a small fraction of the many Fas2 residues which make up the overall functional site provide the critical contacts required for the high affinity interaction.

DISCUSSION

Several groups have produced recombinant three-fingered snake toxins, α- and κ-neurotoxins, as fusion proteins in heterologous bacterial expression systems, and some have reported site mutagenesis studies on these toxins (43, 44, 46–52). The lower activity of the fusion proteins, compared to the natural toxins, however, precludes direct analysis of the mutants before *in vitro* cleavage of the hybrid by chemical or enzymatic means. More recently, a recombinant κ-neurotoxin was produced in yeast with full activity, although possessing a short amino-terminal extension due to altered signal peptide cleavage (53). In our study, we used a mammalian system to express secreted and fully processed rFas2 and 14 Fas2 mutants. Direct expression of rFas2 in its functional conformation demonstrates that the use of the signal peptide sequence of erabutoxin a and the change at position −1 were not critical for post-translational events such as folding, cleavage of signal peptide, and disulfide bond formation of the rFas2 molecule in mammalian cells.

Owing to the use of complementary assays, RIA titration and AChE inhibition, 14 transiently expressed Fas2 mutants could be quantitated and functionally characterized without extensive purification. The polyclonal anti-Fas2 serum is characterized by a high titer in antibodies, likely to be mostly IgGs (35). The shapes of the RIA curves, that generally extend over a concentration range wider than expected for interaction of ^{125}I-Fas2 with a single site (Figs. 3 and 6), suggest that the serum contains at least two IgG populations presumably directed

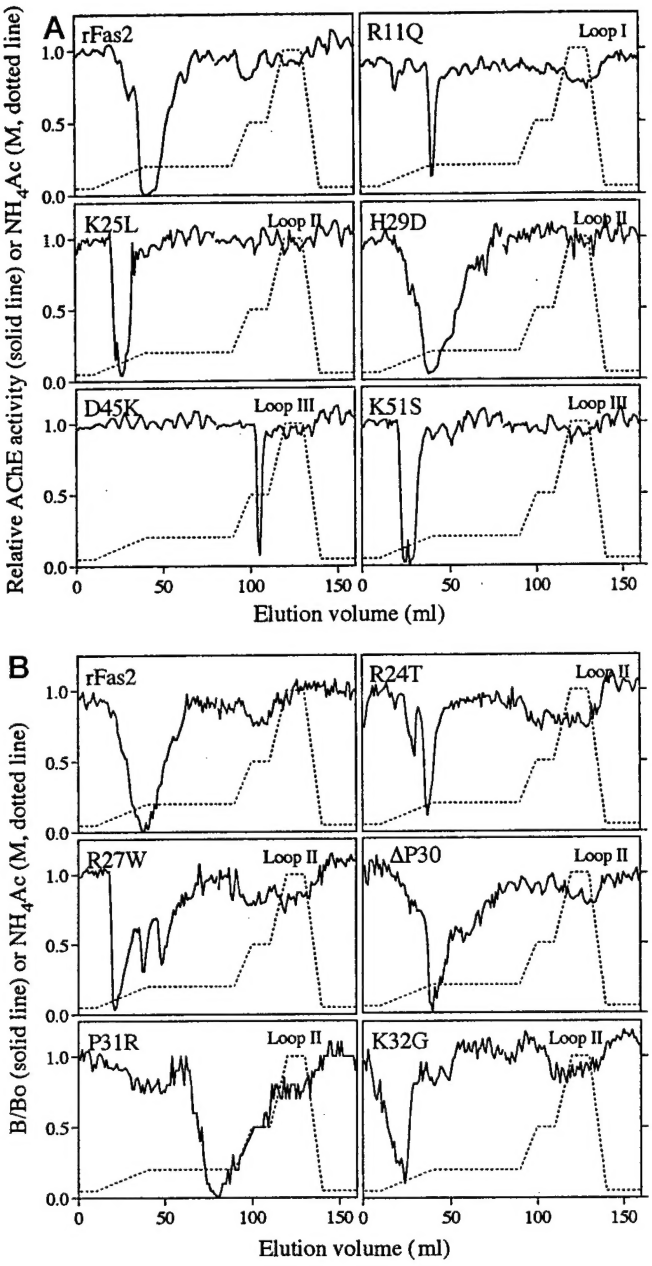

FIG. 5. **Cation-exchange chromatography of rFas2 and rFas2 mutants.** *A*, the chromatographic fractions were monitored for Fas2 activity on mouse AChE for rFas2 (120 ml of culture medium were loaded, 5 μl of each fraction were assayed) and for mutants R11Q (110 ml, 50 μl), K25L (85 ml; 5 μl), H29D (200 ml; 15 μl), D45K (50 ml; 5 μl), and K51S (85 ml; 5 μl); mutants T8A/T9A (165 ml; 5 μl) and R28D (100 ml; 5 μl) are not shown. *B*, the fractions were monitored for reactivity toward a polyclonal anti-Fas2 serum for rFas2 (sample loaded, 150 ml) and for mutants R24T (175 ml), R27W (175 ml), ΔP30 (150 ml), P31R (160 ml), and K32G (200 ml); mutants M33A (185 ml) and V34A/L35A (165 ml) are not shown; 50 μl of each fraction were assayed in each case; B and B_o denote the amounts of ^{125}I-Fas2 specifically bound by the anti-Fas2 serum in the presence and the absence of competing ligand, respectively. The empty pGS vector (sample loaded, 145 ml) yielded no signal for both AChE inhibition (15 μl of each fraction were assayed) and RIA screenings (50 μl were assayed). The absorbance profiles (280 nm) arose primarily from absorption of the culture medium proteins (not shown).

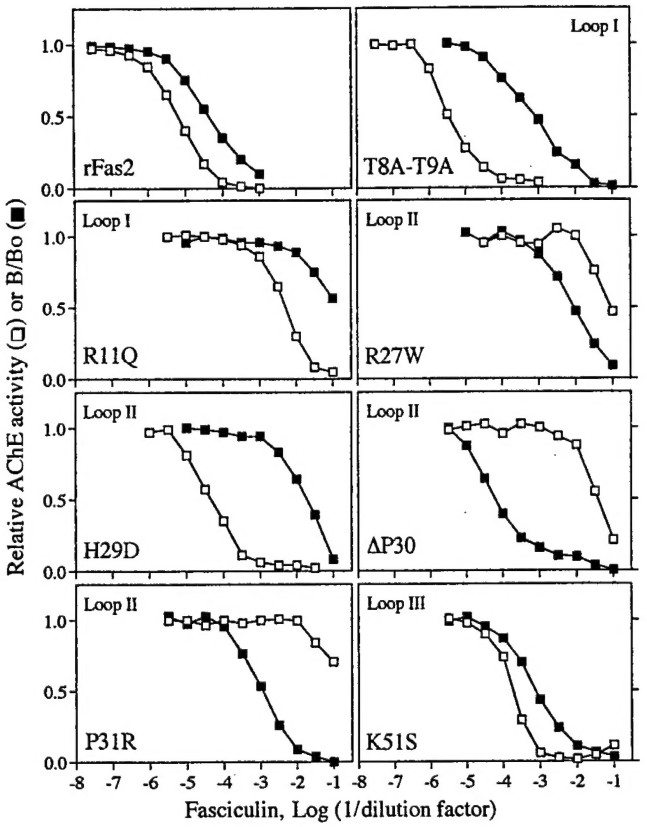

FIG. 6. **Comparative AChE inhibition and radioimmunoassays of rFas2 and Fas2 mutants (primary data).** The rFas2 and mutant rFas2 enriched fractions eluted from the cation-exchange column (*cf.* Fig. 5) were dialyzed and concentrated by ultrafiltration. The AChE inhibition assays (□) were performed with 5 or 10 pM mouse AChE. The RIAs (■) were performed with ^{125}I-Fas2 (10,000 cpm) and the anti-Fas2 serum at its titer; B and B_o denote amounts of ^{125}I-Fas2 specifically bound by the anti-Fas2 serum in the presence and in the absence of competing ligand, respectively. For rFas2, note that the relative positions of the AChE inhibition and RIA curves are similar to those obtained with purified rFas2 (*cf.* Fig. 3). For the mutants, compare the positions of the curves for AChE inhibition relative to the RIA curves with those of rFas2 (*top panel*). For each curve, the dilution yielding 50% competition or inhibition was quantified by reference to an internal standard curve made with Fas2 (not shown). Data are from the major peak when the mutant yielded several peaks on the cation-exchange resin. Data points correspond to the average value of duplicates that differed by less than 5%. The relative Fas2 activities of the mutants, averaged from several experiments, are reported in Table I.

toward distinct epitopes on Fas2. The existence of several antigenic determinants on the fasciculin molecule is in accord with previous reports of three to four distinct epitopes simultaneously accessible to specific antibodies (Fab fragments) directed against α-neurotoxins and of two monoclonal antibodies directed toward distinct areas of a cardiotoxin (*cf.* Ref. 54). Because of the heterogeneity of polyclonal antisera, as well as the multiplicity of residues involved in the contact area between each IgG and its specific epitope, single residue modifications of the three-fingered toxins usually have little influence on polyclonal antibody titers. Antigenic diversity proved to be generally useful for quantifying the loss in the inhibitory activity of the Fas2 mutants based on immunotitration of enriched samples.

Mutants T8A/T9A, R11Q, and H29D, however, displayed greater ratios of inhibitory activity to immunochemical titer than did wild-type Fas2. While this may reflect enhanced inhibitory affinity for AChE, several caveats preclude a precise determination of a dissociation constant. First, with a fasciculin dissociation rate constant of 4.0×10^{-3} min^{-1} (21), extended equilibration times are required for fractional AChE occupation. Extensive dilution of AChE to satisfy the condition of a K_i to total enzyme concentration ratio that assures a reasonable fraction of free ligand (55, 56) would have required unrealistic equilibration times for the putative high affinity

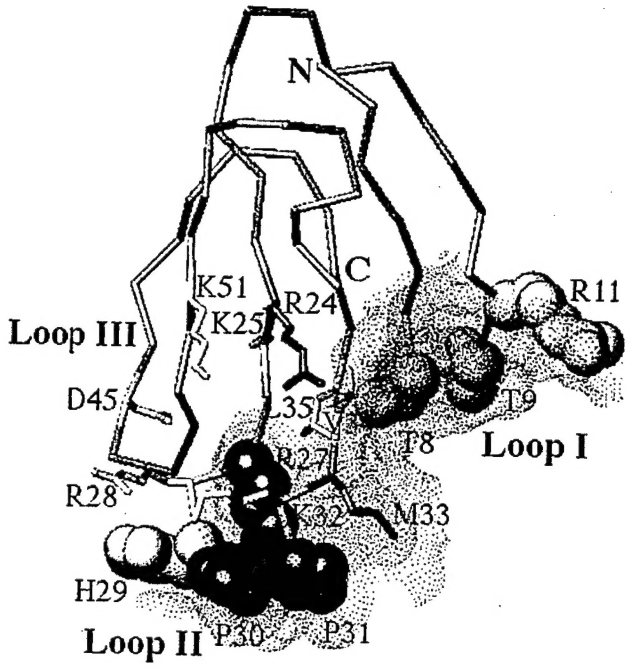

FIG. 7. **Positions of the functionally important residues of Fas2.** The three-dimensional structure of Fas2 complexed with mouse AChE (30) is viewed looking toward the concave side of the molecule; the molecular surface of mAChE buried in the complex is displayed (*dots*). The side chains of the Fas2 residues whose mutation causes virtually no effect on Fas2 activity are displayed as *light gray sticks* (K25L, R28D, K32G, V34A/L35A, D45K, and K51S). Those whose mutation causes a decrease by about one order of magnitude in Fas2 activity are displayed as *dark gray sticks* (R24T and M33A). Those whose mutation causes a decrease by two or more orders of magnitude in Fas2 activity are displayed as *dark gray* CPK (R27W, ΔP30, and P31R). Those whose mutation causes an apparent increase in Fas2 activity are displayed as *light gray* CPK (T8A/T9A, R11Q, and H29D). The two subsets of functionally important residues (CPK mode) reside at the tips of loop I and loop II, respectively. *N* and *C* denote the amino and carboxyl termini of the Fas2 molecule, respectively. This figure was generated with program TURBO-FRODO (70).

mutants. Second, as detailed below, the ratios will be artificially high if a region of Fas2 is a dominant epitope, as mutants of this region would show diminished immunoreactivity.

Mutations in Loop II—Loop II of Fas2 contains 16 residues, located between Cys^{22} and Cys^{39} (Fig. 4). Eleven residues, Arg^{24}, Lys^{25}, and all residues from Arg^{27} through Leu^{35}, were mutated. The Arg^{27}-Pro^{30}-Pro^{31} subset dominates the inhibitory activity of Fas2 (Figs. 6 and 7 and Table I) and interacts with the peripheral anionic site of the enzyme (30). However, the influence of these mutations is particularly complex since they may cause at least three distinct changes. Substitution of Trp for Arg^{27} removes a positive charge, increases the volume of the side chain, and introduces an aromatic indole ring with hydrophobic properties. Thus, the specific conformation of Fas2 loop II is likely to be altered because of the loss of the stabilizing intraloop interaction that Arg^{27} establishes with Pro^{30} and its indirect influence on the Pro^{30}-*cis*-Pro^{31} turn (30, 41). The bulky Trp side chain introduced at position 27 should experience steric hindrance with mAChE-Trp^{286} and would eliminate the potential hydrogen bonds of Arg^{27} with the carbonyl oxygens of Trp^{286} and Leu^{289} in mAChE. A similar steric occlusion might be responsible for the increased K_i seen for Fas2 chemically modified at Arg^{27} (57). Deletion of the amino acid residue Pro^{30} not only removes the cyclic side chain, but also alters both the length of loop II and the *cis* conformation of its tip. As a result, the cavity formed by mAChE residues Glu^{292}, Ser^{293}, Gly^{342}, and Ile^{365} is likely to contain bound water molecules in the complex. The shrinking of loop II, as well as its enhanced flexibility, would diminish the high complementarity of the interactive surface seen in the crystal structure (30). Substitution of Arg for Pro^{31} increases side chain dimensions, introduces a positive charge, and perhaps precludes formation of the *cis* bond in Pro^{30}. The obvious consequences would be steric hindrance of the bulkier Arg side chain with the cluster formed by mAChE residues Leu^{289}, Ser^{293}, and Tyr^{341}, as well as Coulombic repulsion with Fas2-Lys^{32} and/or mAChE-Arg^{296} (30). To resolve these possible interactions, residue substitutions at positions 27, 30, and 31 with progressive changes in side chain properties may help delineate the respective contributions of the charge, volume, and stereochemical characteristics of these three residues to conformation and stability of the complex.

Both the substitutions of Thr for Arg^{24} and Ala for Met^{33} resulted in an order of magnitude decrease in Fas2 activity (Table I). Arg^{24}, located at the base of loop II (Fig. 7), is a structurally important residue that stabilizes the carboxyl-terminal and core regions of Fas2 through hydrogen bonding to the carbonyl atom of Tyr^{61} and stacking interaction with Arg^{37} (30, 41). None of these interactions should be retained by the shorter, uncharged Thr side chain. Thus, a less stable complex forms with mAChE because of indirect destabilization of the mutated peptide molecule. The $Met^{33} \rightarrow$ Ala mutation should have a more direct influence. The loss of the sulfur atom and shortening of the side chain preclude stacking interactions with Trp^{286} and van der Waals contacts with Tyr^{341}, two key mAChE residues located at the peripheral anionic site (21, 58, 59). In addition, the smaller Ala side chain cannot retain secondary hydrophobic interactions with mAChE residues Tyr^{72}, Tyr^{124}, and Tyr^{341} (30). In the Fas2-mAChE complex, most of the solvent-accessible surface area of Met^{33} is lost; in fact, this residue contributes about 10% of the Fas2 surface area buried at the interface (30), a value slightly greater than the individual contributions of neighboring critical Fas2 residues Arg^{27}, Pro^{30}, and Pro^{31}. On the other hand, of the several peripheral anionic site residues that interact with Met^{33}, a single one, Tyr^{124}, does not establish any other contact with Fas2 (30). A decrease in apparent affinity for Fas2 of two orders of magnitude was observed for mAChE mutant Y124Q (21). More than a single order of magnitude in the decrease in Fas2 activity could therefore have been expected upon mutation of Met^{33}; however, the minimal change in the side chain volume with an Ala substitution likely preserves the tight fit of the other loop II residues with the peripheral anionic site.

Substitutions of Leu for Lys^{25}, of Asp for Arg^{28}, and of an Ala doublet for Val^{34}-Leu^{35}, resulted in unaltered Fas2 activity (Table I). These results are in accord with the crystallographic observations that show that the Lys^{25} and Arg^{28} side chains point away from the Fas2-mAChE interface, and that cavities exist between the van der Waals surfaces defined by the side chains of Fas2 residues Val^{34} and Leu^{35} and mAChE residues Leu^{76}, Tyr^{72}, and His^{287}, respectively (30). Replacement of Arg^{28} by Asp probably induces structural rearrangements leading to a different network of internal charge compensation; surprisingly, this does not perturb the activity of the mutant toward the enzyme.

Substitution of Asp for His^{29} resulted in an apparent increase of two orders of magnitude in the Fas2 activity (Figs. 6 and 7 and Table I). In the crystalline complex, the side chain of His^{29} participates in van der Waals interactions with mAChE-Glu^{292} that the newly introduced Asp side chain, negatively charged, cannot establish because of charge repulsion (30). However, the Asp side chain may be sufficiently flexible to rotate toward the side chain of either Arg^{27} or Arg^{28} and

undergo charge compensation. Also, an internal salt bridge could form with Arg^{27}. Thus, an improved fit of the more rigid tip of loop II with the mAChE peripheral anionic site residues might result from stabilization of internal structure. However, as discussed below, a change in structure might also affect the immunoreactivity of this mutant.

Mutations in Loop I—Loop I of Fas2 encompasses 13 residues, located between Cys^3 and Cys^{17} (Fig. 4). Both the mutations made on Thr^8-Thr^9 and Arg^{11} lead to apparent increases of one order of magnitude in the activities of the mutants toward mAChE (Fig. 6 and Table I). The Thr^8-Thr^9-Arg^{11} subset is fully exposed at the tip and external edge of loop I (Fig. 7), which fits in a crevice near the lip of the mAChE catalytic gorge and maximizes the surface area of contact of loop II at the gorge entry (30). In particular, the Thr^8-Thr^9 doublet potentially interacts with eight mAChE residues, Tyr^{70}, Gln^{71}, Tyr^{72}, Val^{73}, Leu^{92}, Gln^{279}, Val^{282}, and Asp^{283} (30). Substitution of an Ala doublet eliminates hydrogen bonding of the Thr side chains with Gln^{279} and Asp^{283}. The smaller size of the two Ala side chains might facilitate a rearrangement of the backbone at the tip of loop I, enabling it to come closer to loop II and establish a stabilizing internal interaction with Fas2-Leu^{35}. In addition, the smaller side chain of Ala^9 may establish more favorable interactions with mAChE residues Tyr^{70}, Leu^{92}, and Val^{282} and provide a tighter fit of the tip of loop I with the furrow that exists on the mAChE surface (30), possibly compensating for the loss of hydrogen bonding energy. On the other hand, Arg^{11} hydrogen bonds with mAChE-residues Glu^{84} and Asn^{87}. Substitution of Gln for Arg^{11} likely preserves the capacity for hydrogen bonding, especially as the smaller size of the Gln side chain should favor a tighter fit between the tip of loop I and the enzyme. Internal stabilization of the Fas2 molecule and/or loop I anchorage at the enzyme surface could thus contribute to tighter occlusion, by the tip of loop II, of the catalytic site gorge of the enzyme. Incidentally, the apparent increase in Fas2 activity that results from the removal of the positive charge does not match with the 40–73% loss in the activity of Fas2 chemically modified at Arg^{11} (57). The modifying agent, however, produces a substantial enlargement in the effective side chain that is not reproduced by the Gln mutation.

Although infrequent, single residue substitutions have shown enhanced affinity with the three-fingered peptidic toxins. The 35-fold higher affinity of Fas3, compared to Fas1, for rat brain AChE likely results from the $Thr^{15} \rightarrow Lys$ substitution in loop I (20). Substitution of Arg for Ile^{36} in erabutoxin a loop II led to a 7-fold increase in this neurotoxin's affinity for the nicotinic receptor (44). Two mutations of *Bungarus* AChE, near the presumed peripheral site, resulted in up to a 14-fold increase in affinity for Fas2 (22). Nevertheless, the uncertainties in the relative activities of the Fas2 mutants T8A/T9A, R11Q, and H29D preclude accurate determinations of specific activity without the availability of homogeneous peptides.

In several three-fingered toxins, the edge of the first loop and the tip and concave side of the second loop are domains immunoreactive to monoclonal antibodies. In Fas2, the bulky side chains of Arg^{11} and His^{29} could be particularly immunogenic, as was found for Trp^{11} of a cardiotoxin, toxin γ, and Lys^{15} of a neurotoxin, toxin α (54). Thus, apart from the structural arguments that may explain increased inhibitory activity, the $Arg^{11} \rightarrow Gln$ and $His^{29} \rightarrow Asp$ mutations may also have altered dominant epitopes located on loop I and loop II. Hence, a diminished, although not eliminated, recognition of the mutant by the anti-Fas2 serum (Fig. 6) may result in an overestimation of their relative inhibitory activities toward AChE. Similar considerations could influence our results for the double mutant T8A/T9A.

Despite the unique conservation of Arg^{11} in the fasciculins (42), the cationic side chain at this position does not appear to be a major contributor to the affinity nor to the inhibitory capacity of Fas2. In the crystalline complex, Arg^{11} associates with the region of Trp^{86}, proposed as a second portal, or "back door," for substrate entry into the enzyme (60, 61). Should translation of the choline cation through the putative back door region be rate-limiting in catalysis in the Fas2-AChE complex, a greater influence of Arg^{11} on AChE inhibition by Fas2 would have been expected. The side chain of Arg^{11}, however, displays high temperature factors (B factors) not only in the structures of unbound Fas1 and Fas2 (41, 62), but also in those of Fas2 bound to mAChE and *Torpedo* AChE (30, 31). In general, the highly flexible loop I may adopt an ensemble of conformations (41, 62); yet, a single conformation is selected in the formation of the high affinity complex (30, 31).

Mutations in Loop III—Loop III of Fas2 encompasses 10 residues, located between Cys^{41} and Cys^{52} (Fig. 4). The unaltered Fas2 activities of the D45K and K51S mutants (Figs. 6 and 7 and Table I) are consistent with the lack of interaction of residues Asp^{45} and Lys^{51} with mAChE, as observed in the crystalline complex. Yet, in the fasciculins, compared to the other members of the three-fingered toxin family, the Asp^{45}-Asp^{46} doublet confers to loop III an exclusive anionic locus which dictates the orientation of the dipole vector of the molecule (18, 42). An internal structural rearrangement in the D45K mutant molecule may occur, since the Lys side chain introduced at position 45 should repel Arg^{28}, which stabilizes Asp^{45} in Fas2 (41, 42). In the mutant, however, it may be compensated by the neighboring side chain of Asp^{46}.

Changes in the Fas2 structure have been proposed earlier to explain the 57% decrease in Fas2 activity upon acetylation of Lys^{51} (63). Two residues of loop III, Asn^{47} and Leu^{48}, interact with mAChE-His^{287}, but at distances of ~4 Å (30); however, Leu48 does not interact with *Torpedo* AChE (31). Loop III residues, therefore, likely play no critical functional role other than internal stabilization of loop II conformation.

Numerous aromatic residues reside at the Fas2-mAChE complex interface: Fas2-Tyr^4, His^6, His^{29}, and Tyr^{61}, and mAChE-Tyr^{70}, Tyr^{72}, Tyr^{77}, Tyr^{124}, Trp^{286}, His^{287}, Tyr^{341}, as well as several nonaromatic residues which undergo hydrophobic interactions: Fas2-Pro^{30}, Pro^{31}, and Met^{33}, and mAChE-Pro^{78} (30). Mutation of Fas2-Pro^{30} and Pro^{31}, which are central to the interface, resulted in two to three orders of magnitude decreases in Fas2 activity. Single-site substitutions of mouse AChE peripheral anionic site residues Tyr^{72}, Tyr^{124}, and Trp^{286}, also central to the interface, reduced the affinity of Fas2 by two to six orders of magnitude (21). Thus, patches of high hydrophobicity at the interface dominate the binding free energy of the Fas2-AChE complex, consistent not only with the tight intermolecular packing areas observed in the crystal structures (30, 31), but also with general structural patterns observed at interfaces of high affinity protein-protein complexes (64–69).

Site-directed mutagenesis of the Fas2 molecule and expression of the mutants from transiently transfected mammalian cells have provided substantial information on the respective contributions of 16 residues of Fas2 positioned for interaction with mouse AChE. The determinants identified by the structural and the functional approaches do coincide, but only a few of the many residues which make up the overall interactive site of the Fas2 molecule provide the strong interactions required for high affinity binding. Mutant cycle analyses, coupled with kinetic and crystallographic studies, should further delineate the contribution of individual residues to the affinity and inhibitory capacity of the fasciculin-AChE complexes.

Acknowledgments—We are grateful to Drs. Tyler White, John Lewicki, Barbara Cordell, and Andy Lin (Scios Nova, Inc.) for the gift of the pGS expression vector, to Dr. Daniel Donoghue (UCSD) for synthesis of the 130-base pair oligonucleotides used in construction of the expression plasmid, to Siv Garod (UCSD) for amino-terminal sequencing of rFas2, to Dr. Igor Tsigelny (UCSD) for three-dimensional superimposition and sequence analysis of the toxins, and to Dr. Yves Bourne (CNRS) for help in structural analysis of the mutants and fruitful discussions. Assistance from Kael Duprey and Jonathan Eads (UCSD) in inhibition and radioimmunoassays and from Maryse Alvitre (CNRS) in rabbit serum production is much appreciated.

REFERENCES

1. Lee, C. Y. & Chang, C. C. (1966) *Mem. Inst. Butantan (Sao Paolo)* **33,** 555–572
2. Changeux, J. P., Kasai, M. & Lee, C. Y. (1970) *Proc. Natl. Acad. Sci. U. S. A.* **67,** 1241–1247
3. Endo, T. & Tamiya, N. (1991) in *Snake Toxins* (Harvey, A. L., ed) pp. 165–222, Pergamon Press, New York
4. Chiappinelli, V. A. (1983) *Brain Res.* **277,** 9–22
5. Oswald, R. E., Sutcliffe, M. J., Bamberger, M., Loring, R. H., Braswell, E. & Dobson, C. M. (1991) *Biochemistry* **30,** 4901–4909
6. Adem, A., Asblom, A., Johansson, G., Mbugua, P. M. & Karlsson, E. (1988) *Biochim. Biophys. Acta* **968,** 340–345
7. Segalas, I., Roumestand, C., Zinn-Justin, S., Gilquin, B., Ménez, R., Ménez, A. & Toma, F. (1995) *Biochemistry* **34,** 1248–1260
8. de Weille, J. R., Schweitz, H., Maes, P., Tartar, A., & Lazdunski, M. (1991) *Proc. Natl. Acad. Sci. U. S. A.* **88,** 2437–2440
9. Albrand, J. P., Blackledge, M. J., Pascaud, F., Holleker, M. & Marion, D. (1995) *Biochemistry* **34,** 5923–5937
10. McDowell, R. S., Dennis, M. S., Louie, A., Shuster, M., Mulkerrin, M. G. & Lazarus, R. A. (1992) *Biochemistry* **31,** 4766–4772
11. Sutcliffe, M. J., Jaseja, M., Hyde, E. I., Lu, X. & Williams, J. A. (1994) *Struct. Biol.* **1,** 802–807
12. Bougis, P., Rochat, H., Piéroni, G. & Verger, R. (1981) *Biochemistry* **20,** 4915–4920
13. Dufton, M. J. & Hider, R. C. (1991) in *Snake Toxins* (Harvey, A. L., ed) pp. 259–302, Pergamon Press, New York
14. Drenth, J., Low, B. W., Richardson, J. S. & Wright, C. S. (1980) *J. Biol. Chem.* **255,** 2652–2655
15. Wright, C. S. (1987) *J. Mol. Biol.* **194,** 501–529
16. Kieffer, B., Driscoll, P. C., Campbell, I. D., Willis, A. C., van der Merwe, P. A. & Davis, S. J. (1994) *Biochemistry* **33,** 4471–4482
17. Ploug, M. & Ellis, V. (1994) *FEBS Lett.* **349,** 163–168
18. Karlsson, E., Mbugua, P. M. & Rodriguez-Ithurralde, D. (1984) *J. Physiol. (Paris)* **79,** 232–240
19. Cerveñansky, C., Dajas, F., Harvey, A. L. & Karlsson, E. (1991) in *Snake Toxins* (Harvey, A. L., ed) pp. 303–321, Pergamon Press, New York
20. Marchot, P., Khélif, A., Ji, Y.-H., Mansuelle, P. & Bougis, P. E. (1993) *J. Biol. Chem.* **268,** 12458–12467
21. Radic, Z., Duran, R., Vellom, D. C., Li, Y., Cervenansky, C. & Taylor, P. (1994) *J. Biol. Chem.* **269,** 11233–11239
22. Cousin, X., Bon, S., Duval, N., Massoulié, J. & Bon, C. (1996) *J. Biol. Chem.* **271,** 15099–15108
23. Radic, Z., Quinn, D. M., Vellom, D. C., Camp, S. & Taylor, P. (1995) *J. Biol. Chem.* **270,** 20391–20399
24. Eastman, J., Wilson, E. J., Cerveñansky, C. & Rosenberry, T. L. (1995) *J. Biol. Chem.* **270,** 19694–19701
25. Marchot, P., Ravelli, R. B. G., Raves, M. L., Bourne, Y., Vellom, D. C., Kanter, J., Camp, S., Sussman, J. L. & Taylor, P. (1996) *Protein Sci.* **5,** 672–679
26. Rosenberry, T. L., Rabl, C.-R. & Neumann, E. (1996) *Biochemistry* **35,** 685–690
27. Sussman, J. L., Harel, M., Frolow, F., Oefner, C., Goldman, A., Toker, L. & Silman, I. (1991) *Science* **253,** 872–879
28. Taylor, P. & Lappi, S. (1975) *Biochemistry* **14,** 1989–1997
29. Taylor, P. & Radić, Z. (1994) *Annu. Rev. Pharmacol. Toxicol.* **34,** 281–320
30. Bourne, Y., Taylor, P. & Marchot, P. (1995) *Cell* **83,** 503–512
31. Harel, M., Kleywegt, G. J., Ravelli, R. B. G., Silman, I. & Sussman, J. L. (1995) *Structure* **3,** 1355–1366
32. le Du, M. H., Marchot, P., Bougis, P. E. & Fontecilla-Camps, J. C. (1989) *J. Biol. Chem.* **264,** 21401–21402
33. Radić, Z., Pickering, N. A., Vellom, D. C., Camp, S. & Taylor, P. (1993) *Biochemistry* **32,** 12074–12084
34. Vellom, D. C., Radić, Z., Li, Y., Pickering, N. A., Camp, S. & Taylor, P. (1993) *Biochemistry* **32,** 12–17
35. Harlow, E. & Lane, D. (1988) *Antibodies, a Laboratory Manual,* Cold Spring Harbor Laboratory, Cold Spring Harbor, NY
36. Tamiya, T., Lamouroux, A., Julien, J. F., Grima, B., Mallet, J., Fromageot, P. & Ménez, A. (1985) *Biochimie* **67,** 185–189
37. Kunkel, T. A., Roberts, J. D. & Zakour, B. A. (1987) *Methods Enzymol.* **154,** 367–382
38. Kalnins, A., Otto, K., Rüther, U. & Müller-Hill, B. (1983) *EMBO J.* **2,** 593–597
39. Laemmli, U. K. (1970) *Nature* **227,** 680–685
40. Ellman, G. L., Courtney, K. D., Andres, V., Jr. Featherstone, R. M. (1961) *Biochem. Pharmacol.* **7,** 88–95
41. le Du, M. H., Marchot, P., Bougis, P. E. & Fontecilla-Camps, J. C. (1992) *J. Biol. Chem.* **267,** 22122–22130
42. van den Born, H. K. L., Radić, Z., Marchot, P., Taylor, P. & Tsigelny, I. (1995) *Protein Sci.* **4,** 703–715
43. Pillet, L., Trémeau, O., Ducancel, F., Drevet, P., Zinn-Justin, S., Pinkasfeld, S., Boulain, J.-C. & Ménez, A. (1993) *J. Biol. Chem.* **268,** 909–916
44. Trémeau, O., Lemaire, C., Drevet, P., Pinkasfeld, S., Ducancel, F., Boulain, J.-C. & Ménez, A (1995) *J. Biol. Chem.* **270,** 9362–9369
45. Mebs, D. & Claus, I. (1991) in *Snake Toxins* (Harvey, A. L., ed) pp. 425–447, Pergamon Press, New York
46. Ducancel, F., Boulain, J. C., Trémeau, O. & Ménez, A. (1989) *Protein Eng.* **3,** 139–143
47. Boyot, P., Pillet, L., Ducancel, F., Boulain, J. C, Trémeau, O. & Ménez, A. (1990) *FEBS Lett.* **266,** 87–90
48. Fiordalisi, J. J., Fetter, C. H., Ten-Harmsel, A., Gigowski, R., Chiappinelli, V. A. & Grant, G. A. (1991) *Biochemistry* **31,** 10337–10343
49. Fiordalisi, J. J., Al-Rabiee, R., Chiappinelli, V. A. & Grant, G. A. (1994) *Biochemistry* **33,** 3872–3877
50. Fiordalisi, J. J., Al-Rabiee, R., Chiappinelli, V. A. & Grant, G. A. (1994) *Biochemistry* **33,** 12962–12967
51. Rosenthal, J. A., Hsu, S. H., Schneider, D., Gentile, L. N., Messier, N. J., Vaslet, C. A. & Hawrot, E. (1994) *J. Biol. Chem.* **269,** 11178–11185
52. Lu, X., Rahman, S., Kakkar, V. V. & Authi, K. S. (1996) *J. Biol. Chem.* **271,** 289–294
53. Fiordalisi, J. J., James, P. L., Zhang, Y. & Grant, G. A. (1996) *Toxicon* **34,** 213–224
54. Ménez, A. (1991) in *Snake Toxins* (Harvey, A. L., ed) pp. 35–90, Pergamon Press, New York
55. Straus, O. H. & Goldstein, A. (1943) *J. Gen. Physiol.* **26,** 559–585
56. Greco, W. R. & Hakala, M. T. (1979) *J. Biol. Chem.* **254,** 12104–12109
57. Cerveñansky, C., Engström, A. & Karlsson, E. (1995) *Eur. J. Biochem.* **229,** 270–275
58. Barak, D., Kronman, C., Ordentlich, A., Ariel, N., Bromberg, A., Marcus, D., Lazar, A., Velan, B. & Shafferman, A. (1994) *J. Biol. Chem.* **269,** 6296–6305
59. Shafferman, A., Velan, B., Ordentlich, A., Kronman, C., Grosfeld, H., Leitner, M., Flashner, Y., Cohen, S., Barak, D. & Ariel, N. (1992) *EMBO J.* **11,** 3561–3568
60. Gilson, M. K., Straatsma, T. P., McCammon, J. A., Ripoll, D. R., Faerman, C. H., Axelsen, P. H., Silman, I. & Sussman, J. L. (1994) *Science* **263,** 1276–1278
61. Axelsen, P. H., Harel, M., Silman, I. & Sussman, J. L. (1994) *Protein Sci.* **3,** 188–197
62. Le Du, M. H., Housset, D., Marchot, P., Bougis, P. E., Navaza, J. & Fontecilla-Camps, J. C. (1996) *Acta Crystallogr. Sec. D* **52,** 87–92
63. Cerveñansky, C., Engström, A. & Karlsson, E. (1994) *Biochim. Biophys. Acta* **1199,** 1–5
64. Chothia, C. & Janin, J. (1975) *Nature* **256,** 705–708
65. Janin, J. & Chothia, C. (1990) *J. Biol. Chem.* **265,** 16027–16030
66. Padlan, E. A. (1990) *Proteins* **7,** 112–124
67. Jin, L., Fendly, B. M. & Wells, J. A. (1992) *J. Mol. Biol.* **226,** 851–865
68. Nuss, J. N., Bossard Whitaker, P. & Air, G. M. (1993) *Proteins* **15,** 121–132
69. Clackson, T. & Wells, J. A. (1995) *Science* **267,** 383–386
70. Roussel, A. & Cambillau, C. (1989) in *Silicon Graphics Geometry Partners Directory* (Silicon Graphics Committee, eds) pp. 77–78, Mountain View, CA